**University of Mohamed Khider –
Biskra**
**Faculty of Exact Sciences and
Science of Nature and life.**

جامعة محمد خيضر ـ بسكرة
كلية العلوم الدقيقة
و علوم الطبيعة
و الحياة

Thesis presented to obtain the degree:

Doctorat LMD

Option**:**

Physics of materials and photonic devices
(Physique des matériaux et composants photoniques)

Entitled:

Simulation of CZTS-based thin-film solar cells

(Simulation des cellules solaires en couches minces à base de CZTS)

Presented by:

Bouslit Sonia

Jury

Toufik Tibermacine	Professor	U.M.K. Biskra	President
Nouredine Sengouga	Professor	U.M.K. Biskra	Supervisor
Widad Laiadi	M.C.A.	U.M.K. Biskra	Examiner
Slimane Chala	M.C.A.	Uni. Boumerdes	Examiner

Acknowledgements

Abstract

Cu₂ZnSnS₄ (CZTS), is a quaternary semiconductor of the thin film with a direct band-gap, has a gap of 1.6-1.4 eV with a large absorption coefficient of 10^4 cm^{-1}, a film absorber with very beneficial properties, in addition to its low production cost. In this work, the effect of many parameters of the absorber layer on the performance of a CZTS solar cell is investigated using the numerical simulation program SCAPS-1D. Also the effect of defects type (donor and acceptor) deep in the band gap of the CZTS was studied. The series and shunt resistances and the interface defects between layer P and layer N were also considered. The effect of the band-gap of energy, thickness, acceptor density and electron affinity were also highlighted. The performance of the solar cell was studied in terms of the short circuit current J_{sc}, the open-circuit voltage V_{oc}, the fill factor FF, and the efficiency η. It was found that when volume defects are considered in the CZTS absorber layer, better results were obtained but not as expected; only the short circuit current is reproduced. On the other hand, interface states are considered between CZTS and CdS give good agreement of the open circuit voltage. The series and shunt resistance lead to a better agreement of the fill factor. Only when all these are considered together that experimental measurements are reproduced.

Keywords: solar cells, thin-film, SCAPS numerical simulation, defects

ملخص

Cu2ZnSnS4 (CZTS) عبارة عن شبه موصل رباعي مع فجوة نطاق مباشرة ، مقداره في المجال eV 1.4 -1.6 مع معامل امتصاص كبير يبلغ 10^4 cm^{-1}، له خصائص مفيدة للغاية ، بالإضافة إلى تكلفة الإنتاج المنخفضة. في هذا البحث تم دراسة تأثير العديد من معاملات الطبقة الممتصة على أداء الخلية الشمسية CZTS باستخدام برنامج المحاكاة الرقمية SCAPS-1D. كما تمت دراسة تأثير نوع العيوب (الآخذة و المانحة) في عمق فجوة النطاق في CZTS. كما تم النظر في المقاومة على التسلسل والتوازي وعيوب الواجهة بين الطبقة P والطبقة N. كما تم تسليط الضوء على تأثير فجوة النطاق للطاقة والسمك وكثافة العيوب الآخذة والألفة الإلكترونية. تمت دراسة أداء الخلية الشمسية من حيث تيار الدائرة القصيرة J_{SC} ، وفلطية الدائرة المفتوحة V_{OC} ، وعامل التعبئة FF ، والكفاءة η. وجد أنه عند النظر إلى عيوب الحجم في الطبقة الماصة CZTS ، تم الحصول على نتائج

أفضل ولكن ليس كما هو متوقع و يتم فقط إنتاج تيار الدائرة القصيرة. من ناحية أخرى ، حالات الواجهة بين CZTS و CdS تعطي توافقًا جيدًا على جهد الدائرة المفتوحة. تؤدي المقاومة التسلسلية والتحويلة إلى اتفاق أفضل لعامل التعبئة. فقط عندما يتم أخذ كل هذه العوامل معًا في الاعتبار ، يتم إعادة إنتاج القياسات التجريبية

كلمات مفتاحية: الخلايا الشمسية ،الشرائح الرقيقة ، محاكاة رقمية SCAPS، العيوب.

Table of Contents

List of figures

List of tables

List of symbols and abbreviations

2D	Two-Dimensional
AM0	Air Mass zero
AM1.5	Air Mass 1.5 Global solar spectrum
CB	Conduction band
CBM	Minimum conduction band
CBO	The conduction band Offset
D_n [cm^2/s]	Electron diffusion constant
D_p [cm^2/s]	Hole diffusion constant
E [V/cm]	Electric field
E_A, E_a [eV]	Apparent activation energy
E_C [eV]	Bottom edge of conduction band
E_{CBM}	Minimum conduction band, the bottom of the conduction bands
E_F [eV]	(Equilibrium) Fermi level
E_{Fn} [eV]	Electron Fermi level
E_{Fp} [eV]	Hole Fermi level
E_g (eV)	Gap optique
E_T [eV]	Trap level; energy level of a defect
Evac	The vacuum level, free electron energy
f [Hz]	Frequency
FF [%]	Fill factor
G_n	The electron generation rates
G_p	The hole generation rates
hν [J or eV]	Photon energy
I	Current
I_{ph}	Photogenrated current
J	Current density
J [A/cm^2]	Current density
J_0 [A/cm^2]	(Dark) saturation current density
J_m [A/cm^2]	Current density at maximum power

J_n [A/cm^2]	Electron particle current density
J_p [A/cm^2]	Hole particle current density
J_{sc} [A/cm^2]	Short circuit current density
K_B	Boltzmann constant
L_e	The minority-carrier-diffusion lengths for electron
L_h	The minority-carrier-diffusion lengths for hole
n	Electron concentrations
N_A [1/cm^3]	Shallow acceptor density
N_C (cm^{-3})	Densité effective d'états dans la bande de conduction
N_D [1/cm^3]	Shallow donor density
N_D^+ [cm^{-3}]	Density of ionised shallow donors
nm	Nanometer
N_t, N_T [1/cm^3]	Density of traps, defects
N_V (cm^{-3})	Densité effective d'états dans la bande de valence
p	Hole concentrations
P_i	Incident power
P_m	Maximum produced power
q	Elemantary charge
QE [%]	External quantum efficiency
R_n	The electron recombination rates
R_p	The hole recombination rates
R_s [Ω]	Series resistance
R_{sh} [Ω]	Shunt resistance
SRH	Shockley-Read-Hall recombination mechanism
T [K]	Absolute temperature
TCO	Transparent Conducting Oxide
V [V]	Voltage, applied voltage
VB	Valence band
VBM	Valence-band minimum
V_m [V]	Voltage at maximum power
V_{oc} [V]	Open circuit voltage

W [cm, μm or nm]	Depletion layer width
α [/cm]	Optical absorption constant
ε	Relative permittivity
ε_0 [F/cm]	Permittivity of vacuum
η [%]	Photovoltaic conversion efficiency
λ [nm] or [μm]	Wavelength
μ_n [cm^2/Vs]	Electron mobility
μ_p [cm^2/Vs]	Hole mobility
ρ (Ω.cm)	Résistivité
ρ_n	Electrons distribution
ρ_p	Holes distribution
σ (Ω^{-1}.cm^{-1})	Conductivité, inverse de la résistivité
σ_n [cm^2]	Capture cross section for electrons
σ_p [cm^2]	Capture cross section for holes
ψ	Electrostatic potential
Φ	The flat band metal work function

GENERAL

INTRODUCTION

GENERAL INTRODUCTION

Technological progress is closely linked to the evolution of different materials and tools made from those materials. Only the different ages were described with respect to the materials used. Several of today's main attributes (i.e., the age of electronic materials) are modern instruments such computers and fiber-optic telecommunication networks, in which semiconductor materials provide critical components for various microelectronic and optoelectronic devices in applications, like: computing, memory storage, and communication [1].

Photovoltaics is the direct transformation of sunlight into electricity using solar cells. Edmond Becquerel, as a young 19-year-old employed in his father's laboratory in France, demonstrated the first photovoltaic system in 1839. However, understanding and exploiting this effect was to depend on some of the 20th century's most significant scientific and technological developments. One is the invention of quantum mechanics, which is one of the 20th century's great scientific achievements. The production of semiconductors is another, which is based on the first technology that was responsible for the omnipresent revolution in electronics and photonics revolution now gathering pace. Loferski (1993) provides a fascinating overview of modern photovoltaic innovations and Crossley et al. (1968) explains the early history, dating back to 1839, in more technical detail [2, 3].

The use of photovoltaics has become ever more systematic processes to manufacture ever thinner cells with higher efficiencies and lower costs in greater quantities. Advances in photovoltaic materials and manufacturing will continue to improve cost-competitiveness of the technology and slowly extend its applications without the need for scientific breakthroughs that change game. If true breakthroughs are made, the kind that exploits new understanding of physics and material science to overcome old efficiency and cost limitations then the current solar power evolution could turn into a revolution with a more rapid pace. Several broad routes have been pursued to reduce production costs, including increasing the efficiency of traditional Si-based photovoltaics, using thin film absorbers (amorphous Si, CdTe, and $CuIn_xGa_{1-x}Se_2$; CIGS), and developing novel low-cost platform technologies such as organic photovoltaics (OPVs) and dye-sensitized solar cells (DSSCs)[4].

Copper zinc tin sulfide (CZTS) is a quaternary semiconducting compound that has gained growing popularity in thin film solar cells since the late 2000s. Many I_2-II-IV-VI$_4$, such as copper zinc tin selenide (CZTSe) and sulfur-selenium alloy CZTSSe, are included in the associated content class. CZTS is a p-type semiconductor, provides favorable optical and electronic properties similar to CIGS (copper indium gallium selenide), making it well-suited for use as a thin film solar cell absorber layer, but unlike CIGS (or other thin films such as CdTe), CZTS is composed of only abundant and non-toxic materials. Concerns about the price and quality of Indium in CIGS and Tellurium in CdTe, as well as the toxicity of cadmium, the quest for alternative thin film solar cell materials has been a significant motivator [5, 6]. CZTS has sufficient optical bandgap energy of 1.4-1.68 eV and a high optical absorption coefficient bigger than 10^4 cm^{-1} in visible wavelength range [7-12].

This thesis is organised over three chapters.

Chapter I is a comprehensive and general theoretical study of the basic concepts of semiconductors, and their evolution over time, as well as to provide a summary of some of their types, crystal structure, summary of defects in semiconductors, and the characteristics and defects of CZTS semiconductors. CZTS solar cells are presented in this chapter. Their characteristics, different configurations and structures are discussed.

Chapter II presents the definition and description of the numerical simulation by SCAPS, used in this study.

Chapter III summarizes simulation results and discussions of thin films and solar cells. First , CZTS parameters are taken from experimental measurements in the litterature [13]. Second, a simulation of thin film solar cells base on these CZTS films is conducted before adjusting these parameters and the presence of defects to achieve acceptable fitting to experimental measurements. The results and discussion of solar cell performance are based on the open voltage circuit Voc, the short circuit current Jsc, efficiency η and the fill factor FF.

REFERENCES

[1]   B. G. Yacobi, *Semiconductor materials: an introduction to basic principles*: Springer Science & Business Media, 2003.

[2]   S. Wenham, M. Green, M. Watt, and R. Corkish, *Applied photovoltaics, second edition*, 2013.

[3]   A. E. Becquerel, "Recherches sur les effets de la radiation chimique de la lumiere solaire au moyen des courants electriques," *Comptes Rendus de L´Academie des Sciences,* vol. 9, 1839.

[4]   C. Tong, "Materials-Based Solutions to Advanced Energy Systems," in *Introduction to Materials for Advanced Energy Systems*, ed: Springer, 2019, pp. 1-86.

[5]   H. Katagiri, "Cu2ZnSnS4 thin film solar cells," *Thin Solid Films,* vol. 480, pp. 426-432, 2005.

[6]   G. Altamura, "Development of CZTSSe thin films based solar cells," Université Joseph-Fourier-Grenoble I, 2014.

[7]   T. Kobayashi, K. Jimbo, K. Tsuchida, S. Shinoda, T. Oyanagi, and H. Katagiri, "Investigation of Cu2ZnSnS4-based thin film solar cells using abundant materials," *Japanese journal of applied physics,* vol. 44, p. 783, 2005.

[8]   S. Chen, X. G. Gong, A. Walsh, and S.-H. Wei, "Crystal and electronic band structure of Cu2ZnSnX4 (X=S and Se) photovoltaic absorbers: First-principles insights," *Applied Physics Letters,* vol. 94, p. 041903, 2009.

[9]   S. Chen, J.-H. Yang, X.-G. Gong, A. Walsh, and S.-H. Wei, "Intrinsic point defects and complexes in the quaternary kesterite semiconductor Cu 2 ZnSnS 4," *Physical Review B,* vol. 81, p. 245204, 2010.

[10]   M. Suryawanshi, S. Shin, U. Ghorpade, K. Gurav, G. Agawane, C. W. Hong, J. H. Yun, P. Patil, J. H. Kim, and A. Moholkar, "A chemical approach for synthesis of

photoelectrochemically active Cu2ZnSnS4 (CZTS) thin films," *Solar Energy,* vol. 110, pp. 221-230, 2014.

[11]   M. Patel and A. Ray, "Enhancement of output performance of Cu2ZnSnS4 thin film solar cells—A numerical simulation approach and comparison to experiments," *Physica B: Condensed Matter,* vol. 407, pp. 4391-4397, 2012.

[12]   W. Li, J. Chen, C. Yan, and X. Hao, "The effect of ZnS segregation on Zn-rich CZTS thin film solar cells," *Journal of Alloys and Compounds,* vol. 632, pp. 178-184, 2015.

[13]   T. P. Dhakal, C. Y. Peng, R. R. Tobias, R. Dasharathy, and C. R. Westgate, "Characterization of a CZTS thin film solar cell grown by sputtering method," *Solar Energy,* vol. 100, pp. 23-30, 2014.

CHAPTER I

Solar cells

Chapter I.   Solar cells

I.1. Introduction

Since the discovery of electricity, humans cannot do without it due to its significance in their daily life. For instance, our mobile devices need electricity, our street lighting needs illumination and our cars need gasoline. We supply our homes with household oil, propane, or electricity for lighting, heating, and powering our appliances from a national or local grid. All these things take energy from fuel. Those sources have polluting emissions and harmful impacts on the environment. While electricity generation from carbon fuels can lead to these problems, renewable energy which is produced from clean and sustainable resources, such as solar radiation, solar photovoltaic technologies directly convert solar radiation into power. The planet is doing its utmost to minimize carbon emissions and limit the global average that increases its temperature. We need to move to renewable sources to generate our energy to help preserving the environment and secure the future of the planet.

This chapter introduces the photoelectric effect, followed by a brief presentation of the essential solar energy aspect for radiation. We will discuss the photovoltaic cell's operating theory, its various properties, and provide a brief presentation of thin-film solar cells based on CZTS.

I.2. Semiconductors

A semiconductor is a substance with a certain degree of conductivity between a conductor and an insulator. Physical conductivity is tied to its resistance to current flow. In other words, the higher the conductivity level and the lower is the resistance. Figure I.1 illustrates the electrical conductivity σ of certain materials from the three parts (and the corresponding resistivity $\rho = 1/\sigma$). Insulators have very low conductivity and high resistivity in the range of 10^{-18}–10^{-8} S/cm such as a diamond (pure), fused quartz, and sulfur; and conductors have low resistivity and high conductivity such as copper and platinum, typically between 10^4 and 10^6 S/cm. Semiconductor's conductivities occur between insulators and conductors. The temperature, illumination, magnetic field, and minute amounts of impurity atoms affect a semiconductor's conductivity The semiconductor becomes one of the important materials in conductivity for that purpose [1].
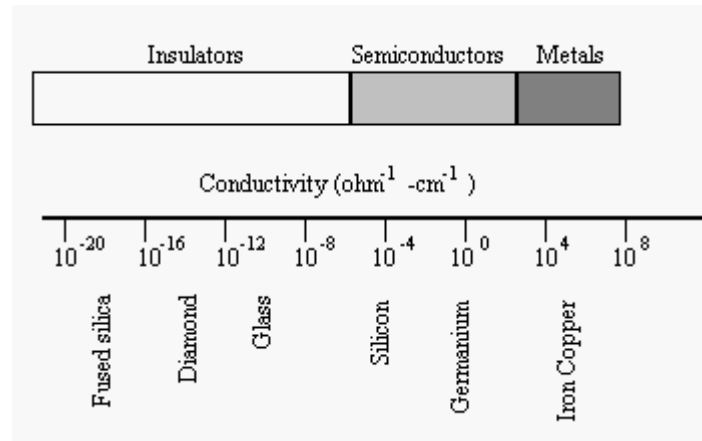
Figure I.1: Electrical conductivity at room temperature of some solid bodies; boundaries between semiconductors, metals and insulators.

I.3. Different types of doping

Intrinsic semiconductors are of little use. In fact, the semiconductor materials' properties can be substantially altered by adding impurity atoms to the proportionally pure semiconductor content. Though added, these impurities will reasonably alter the band structure to fully transform the material's electrical properties [2]. There are two types of semiconductors:

I.3.1. N-doped semiconductors

N-type doping is about amplifying the semiconductor electron density. Thus, the acceptor concentration will be lower than the donor concentration ($N_A < N_D$). For this, we include several rich atoms in electrons in the semiconductor.

I.3.2. P-doped semiconductors

P-type doping is designed to increase the density of holes in the semiconductor, the concentration of acceptors would be higher than that of donors ($N_A > N_D$). For this reason, we include several poor atoms in electrons in the semiconductor.

I.4. The p-n junction

The interaction between an n-type semiconductor and a p-type semiconductor produces a diode or a p-n junction. Under the influence of the concentration gradient, some

of the majority holes in the p-type component are transferred to the n-type region leaving negative acceptor ions N_A^-. It is the same for the other-way electrons leaving some positive donor ions N_D^+. As a result, near the n-side is formed a positive spatial charge, and near the p-side of the junction is formed a negative spatial charge (see Figure I.2). An area without mobile charges is formed, called space charge region (depletion zone or space charge layer), where an extreme electric field prevails. The role this region in solar cells is fundamental. The photogenerated carriers inside the depletion region are immediately separated, diffused outside the depletion zone, and collected at the external contact point. The photogenerated charges outside the depletion zone must first be diffused into the depletion zone and then guided through by the electric field. The classical homojunction structure can be expressed in terms of energy bands, and the structure of which it is shown in Figure I.2: 1.Figure I-2-2 (a) shows the characteristic band structure of the p and n-type materials. Figure 1-2: 2 (b) demonstrates the processes of absorption and aggregation given the band structure. Where the space charge area produces an electric field, which counterbalance the charge exchange and restores thermodynamic equilibrium.
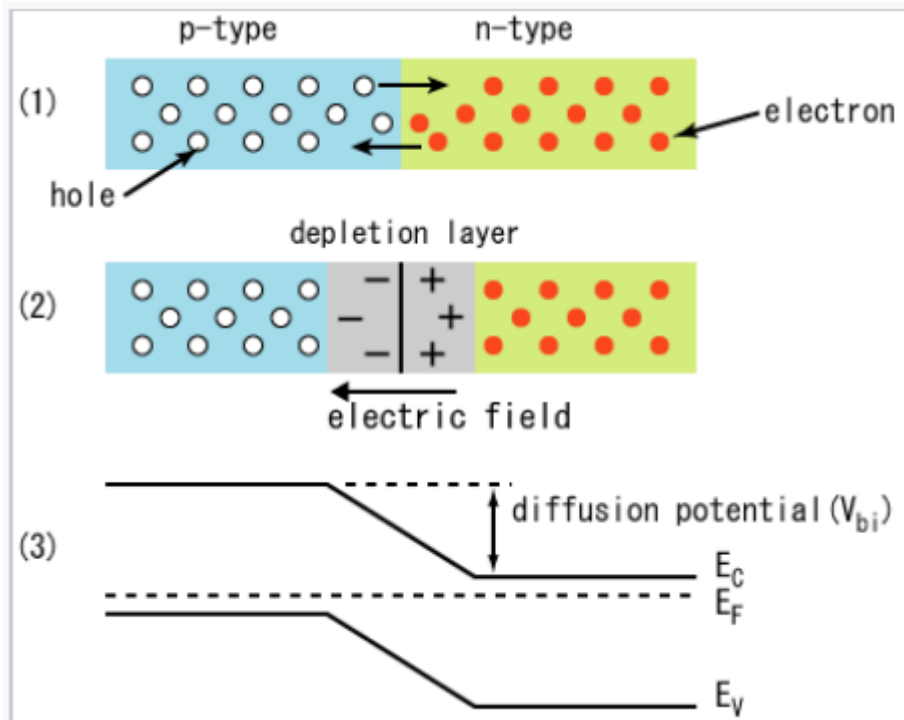
Figure I.2: Schematic illustration of the p-n junction. Solar radiation

Though the sun's surface radiation is constant [3, 4], because of its absorption and diffusion in its atmosphere, it is very unpredictable when it hits the Earth's surface. The highest radiation hits the surface of the Earth when the sun is directly overhead in the

clearness of the sky. The spectral distribution of sunlight outside the ambient atmosphere (Air Mass Zero or AM0) and AM1.5 are illustrated (see Figure 1.3). Air mass Zero does not essentially change, and the total density of its embodied power in the spectrum is called the solar constant which is given by the generally accepted value of 1.3661 kW / m^2 [3, 5]. It is common to look at the "direct" (or "beam") solar radiation and the "diffuse" radiation somewhere else in the sky, the sum of which is known as "global" radiation, separately [6].

Then Becquerel is one of the first to discover the photoelectric effect, after noticing in 1839 that some of the materials exposed to light created an electrical current and permitted direct conversion of light energy to electrical energy. This effect is now called the photovoltaic effect. This conversion of energy can be divided down into solar radiation absorption, separating and collecting optical charges. When the solar cell is illuminated, photons whose energy is larger than the material bandgap are absorbed resulting in electron-hole pairs [7, 8].
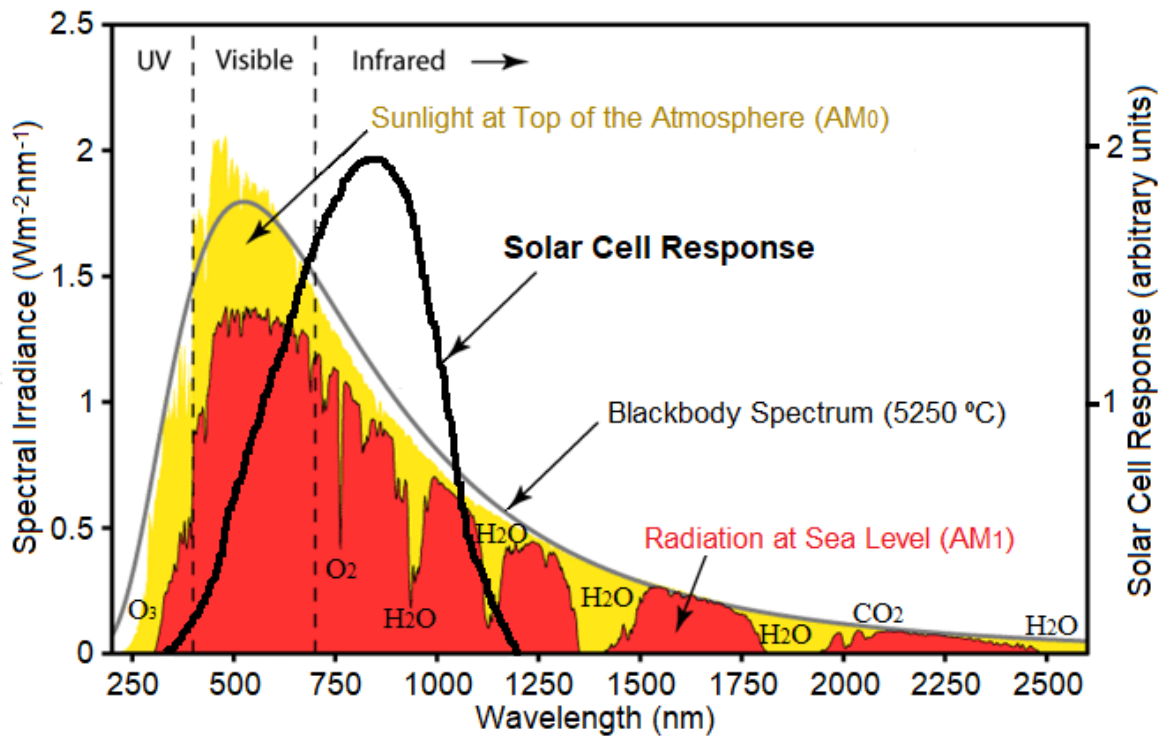
Figure I.3: The spectral power density of sunlight, outside the atmosphere (AM0), and at the earth's surface (AM1.5), shows absorption from various atmospheric component [9].

I.5. Characteristic parameters of a photovoltaic cell

A solar cell is most often a p-n (or n-p) junction to which contacts are added to collect the current [10]. Once the solar cell is exposed to light, pairs of electron- hole are formed and thus the photogenerated I_{ph} current is created which depends on the amount of incident light. Figure I-4 shows the solar cell's two I-V characteristics in the dark and under the illumination. The following equation defines the curve [11]:

$$I = I_0 \left(e^{qV/kT} - 1 \right) - I_{ph} \qquad\qquad\qquad \text{I-1}$$

$$I_0 = Aqn_i^2 \left(\frac{D_e}{L_e N_A} + \frac{D_h}{L_h N_D} \right) \qquad\qquad\qquad \text{I-2}$$

Where: k_B is Boltzmann's constant, T is the absolute temperature, q is the electron charge, V is the voltage on the terminals of the cell, I_0 is the diode saturation current and I_{ph} is the photogenerated current. The diode saturation current is a reminder that a solar cell in the dark is simply a current rectifier semiconductor or diode.
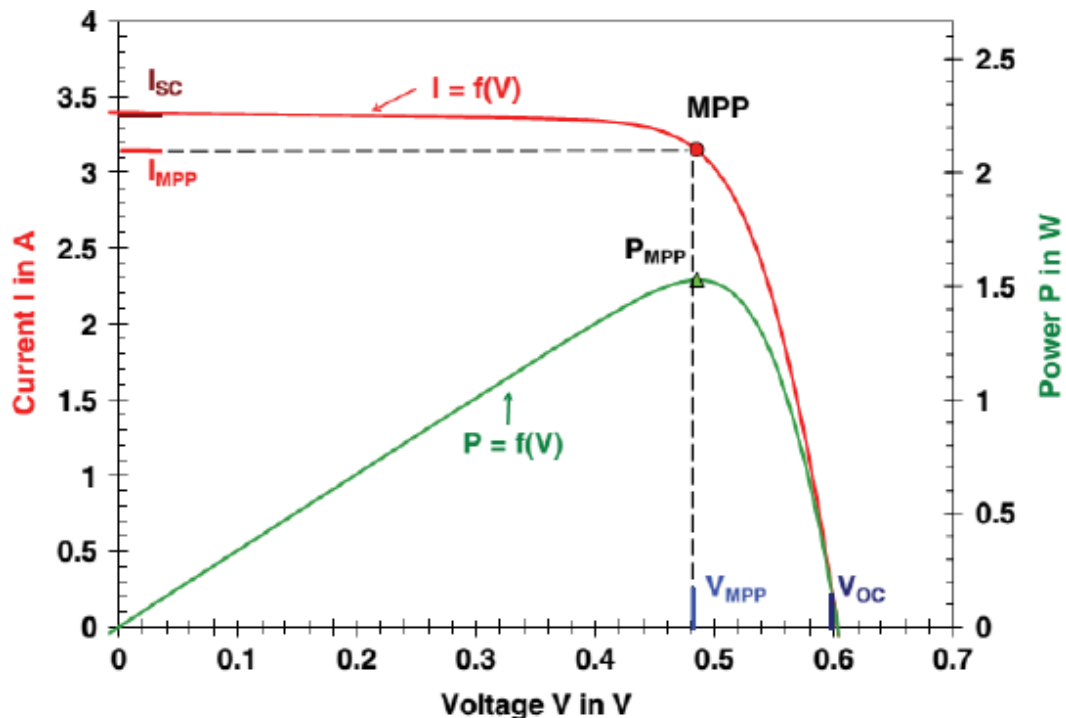
Figure I.4: I-V characteristics of the PV cell and its equivalent electric circuit[12].

I.5.1. Short circuit current I_{sc}

It is noticed that the curve under illumination is displaced concerning the first value of I_{sc} which explains the constant generation of current by light. This value is known as the short-circuit current, or it is the current that generates the cell under zero voltage under light.

I.5.2. Open circuit voltage in V_{oc}

This is the open-circuit voltage, the voltage of the cell under zero current. In the ideal case, the short circuit current I_{sc} is equal to the photogenerated current I_{ph}

$$V_{oc} = \left(\frac{kT}{q}\right)\left[\left(\frac{I_{ph}}{I_0}\right)+1\right] \qquad \text{I-3}$$

I.5.3. Fill factor FF

The fill (form) factor indicates the cell quality that it develops the maximum power P_{max} at a voltage V_m and a current I_m, and it is handy to define the fill factor FF by:

$$FF = \frac{I_m V_m}{I_{sc} V_{oc}} = \frac{P_m}{I_{sc} V_{oc}} \qquad \text{I-4}$$

I.5.4. Energy conversion efficiency η

The energy efficiency or the conversion efficiency is defined as the ratio between the maximum power produced by the cell and the incident power P_i of the solar radiation that arrives on the photovoltaic cell, which is normalized to 1000 W/m^2 for an AM1.5 spectrum.

$$\eta = \frac{P_m}{P_i} = \frac{FF.V_{oc}.I_{sc}}{P_i} \qquad \text{I-5}$$

I.6. Series and parallel (shunt) resistances R_S and R_{shunt}

The photovoltaic cell is not ideal in reality. The parameters that lead to resistance effects: edge leaks, recombination and contacts. Figure I.5 indicates the two resistors.

The series resistance (R_s) is an interpretation of the interface resistance of the front and rear contact. The short circuit resistance (R_{shunt}) is in parallel with the diode and the current generator. It reduces the short circuit through the cell. In general, by at least one order of magnitude, the value of R_{sh} is greater than that of R_s. Reduce R_s, and boost R_{sh} to reduce losses. The ideal case is R_{sh} equal to infinity, and R_s equal to zero [13].
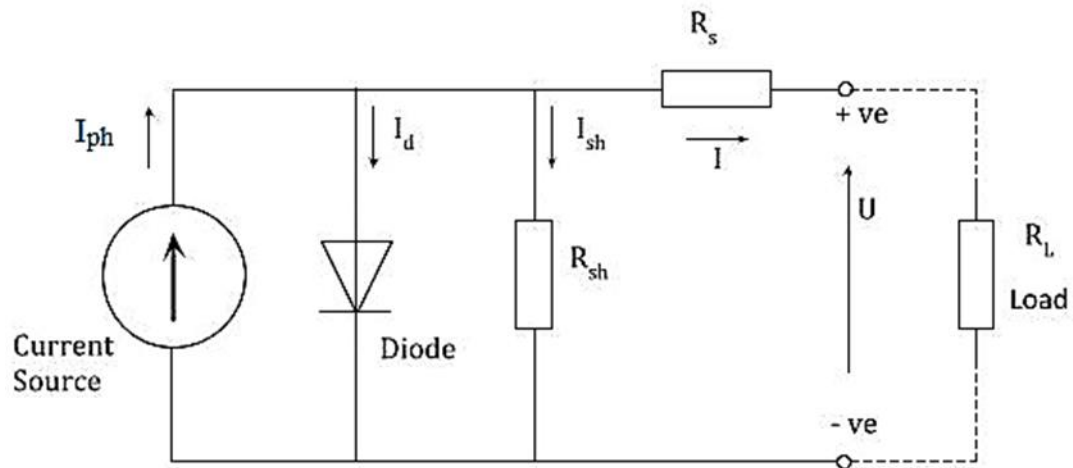
Figure I.5: Equivalent circuit of a photovoltaic cell.
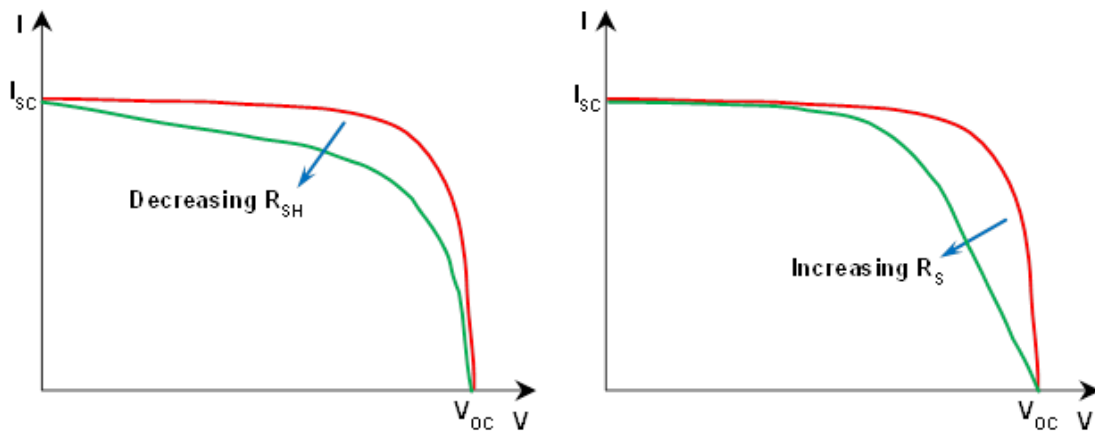
Figure I.6: The effect of the series resistance (a) and shunt resistance (b) on the I-V characteristic of the solar cell.

I.7. Photovoltaic cell technologies

I.7.1. First generation (silicon-based)

Solar cells are typically made of semiconductor materials, such as crystalline silicon; the explanation for the plentiful use of silicon in the solar cell industry is due to the materials large availability in nature and its fair price. Including silicon cells, the first generation of solar cells has evolved over 60 years as it has the longest production history, which includes up to 90% of all solar cells produced in 2008. Silicon is considered environmentally friendly and one of the most abundant commodities on Earth, accounting for 26 % of crustal materials [14, 15].

For current PV production, the mono-junction solar cells based on silicon wafers like monocrystal (c-Si) and multi-crystalline silicon (mc-Si) dominate. Mono-crystalline cells consist of a single large silicon wafer, as shown in Figure I.7. These types of mono-junction, silicon-wafer devices are now called first generation technology (1 G), these cells are highly effective, but they are very expensive due to the production process which requires a huge effort. Such crystals are grown in cylindrical ingots using the Czochralski process and therefore do not cover the entire region of a square solar cell, this method was developed in the late 1940s and early 1950s, forming p-n junctions by spreading high temperature vapor [16].
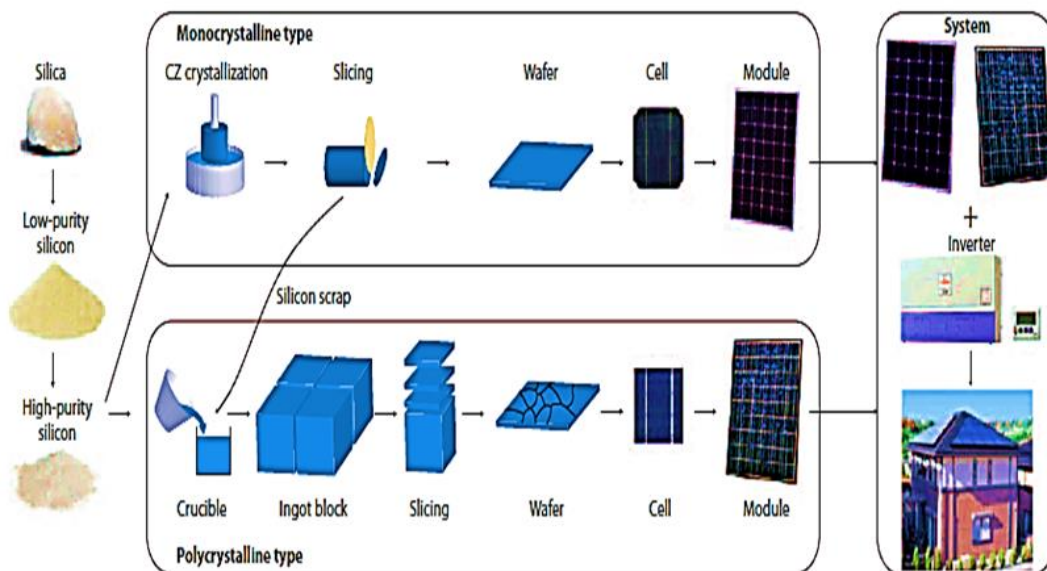
Figure I.7: Production process for typical commercial crystalline silicon solar cells [15].

This type of cell is the most commonly used and will remain a pioneer until the development of yet another more cost-effective technology. The amount of energy emitted

by photons decreases at high wavelengths so today's efforts are limited to improve performance. Furthermore, radiation with longer wavelengths contributes to thermal dissipation, which mostly causes the cell to heat up and thus lowers its efficiency. Silicon solar processing technology has a lot to do with the microelectronics industry and the advantages of significant developments in wafer processing technologies used in microelectronic applications are to increase the efficiency of laboratory cells, making this technology the most suitable [14].

The polycrystalline solar panels or multi-crystalline (mc-Si), and it differs from the monotype in the form in which the cells are compact squares, and their capacity is medium, contributing to the need for more of them to produce the same energy that is less costly than the mono type. The construction is less energy-consuming, but it is cheaper than monocrystalline growth. Its performance under bad lighting is poor.

I.7.2. Second generation (non-silicon- based, thin film)

Thin-film solar cells are thin films of semiconductor materials added to a substrate with solid support. Compared to silicon wafers, it is lower in the cost of production as it significantly decreases the number of semiconductor materials required for each cell. Amorphous silicon (a-Si), selenium-copper indium ($CuIn_xGa_{1-x}Se_2$ or CIGS), and cadmium telluride (CdTe) are among the materials commonly used for thin-film PV cells.[14, 17].

Thin-film cells are produced using sputtering techniques, depositing thin layers of some materials on glass or stainless steel substrates (SS). Indeed, this methodology is distinguished by the fact that the thickness of the depositing layers is barely a small micrometer thickness (less than 10 μm) compared to the multi-hundred micron thick crystalline wafers, in addition to the films placed on the SS sheet which allow flexible PV modules to be created. The resulting disadvantage decreased the production costs in addition to lower material costs due to the high production precipitation technique. Technically, the efficiency of thin-film solar modules is less than crystalline since it produces light materials that are less absorbable from much thinner layers for solar radiation, although the ability to deposit many different materials and alloys has allowed significant efficiencies to be improved [14].

The photovoltaic effect was first reported in material from gallium arsenide (GaAs) in 1954. In 1955, solar cell efficiencies for cadmium diffused GaAs wafers of 6.5 % and for small polycrystalline devices of 1 to 4 % were registered. A cell structure of the GaAlAs / GaAs is reported in 1971. A thin layer of GaAlAs, known as the "window", is deposited on a p-on-n GaAs cell and greatly decreases losses in surface recombination. The new design paved the way for the cell to increase its efficiency, reaching 16 % in sizes of 2 x 2 cm at AM0 in 1977. The research was sought to increase the efficiency of 0.25 cm cells above 23 % under AM1 lighting[16].

Amorphous silicon (a-Si), the non-crystalline form of silicon; distinct from the first-generation photovoltaic of crystalline silicon (a-Si) is a material whose behavior can be contrasted with the conduct of a direct gap material [18]. The structural arrangement of the atoms has no long-range arrangement in amorphous silicon. Chittick et al- was the first to deposit a-Si by a discharge of the radio frequency glow in silane in 1969 [19]. This can also be produced, much cheaper than polysilicon. Successively, in 1976, Carlson et al achieved high efficiency of 2.4 % [20]. The most advanced thin-film technology with 5 to 7 % cell efficiency and double and triple junction designs that promote it to 8-10 %[14]. Amorphous silicon types include amorphous silicon germanium (a-SiGe), amorphous silicon carbide (a-SiC), microcrystalline silicon (μc-Si), and amorphous silicon nitride (a- SiN) [14, 21].

Cadmium telluride (CdTe) is a photovoltaic element; it has a high coefficient of direct absorption for a 1.45eV solar absorber material and direct bandgap. A limited area of CdTe cells has given efficiency supremacy of 16%. CdTe is simpler to deposit and more appropriate for large-scale dissimilarity to the other thin-film technology, CdTe solar cells make use of only 1% of the semiconductor content used by bulk silicon cells; this is because of their effectiveness. But they have lower costs because of smaller amounts of materials used and simpler manufacturing methods and are typically much less effective than large quantities of silicon cells [14].

Although low-price sales of CdTe cells fell sharply; the increased demand for rare mineral tellurium pushed the price of this product sharply higher. Concerns about the risk of CdTe solar cells have been increased, as CdTe is a carcinogenic and toxic element. Such questions were answered by suggesting that one square meter of cadmium in the CdTe cell is less than that in the C-NiCd lamp battery and that CdTe is well lined with metal. [14].

For any thin-film cell, a combination of copper selenide (CIS) and copper indium gallium selenide (CIGS) demonstrated the highest efficiency where the junction consists of an asymmetric semiconductor bandgap, instead of a traditional junction consisting of p-type silicon and n-type silicon which have similar bandgap energies. The bandgap of semiconductors in CIGS cells can be adjusted by changing the ratio of indium to gallium, allowing the bandgap in the cell to continuously range from 1.0 volts to 1.7 volts, which corresponds well to the solar spectrum. In contrast to what some optical semiconductors need in a complex vacuum precipitation cycle, CIGS is also fairly easy material to produce [14].

CIS and CIGS are polycrystalline p-type semiconductors with direct-gap and high optical absorption, they are used in solar cells (heterojunctions) by positioning them with n-type layers (commonly CdS or ZnO), and the effective bandgap between 1.1 and 1.2 eV is the reason why CIS and CIGS are highly successful. These are also optical devices that contain elements of the group I, III, and VI semiconductors in the periodic table, giving them good optical and electrical properties[14].

I.7.3. Third generation (new emerging technology)

This category aims to reduce the costs of production by introducing new technologies (organic solar cells, Gratzel ...). It also needs to solve the current limitations of productivity by using original ideas such as multijunction cells, intermediate gap cells, or using hot carriers.

Organic semiconductors were set up by Alan J. Heeger, Alan G. MacDiarmid, and Hideki Shirakawa, in 1977 [22]. Organic solar cells and solar polymers are made from thin films (usually 100 nm) of organic semiconductors such as polymers and small-molecule compounds such as pentacene, multiphenylene, vinylene, copper phthalocyanine (a blue or green organic pigment). Phenyl-C61-butyric acid methyl ester (PCBM) between the different active layers of solar cell poly(3-hexylthiophene)(P3HT)[14, 23].

This material is of importance on account of its mechanical flexibility and the likelihood of disposal. Because they are largely made from traditional silicone-contrast plastics, the manufacturing process is efficient with limited technical challenges (not

requiring high temperature conditions or high vacuum) and also cost-effective (low-cost materials, high production industries); these are much thinner than cells made from silicone. Hence, it is less in weight and does not require a lot of manufacturing materials, which means that it is cheaper than silicon, and this is an essential advantage [14].

Such organic cells are extremely transparent and can be mixed with any color, giving them an aesthetic look that can be used in buildings. On the other hand, these cells have weak efficiency compared to silicon, and their shelf life is lower than that of silicon cells. Given what has been said about the defects of these cells, this technology can outperform silicon technology in very rapid growth, but it can fold down low-cost organic carbon-based solar cells. It can be turned into flat, foldable rolls, inserted around structures or in clothing, to be part of our surroundings to fit all tastes[14, 24].

To create an organic photovoltaic cell, molecular sensitizers (dye molecules) which are the absorbing material of sunlight are connected to the titanium surface with the anode (the first electrode), which is a thick film of titanium dioxide nanoparticles (about 100 nm) formed on the conducting side of a transparent glass covered with an electrolyte material such as fluorine-doped tin oxide. The electrolyte is in between the two electrode layers. The cathode (second electrode) is yet another transparent platinum-covered glass plate. This kind of color-sensitized solar cell is also known as the Grätzel Dye-Sensitized Solar Cells (DSSC), which has a short-length diffusion defect. Furthermore, super-molecular or multifunctional particle sensitizers were tested for increasing the carrier diffusion's lifetime. For instance, adding secondary electron donors varied the dye chromophore. Minority carriers (holes in this case) diffuse for recombination to the attached electron donors. Consequently, the recombination of the electron-hole is hindered by the physical separation between the moiety of dye-cation and the surface of TiO2. Lastly, this process increases the diffusion length of the carrier's which results in an increased carrier lifetime [12, 23].

Approximately the quantitative conversion of the incident photon into electric current occurs over a wide spectral range from the UV to the near IR region. The concept of working dye solar cells makes it possible to utilize them in light illumination conditions such as indoor or overcast sky, as their efficiency increases in the case of high temperature, whereas the semiconductor-based solar cells decrease their efficiency with increased temperature. The design of the coloring solar cells makes them better; they are able to dissipate internal heat, which assists to operate at lower temperatures. The key flaw in the pigment cells is that

their model employs electrolyte, which has problems with temperature change related to its stability. This liquid, can freeze at a low temperature which causes breakdowns in the cell. The leakage of the liquid allows it to spill out of the containment of the cell at high temperatures and this leads to a physical imbalance within the cell.
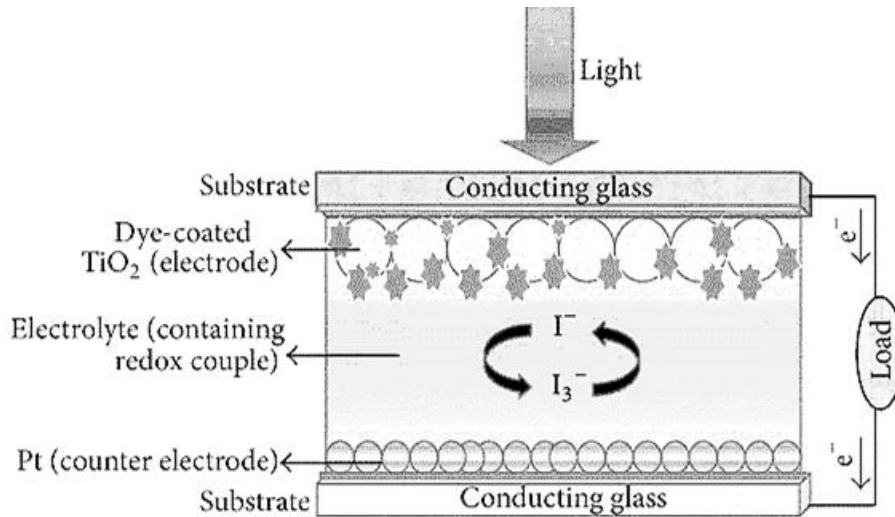
Figure I.8: Schematic representation of the components and of the basic operating principle of a DSSC [25].

The electrolyte is also an organic solvent, which must contain a well and must not cause it to leak out. Replacing the conductive liquid with a solid in this field is a big challenge and a lot of work is being done to solve this problem. Solid mineral salts have been used as an alternative to the electrolyte in recent studies, but with some problems linked to the short life of these cells, particularly when working continuously [12, 22].

I.8. Photovoltaic solar cell based on CZTS

From a technical point of view, commercially accessible thin film solar cells suffer from low efficiencies, such as a-Si, raw material shortages such as Te in the case of CdTe, and In in the case of CIGS technology, or toxicity of materials such as Cd in CdTe technology [26]. For this reason, researchers have attempted to find some alternative solutions, and they prepared the solar cells based on $CZTS(Cu_2^I Zn^{II} Sn^{IV} S_4^{VI})$.

Naturally, CZTS semiconductors are non-toxic and plentiful, with a direct bandgap of about 1.5 V and an absorption coefficient above 10^4 cm^{-1} [27]. In 1988, Ito and Nakazawa stated for the first time that the photovoltaic effect was observed in CZTS heterojunction by

atom beam sputtering, which consists of a transparent conductive film cadmium-tin-oxide and CZTS [28]. The conversion efficiency for CZTS thin-film solar cells of 0.66 % was achieved in 1996 [29]. Katagiri and co-workers developed a new type of thin-film solar cell used vapor-phase sulfurization of E-B (electron beam) from evaporated precursors in 1997 [29]. They presented a 4.53 % conversion efficiency for CZTS-based solar cells in 2005 [30].

Additionally, the conversion efficiency in laboratories has been enhanced over the years, Dhakal and co-workers obtained an efficiency of 6.2 %for CZTS/CdS solar cell devices produced using co-sputtering supported by H_2S annealing [31], through optimizing the experimental conditions including target composition, Katagiri and co-workers obtained an efficiency of 6.89 percent [32]. An efficiency of 8.76% is accomplished by Liu and co-workers [33].

I.8.1. Solar cell structures

The structure of the CZTS based solar cell is shown in Figure I.9 which consists of
- A back metal electrode made of molybdenum deposited on a glass substrate.
- CZTS absorber layer whose thickness varies from 1 to 3 μm.
- A buffer layer (CdS, ZnO and ZnS) with a thickness between 10 and 100 nm each, guaranteeing the junction and absence of short circuits respectively.
- An optical window of aluminum-doped ZnO (ZnO: Al) that must combine two significant properties: electrical conductivity and optical transparency (TCO);
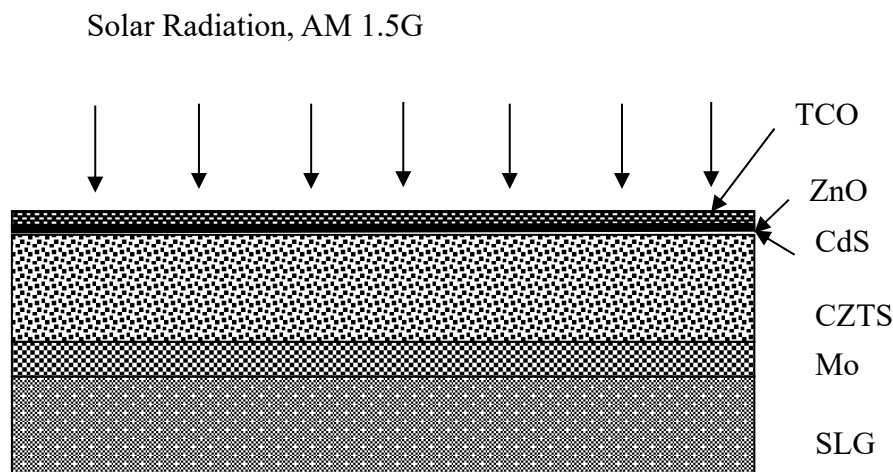
Figure I.9: A schematic representation of the CZTS solar cell.

a. Absorber layer

Due to the low cost and appropriate photovoltaic properties of the materials, copper-zinc-tin-chalcogenide Cu_2ZnSnS_4 (CZTS) has become an essential candidate for use as an absorber layer in solar cells.

b. Buffer layer

The buffer layer is positioned between the optical window and the absorber layer. When communication is directly realized (absorber layer / optical window), there could be a photovoltaic junction. On the other hand, due to the presence of disordered areas at grain joints, its performance is limited by the inadequacy of the bandgap and leakage currents. It is therefore preferable to insert a thin layer, called a buffer layer, between these two compounds to optimize cell performance such as In_2S_3, ZnS, and CdS [13]. The n-type conductivity of the buffer layer forms a junction with the absorber layer. In fact, its conductivity must be lower than that of the absorber layer to avoid the consequences of current leakage. An intermediate bandgap allowing a "flexible" transition between the absorber and the optical window with a value of 2.4 to 3.2 eV.

c. Optical window

Thin films of transparent conducting oxides (TCO) with high electrical conductivity and optical transparency are widely used, as they have produced many industrial and technical applications. Usually, n-type TCO materials such as ZnO, In_2O_3, SnO_2, and CdO are structured using different deposition methods, In_2O_3: Sn (ITO), SnO_2: F (FTO), ZnO: Al (AZO) thin films are the best n-type TCO materials. Their transparency is related to their gap value while their electrical properties depend on the layer composition and possible doping [34].

I.8.2. Crystal Structure

The binary semiconductors II-VI follow a cubic zincblende (Or hexagonal wurtzite) structure where two interpenetration fcc of group II and VI networks atoms have tetrahedral coordination. The ternary I–III–VI$_2$ compounds by mutating the group II atoms into group I and group III pairs. This progression incorporates the possibility of ordering the cation: the

smallest energy structures are those where the group I and group III atoms are arranged in (201) (chalcopyrite structure "CH") and (001) (Cu-Au structure"(CA)-like") planes. These structures are preferred because they satisfy the local charging neutrality requirement. Each anion is coordinated by two group I and two group III cations (Shown Figure 1.10) [35, 36].

One way to develop novel materials is by adopting the principle of mutation to further segment the ternary I – III – VI$_2$ structures into quaternary compounds (see Figure 1.10). There are two methods of this cation mutation:

1) Replacing two group III atoms with one group II and one group IV atom, creating a compound I$_2$–II–IV–VI$_4$;

2) Replacing one group I atom and one group III with two group II atoms, creating a compound I–III–II$_2$–VI$_4$. Similar tetrahedral crystal structures are holding for the quaternary compounds to their parent materials.
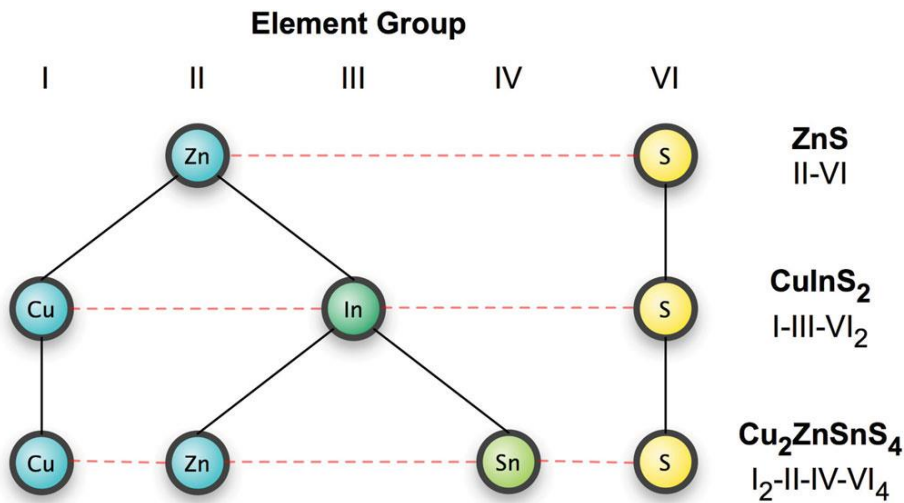
Figure I.10: Relationship between binary, ternary, and quaternary semiconductors to produce Cu$_2$ZnSnS$_4$, starting from a II–VI parent compound.

Figure I.11 shows the structural transition from binary to quaternary semiconductors. There is a possibility of cation arranging, with the complexity of the problem increasing to three quaternary material lattice locations, e.g. Cu, Zn, and Sn in CZTS. The ordering of the I$_2$–II sublattice: kesterite derives from the ordering of chalcopyrite (201) and stannite derives from the ordering of Cu-Au (001), as indicated in Figure I.10 a third form of order can be

extracted from the structure of CuAu, the primitive-mixed CuAu structure (PMCA) [35, 36].

Moreover, $Cu_2(MII)(MIV)(S, Se)4$ (MII= Mn, Fe, Co, Ni, Zn, Cd, Hg; MIV = Si, Ge, Sn) are Chalcogenide compounds that have been significant for many years due to their suitable direct band gaps and also appearance as naturally occurring minerals for use in solar cells and other optical devices. Cu_2ZnSnS_4 crystallizes in the kesterite structure and stannite that are observed for the closely related minerals; Cu_2FeSnS_4 (CFTS); Comparable to ZnS or ZnO, all cations and anions are placed in a tetrahedral bonding system, with a zinc-blend-like stacking (face-centered cube); the different structural changes are related to a different order in the cation sublattice [37, 38].

One way to test these structures is by starting from the $CuM_{III}(S, Se)_2$ ternary chalcopyrite structure and replacing the trivalent M_{III} ions with an equal number of divalent M_{II} and tetravalent M_{IV} metals. When M_{II} and M_{IV} atoms alternate on the $z = 0$ and $1/2$ planes and only Cu exists on the $z = 1/4$ and $3/4$ planes, this is known as the stannite structure, while Cu and M_{IV} atoms (CuSn) alternate on the $z = 0$ and $1/2$ planes (z =fractional coordinates along the long c-axis of the structure) and Cu and M_{II} atoms (CuZn) alternate on the $z = 1/4$ and $3/4$ planes. While the kesterite structure has the same basic Cu/S structure as chalcopyrite, some reorganization of the Cu sublattice is required in the stannite structure [37].
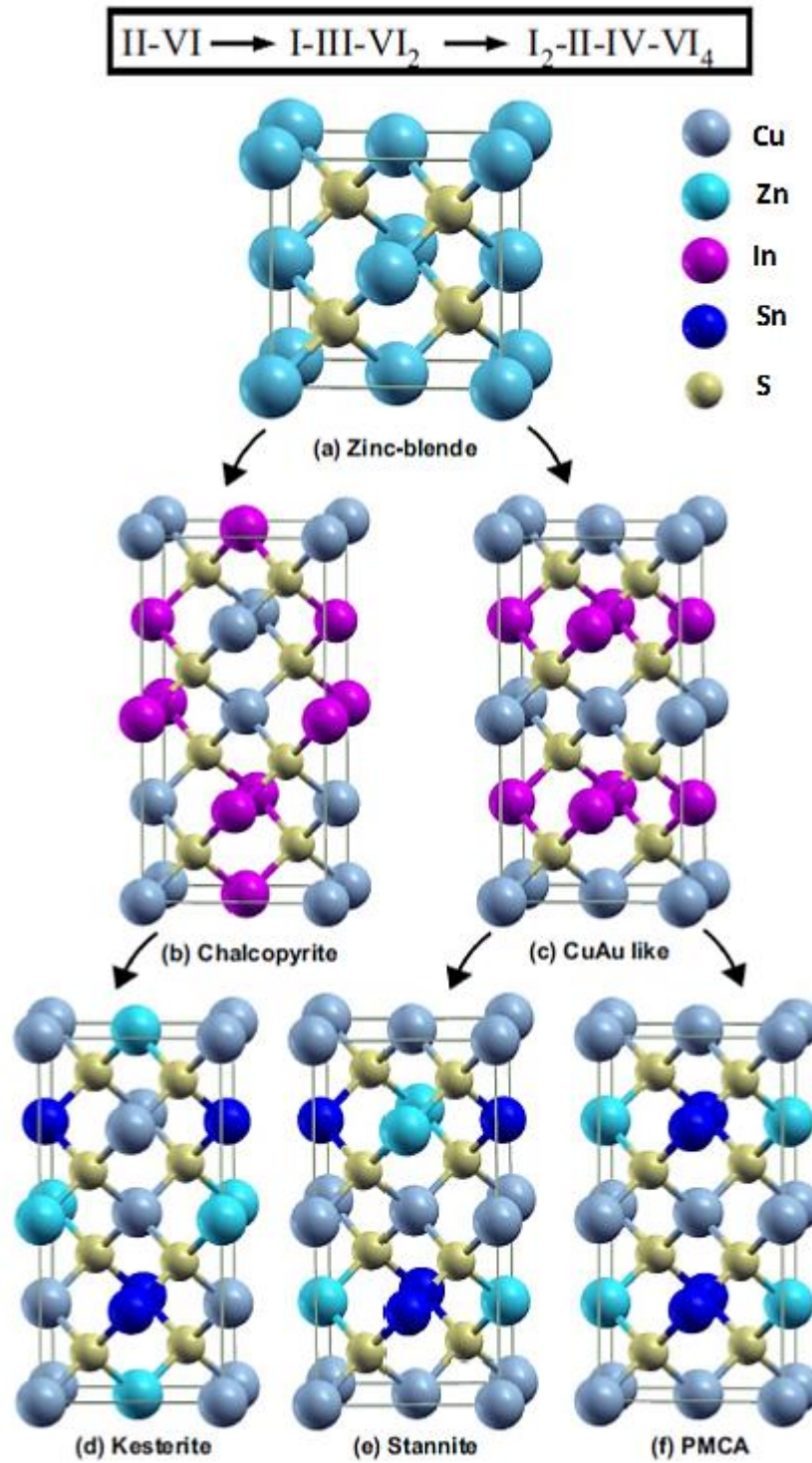
Figure I.11: Crystal structure representations of zinc-blende ZnS; (201) ordered chalcopyrite $CuInS_2$; (001) ordered CuAu-like $CuInS_2$; kesteriteCu_2ZnSnS_4; stannite Cu_2ZnSnS_4, and mixed-CuAu Cu_2ZnSn_4[39].

I.8.3. Affinity

The electron affinity χ is known as the energy needed to remove an electron from the semiconductor surface to the vacuum level, or it is the energy difference between the vacuum level (E_{vac} free electron energy) and the bottom of the conduction bands (E_{CBM} minimum conduction band) [11, 40] as shown in Figure I.12.

$$\chi = E_{vac} - E_{CBM} \qquad \text{I-6}$$
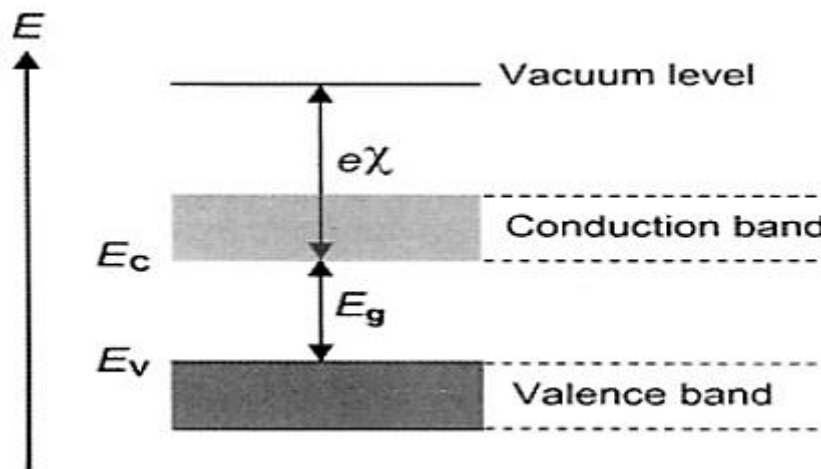
Figure I.12: Schematic illustration of the electron affinity (χ) [11].

I.8.4. Band structure (the conduction band Offset CBO)

Anderson suggested that the difference in electron affinities may account for the offset of the conduction band (the barrier energy for an electron)

$$\Delta E_c = E_{c1} - E_{c2} = \chi_1 - \chi_2 \qquad \text{I-7}$$

Then, the buffer layer plays an important role in the performance of solar cells, since a (spike-like or type I) structure in the band alignment($E_{c,buffer} > E_{c,absorber}$) when the CBO is positive, whereas a (cliff-like or type II) structure ($E_{c,buffer} < E_{c,absorber}$) when the CBO is negative [41, 42].

I.9. Crystal defects

The atoms are regularly arranged without defects in ideal crystals, but in fact, there is no ideal crystal free of defects. Where the defect is present, any difference in the consistency of the crystal network's systemic composition of the atoms is. Also, defects play an important role in solid state physics, as they greatly affect physical properties namely: electrical conductivity, thermal conductivity, and the optical and mechanical properties of solid materials. There are several types of defects.

I.9.1. Point defects

A point defect in the position of an atom or the location of a few adjacent atoms is known as a deviation or anomaly. This defect is called a point defect and the reason for this is that it occurs in a very small area compared to the size of the crystal (0-dimensional defects), and it is classified as a point defect because of the presence of additional voids or atoms within the crystal structure:

a. Vacancies (intrinsic point defect)

A vacancy implies a crystalline pattern in space. This space typically occurs when one or more atoms (or ions) of one or more of the original atoms (Self-atoms) are lost or displaced from their normal lattice site to another position in a crystal, leaving a vacant lattice site. More present at elevated temperatures. These are particularly common in high temperatures when atoms change their positions regularly and randomly, leaving empty lattices behind [11].

b. Self-interstitial (intrinsic point defect)

This type of defect can be regarded as a type of inverse vacancy that transfers an atom from the crystal surface to its interior (an atom may exist in the crystal structure between the lattice sites). However, due to the lack of an unoccupied lattice site location, the excess corn must be "pressed" into an interstitial site within the crystal structure [11].

c. Substitution impurity (extrinsic point defect)

It is a foreign atom, an atom of a different nature than the original atom, being in the lattice occupying the place of the original atom. Alternative atoms with impurities typically similar to the size of the original atom[11, 43].

d. Interstitial impurity (extrinsic point defect)

In this case, the size of the foreign atoms is smaller than the host atoms, as they are situated in the interstitial space between the atoms in the lattice structure [43].
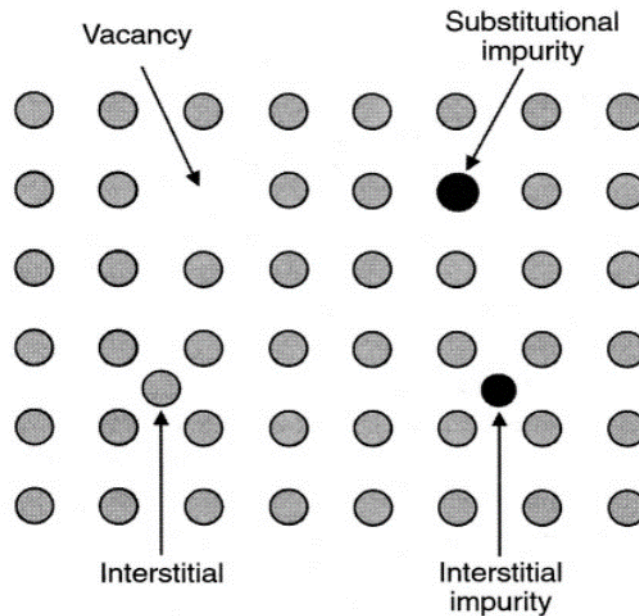
Figure I.13: Schematic for vacancy and self-interstitial defects, for Substitution and Interstitial defects.

In the case of moving atoms, they can migrate in successive stages to eventually settle at the surface of the crystal, causing the expansion of the crystal. It refers to the existence of holes in the crystal without the presence of additional initial atoms that lead to those holes. Such a defect is considered a Schottky defect [11].

If the atom travels from its normal web site to interstitial locations, the defect would contain a void and an additional initial atom; this defect resulting from an initial interstitial distance and atom is called the Frenkel defect [11].
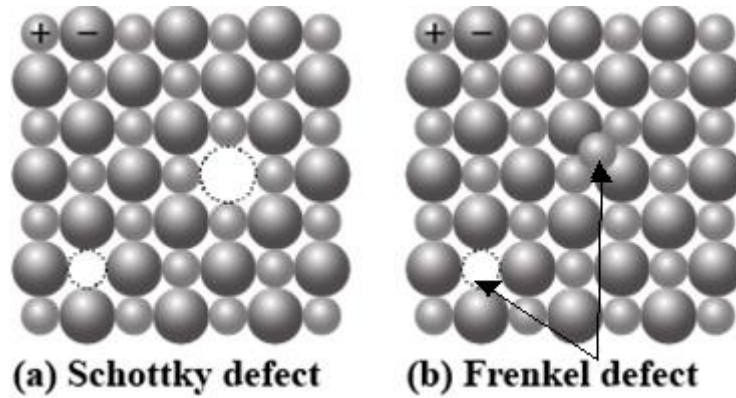
Figure I.14: Schematic for Frenkel and Schottky defects.

I.9.2. Line defect

Line defect is also known as dislocation. The dislocation is a major source of irregularity in the crystal, and as a result of a type of stress on the crystal a region can slide onto another region, and the line separating the two regions is called the line of dislocation. There are two ideal disorders forms, the edge, and the screw. The dislocation of the edges is amongst these the simplest form of dislocation [43, 44].

a. Edge dislocation

A dislocation in a crystal lattice may result from the introduction of an additional level of atoms that ends at the dislocation line, the difference of uniformity of atoms row along a straight edge in the crystal structure. The optimal offset of the edges can be considered the result of insertion along with one of the crystalline directions, from "half-level" foreign atoms in an unblemished crystal network. By definition, the edge of the inserted hemisphere corresponds to the dissociation line or axis. The crystal lattice is disrupted near the dislocation; however, out of dislocation, the crystal lattice remains relatively "perfect". It can be described as half of a row of the outer atoms of an ideal crystal that distinguishes the edge boundaries of a portion of an atomic layer and then shifts the levels near it to fill the void. This dislocation line is with greater energy in contrast to the crystal parts because the network above the dislocation line is in a compressed state while below the dislocation line is in a tensile state in which a strong interstitial vacuum may occur, and the dislocation line acts as a property of the atoms collection and chemical impurities[43, 44].

b. Screw dislocation

To obtain a pure spiral dislocation, a strange level of atoms is not required; however, the atomic planes inside the network turn into an arrangement similar to a "spiral staircase". Once again, the corresponding imbalance of the crystal structure near the dislocation axis leads to a local increase in the crystal stress energy. It is produced by a successive transfer of atomic levels in a spiral or spiral shape around the emission line and may be accompanied by some tensile and compression stresses that affect the solid materials' mechanical and physical properties. The process of displacing one part of the crystal lattice relative to another part in a spiral shape, the following figure shows the removal of the edges and screws[43, 44].
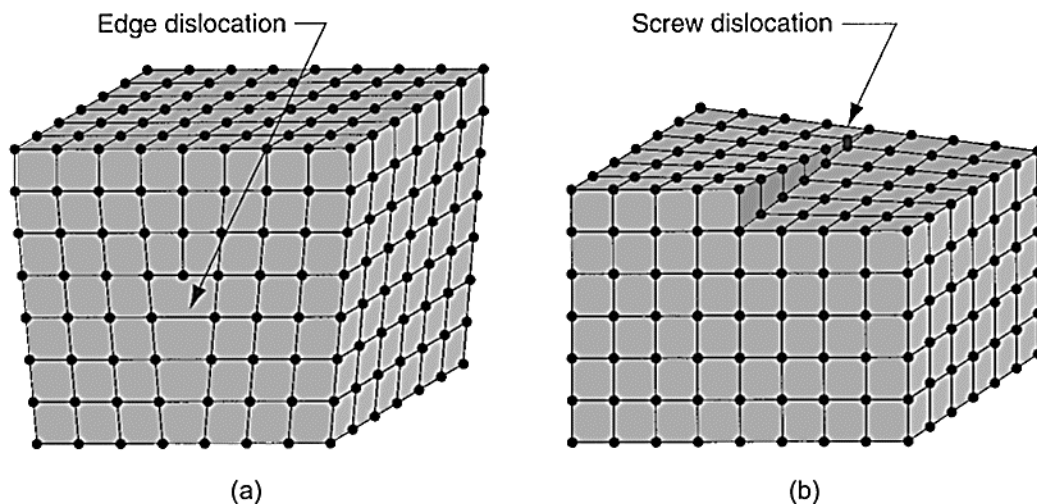
Figure I.15: (a) edge dislocation; (b) screw dislocation.

I.9.3. Planer defects (Surface defects)

These defects are named after this name because they arise from the accumulation of many linear defects, which constitutes a surface of defects. This type has a full crystalline where the defects extend in two dimensions, and the crystal surface itself is a defect because the patrol of the network is flawed on the surface and this is shown through the study of thin film and divided into external surfaces, grain boundaries, twins, etc.[11, 43].

a. Grain boundaries

That some solid materials do not consist of a crystalline structure from one crystal, but rather from many small-sized crystals that are called grains in which each granule inside the structure of the solid material differs in terms of its direction, size, shape, and distance from its neighbor. Therefore, it must be separated from each other by separating boundaries called grains boundaries. The grain boundaries impede the movement of free electrons, thereby creating additional resistance to metallic materials, as the electrical conductivity in them decreases; this type of defect occurs during the hardening of molten metal's.
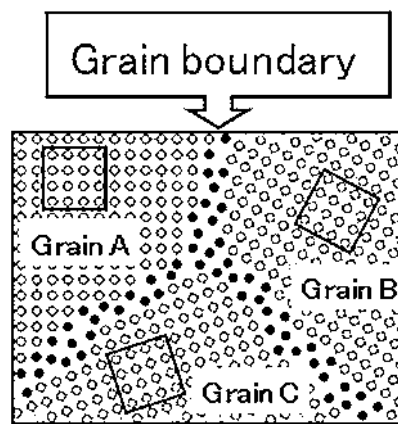
Figure I.16: Schematic of the grain boundary.

b. Twins boundaries

Twins are common superficial defects that occur as a result of the lack of continuity of the network patrol, and the twins' formation process is a pattern of malformation of the skin and during the twinning process, a small displacement occurs between many adjacent levels which the crystal's distorted part has a mirror similar to the non-deformed part. Twinning is of two types depending on the way it is formed, it is called developing twins if formed in a crystalline growth method, and it is called deformed twins if formed in a mechanical distortion method such as knocking and pressing.

c. Packing defects (stacking fault)

Assuming that the crystal is stacks of levels consisting of atoms on top of each other, one of the levels was joking about the adjacent level with an offset that is not equal to a

vector in the crystalline grille which consists of a defect in the composition called a stacking error. These errors occur in compact crystals such as the concentrated cubic crystal. The stacking in this crystal has multiple patterns, as stacking on ABCABC or stacking on the ABAB body as shown in the form when the ABABC arrangement is produced, for instance, instead of the ABCABC arrangement, we say that there was an error in stacking.

I.9.4. Volume defect

A volume defect is any volume within a semiconductor that differs in composition, structure, and/or orientation of the rest of the crystal. Volume defects are formed from vacancy clusters that can expand to form dislocation loops and ultimately collapse. Some impurities may precipitate into a separate process, and large, three-dimensional aggregates may also form impurity atoms and vacancies[11].

I.10. CZTS defect

CZTS normally comprises a high concentration of neutral and charged point defects. These defects include the vacancies (V_{Cu}, V_{Zn}, V_S), antisites (Cu_{Zn}, Zn_{Sn}, Zn_{Cu}), and interstitials (Cu_i, Zn_i) in their unionized state and complexes. These defects and defect-complexes form shallow donor levels, shallow acceptor levels, mid-gap states, and deep trap states within the bandgap of CZTS absorbing material. The defect-complexes are self-compensated defects that form because of the presence of donor and acceptor vacancies, interstitials, and antisites in CZTS. These defect complexes include ($Cu_{Zn}+Zn_{Cu}$), ($Sn_{Zn}+Zn_{Sn}$), ($Cu_{Sn}+Sn_{Cu}$), ($V_{Cu}+Zn_{Cu}$), ($V_{Zn}+Sn_{Zn}$), ($Zn_{Sn}+2Zn_{Cu}$).They are created because their formation energy is lower than the formation energy of individual antisite defects[45, 46].

The concentration of point defects in materials in equilibrium is determined by their formation energy, which depends on the atomic thermodynamic chemical potential (growth conditions) as well as electron chemical potential (Fermi energy) for charged defects[35].

Each anion in kesterite CZTS (CZTSe) is tetrahedrally coordinated by four cations (in nominal valence two Cu+1, one Zn in +2, and one Sn in +4). An acceptor level is created above the maximum valence band (VBM)when Cu replaces Zn (Cu_{Zn} antisite), and two electrons occupy a donor level below the minimum conduction band (CBM) b when Sn

replaces Zn(Sn_{Zn} antisite), Since Sn_{Zn} is a double donor defect, (Cu_{Zn}+ Sn_{Zn})there's only one donor electron can compensate for another Cu_{Zn} acceptor forming the $2Cu_{Zn}+Sn_{Zn}$ tri-cluster[47].The measured energy-transition levels for all intrinsic defects are shown in

Table I-1: Possible defects and defect-complexes in CZTS[45]

	Details of defects	**Ionization levels (Donor/Acceptor)**
vacancies	Copper vacancy (V_{Cu})	One, Acceptor
	Zinc vacancy (V_{Zn})	Two, Acceptor
	Tin vacancy (V_{Sn})	Four, Acceptor
	Sulfur/Selenium vacancy (V_S/V_{Se})	One/One, Donor/Donor
Antisites	Copper-on-Zinc antisite (Cu_{Zn})	One, Acceptor
	Zinc-on-Copper antisite (Zn_{Cu})	One, Donor
	Copper-on-Tin antisite (Cu_{Sn})	Three, Acceptor
	Tin-on-Copper antisite (Sn_{Cu})	Two, Donor
	Zinc-on-Tin antisite (Zn_{Sn})	Two, Acceptor
	Tin-on-Zinc antisite (Sn_{Zn})	Two, Donor
Interstitials	Copper interstitial (Cu_i)	One, Donor
	Zinc interstitial (Zn_i)	Two, Donor
Defect complexes	Stoichiometric-conserving defect complex($Cu_{Zn}+Zn_{Cu}$), ($Cu_{Sn}+Sn_{Cu}$),($Zn_{Sn}+Sn_{Zn}$)	($Cu_{Zn}+Zn_{Cu}$): ~0.2 eV formationenergy, for other two >0.2 eV
	Non-stoichiometric-conserving defect complex($V_{Cu}+Zn_{Cu}$), ($V_{Zn}+Sn_{Zn}$),($Zn_{Sn}+2Zn_{Cu}$)	Formation energy ~0.3-0.6 eV

REFERENCES

[1]   F. Lévy, *Physique et technologie des semiconducteurs* vol. 18: PPUR presses polytechniques, 1995.

[2]   R. L. Boylestad, L. Nashelsky, and L. Li, *Electronic devices and circuit theory* vol. 11: Prentice Hall Englewood Cliffs, NJ, 2002.

[3]   C. A. Gueymard, "The sun's total and spectral irradiance for solar energy applications and solar radiation models," *Solar Energy,* vol. 76, pp. 423-453, 2004.

[4]   R. C. Willson and H. S. Hudson, "Solar luminosity variations in solar cycle 21," *Nature,* vol. 332, p. 810, 1988.

[5]   (2019). *2000 ASTM Standard Extraterrestrial Spectrum Reference E-490-00 | Grid Modernization | NREL.* Available: https://www.nrel.gov/grid/solar-resource/spectra-astm-e490.html

[6]   S. Wenham, M. Green, M. Watt, and R. Corkish, *Applied photovoltaics, second edition*, 2013.

[7]   A. E. Becquerel, "Recherches sur les effets de la radiation chimique de la lumiere solaire au moyen des courants electriques," *Comptes Rendus de L´Academie des Sciences,* vol. 9, 1839.

[8]   E. Leonard, "Cellules solaires à base de couche mince de $Cu(In,Ga)Se_2$ submicrométrique : optimisation des performances par ingénierie optique et électronique," PhD thesis, Université NANTES, 2013.

[9]   C. A. Figueiredo Ramos, A. Alcaso, and A. J. M. Cardoso, "Photovoltaic-thermal (PVT) technology: Review and case study," *IOP Conference Series: Earth and Environmental Science,* vol. 354, p. 012048, 2019.

[10]   H. Mathieu and H. Fanet, *Physique des semiconducteurs et des composants électriques: cours et exercices corrigés*: Dunod, 2009.

[11]   B. G. Yacobi, *Semiconductor materials: an introduction to basic principles*: Springer Science & Business Media, 2003.

[12]   A. Al-Khazzar and E. Hashim, *Temperature Effect on Power Drop of Different Photovoltaic Modules*, 2015.

[13]   A. McEvoy, T. Markvart, L. Castañer, T. Markvart, and L. Castaner, *Practical handbook of photovoltaics: fundamentals and applications*: Elsevier, 2003.

[14]   C. Tong, "Materials-Based Solutions to Advanced Energy Systems," in *Introduction to Materials for Advanced Energy Systems*, ed: Springer, 2019, pp. 1-86.

[15]   T. Saga, "Advances in crystalline silicon solar cell technology for industrial mass production," *npg asia materials,* vol. 2, p. 96, 2010.

[16]   H. S. Rauschenbach, *Solar cell array design handbook: the principles and technology of photovoltaic energy conversion*: Springer Science & Business Media, 2012.

[17]   H. Flammersberger, *Experimental study of Cu2ZnSnS4 thin films for solar cells*, 2010.

[18]   V. Foncrose, "Nanocristaux, films et cellules photovoltaïques de Cu2ZnSn (SSe) 4 par impression d'encres," Université de Toulouse, Université Toulouse III-Paul Sabatier, 2015.

[19]   R. Chittick, J. Alexander, and H. Sterling, "The preparation and properties of amorphous silicon," *Journal of the Electrochemical Society,* vol. 116, pp. 77-81, 1969.

[20]   D. E. Carlson and C. R. Wronski, "Amorphous silicon solar cell," *Applied Physics Letters,* vol. 28, pp. 671-673, 1976.

[21]   B. Parida, S. Iniyan, and R. Goic, "A review of solar photovoltaic technologies," *Renewable and sustainable energy reviews,* vol. 15, pp. 1625-1636, 2011.

[22]   H. Shirakawa, E. J. Louis, A. G. MacDiarmid, C. K. Chiang, and A. J. Heeger, "Synthesis of electrically conducting organic polymers: halogen derivatives of polyacetylene,(CH) x," *Journal of the Chemical Society, Chemical Communications,* pp. 578-580, 1977.

[23]   T. Kuwabara, T. Nakayama, K. Uozumi, T. Yamaguchi, and K. Takahashi, "Highly durable inverted-type organic solar cell using amorphous titanium oxide as electron collection electrode inserted between ITO and organic layer," *Solar Energy Materials and Solar Cells,* vol. 92, pp. 1476-1482, 2008.

[24]   M. Grätzel, "Dye-sensitized solar cells," *Journal of Photochemistry and Photobiology C: Photochemistry Reviews,* vol. 4, pp. 145-153, 2003.

[25]   R. Kushwaha, P. Srivastava, and L. Bahadur, "Natural Pigments from Plants Used as Sensitizers for TiO2 Based Dye-Sensitized Solar Cells," *Journal of Energy,* vol. 2013, pp. 1-8, 2013.

[26]   G. Altamura, "Development of CZTSSe thin films based solar cells," Université Joseph-Fourier-Grenoble I, 2014.

[27]   S. Guitouni and N. Attaf, "Elaboration et étude de structures à base de couches minces de ZnO et de chalcogénures (CIS, CZTS) pour des applications photovoltaïques," جامعة الإخوة منتوري قسنطينة, 2016.

[28]   K. Ito and T. Nakazawa, "Electrical and optical properties of stannite-type quaternary semiconductor thin films," *Japanese Journal of Applied Physics,* vol. 27, p. 2094, 1988.

[29]   H. Katagiri, N. Sasaguchi, S. Hando, S. Hoshino, J. Ohashi, and T. Yokota, "Preparation and evaluation of Cu2ZnSnS4 thin films by sulfurization of E-B evaporated precursors," *Solar Energy Materials and Solar Cells,* vol. 49, pp. 407-414, 1997.

[30]   H. Katagiri, "Cu2ZnSnS4 thin film solar cells," *Thin Solid Films,* vol. 480, pp. 426-432, 2005.

[31]   T. P. Dhakal, C. Y. Peng, R. R. Tobias, R. Dasharathy, and C. R. Westgate, "Characterization of a CZTS thin film solar cell grown by sputtering method," *Solar Energy,* vol. 100, pp. 23-30, 2014.

[32]   H. Katagiri and K. Jimbo, "Fabrication of earth-abundant CZTS thin film solar cells," in *2016 23rd International Workshop on Active-Matrix Flatpanel Displays and Devices (AM-FPD)*, 2016, pp. 54-55.

[33]   F. Liu, C. Yan, J. Huang, K. Sun, F. Zhou, J. A. Stride, M. A. Green, and X. Hao, "Nanoscale microstructure and chemistry of Cu2ZnSnS4/CdS interface in kesterite Cu2ZnSnS4 solar cells," *Advanced Energy Materials,* vol. 6, p. 1600706, 2016.

[34]   M.-M. Bagheri-Mohagheghi and M. Shokooh-Saremi, "The influence of Al doping on the electrical, optical and structural properties of SnO2 transparent conducting films deposited by the spray pyrolysis technique," *Journal of Physics D: Applied Physics,* vol. 37, p. 1248, 2004.

[35]   A. Walsh, S. Chen, S. H. Wei, and X. G. Gong, "Kesterite thin-film solar cells: Advances in materials modelling of Cu2ZnSnS4," *Advanced Energy Materials,* vol. 2, pp. 400-409, 2012.

[36]   S. Chen, X. G. Gong, A. Walsh, and S.-H. Wei, "Crystal and electronic band structure of Cu2ZnSnX4 (X=S and Se) photovoltaic absorbers: First-principles insights," *Applied Physics Letters,* vol. 94, p. 041903, 2009.

[37]   D. B. Mitzi, O. Gunawan, T. K. Todorov, K. Wang, and S. Guha, "The path towards a high-performance solution-processed kesterite solar cell," *Solar Energy Materials and Solar Cells,* vol. 95, pp. 1421-1436, 2011.

[38]   J. Paier, R. Asahi, A. Nagoya, and G. Kresse, "Cu2ZnSnS4as a potential photovoltaic material: A hybrid Hartree-Fock density functional theory study," *Physical Review B,* vol. 79, 2009.

[39]   S. Chen, X. Gong, A. Walsh, and S.-H. Wei, "Crystal and electronic band structure of Cu2ZnSnX4 (X= S and Se) photovoltaic absorbers: First-principles insights," *Applied Physics Letters,* vol. 94, 2009.

[40]   F. Maier, J. Ristein, and L. Ley, "Electron affinity of plasma-hydrogenated and chemically oxidized diamond (100) surfaces," *Physical Review B,* vol. 64, p. 165411, 2001.

[41]   D. V. Morgan and R. H. Williams, *Physics and technology of heterojunction devices*: IET, 1991.

[42]   J. Li, M. Wei, Q. Du, W. Liu, G. Jiang, and C. Zhu, "The band alignment at CdS/Cu2ZnSnSe4heterojunction interface," *Surface and Interface Analysis,* vol. 45, pp. 682-684, 2013.

[43]   R. Phillips and P. Rob, *Crystals, defects and microstructures: modeling across scales*: Cambridge University Press, 2001.

[44]   Z. Zhuang, Z. Liu, and Y. Cui, "Chapter 4 - Dislocation-Based Single-Crystal Plasticity Model," in *Dislocation Mechanism-Based Crystal Plasticity*, Z. Zhuang, Z. Liu, and Y. Cui, Eds., ed: Academic Press, 2019, pp. 91-119.

[45]   M. Kumar, A. Dubey, N. Adhikari, S. Venkatesan, and Q. Qiao, "Strategic review of secondary phases, defects and defect-complexes in kesterite CZTS–Se solar cells," *Energy & Environmental Science,* vol. 8, pp. 3134-3159, 2015.

[46]   S. Meher, L. Balakrishnan, and Z. Alex, "Analysis of Cu 2 ZnSnS 4/CdS based photovoltaic cell: a numerical simulation approach," *Superlattices and Microstructures,* vol. 100, pp. 703-722, 2016.

[47]   S. Chen, L.-W. Wang, A. Walsh, X. Gong, and S.-H. Wei, "Abundance of Cu Zn+ Sn Zn and 2Cu Zn+ Sn Zn defect clusters in kesterite solar cells," *Applied Physics Letters,* vol. 101, p. 223901, 2012.

CHAPTER II

NUMERICAL

SIMULATION BY

SCAPS

Chapter II.   Numerical Simulation by SCAPS

II.1. Introduction

The performance solar cells were studied by numerical simulation for approximately 40 years [1]. In 1975, Jerry developed a method for discussing the carrier transport problem of silicon solar cells by solving Poisson's equation and continuity equations for electrons and holes [2, 3]. There are many software programs used recently for this purpose such as SCAPS-1D, PC1D and AMPS-1D[3]. Many researchers also studied and analyzed dye sensitized solar cells (DSCS) [4-6].

In this thesis, we have used SCAPS for our simulation. Firstly, we have given some explanations of the Solar Cell Capacitance Simulator in one Dimension (SCAPS-1D) which is used for the study and analysis of solar cell performance and the way it works and explains the its control panel. Then, we explain the solar cell structure is defined and how to enter its various parameters.

II.2. Program Overview

SCAPS-ID (Solar Cell Capacitance Simulator) is a Windows application program that is developed by Marc Burgelmann at the Department of Electronics and Information Systems (ELIS) of the University of Gent, Belgium, as a 1-D (one dimensional) numerical optoelectronic device solver specifically targeted at solar cell [7, 8]. It was originally developed for $CuInSe_2$ and CdTe based solar cells , then has evolved to study CIGS solar cells [9]. It is also used for amorphous silicon cells (a-Si and micro-amorphous Si) and crystalline solar cells (Si and GaAs family) as the latest of the uses of the program now. SCAPS contains several panels (or pages or windows), where the user can enter parameters related to his works and observes the results. It is possible to enter several panel points while opening the program like temperature, voltage, frequency, illumination and can show an action list of calculations (I-V, C- V, C-f, Q (λ)) [8, 10]. The program solves the Poisson (2-1) and continuity, equations simultaneously for electrons (2-2) and holes (2-3) with appropriate limit conditions [8, 11-15].

$$\frac{\partial^2}{\partial x^2}\Psi(x) = \frac{q}{\varepsilon_0 \varepsilon_r}\left(p(x) - n(x) + N_D - N_A + \rho_p - \rho_n\right) \qquad \text{II-1}$$

$$\frac{\partial n}{\partial p} = \frac{1}{q}\frac{\partial}{\partial x}J_n(x) + (G_n - R_n)$$

II-2

$$\frac{\partial}{\partial} = -\frac{1}{q}\frac{\partial}{\partial x}J_p(x) + (G_p - R_p)$$

II-3

Where ψ is electrostatic potential, q is the electrical charge, ε_r and ε_0 are the relative and vacuum permittivities respectively, p and n are hole and electron concentrations respectively, N_D and N_A are the donor and acceptor type impurities concentrations respectively, ρ_p, and ρ_n are holes and electrons distribution, respectively, J_n and J_p are electron and hole current densities, G_n and G_p are the electron and hole generation rates, R_n and R_p are electron and hole recombination rates, μ_n is the electron mobility and μ_p is the hole mobility, D_n is the electron diffusion coefficient, D_p is the hole diffusion coefficient. Carrier transport in semiconductors occurs by drift and diffusion and can be described by the equations:

$$J_n = -q_n\mu_n n\frac{\partial\Psi}{\partial x} + q_n D_n\frac{\partial n}{\partial x}$$

II-4

$$J_p = q_p\mu_p p\frac{\partial\Psi}{\partial x} + q_p D_p\frac{\partial p}{\partial x}$$

II-5

We have relied on the work by simulation package SCAPS 1D, most of the information is taken from the SCAPS manual[16]. The simulation stages SCAPS are shown in Figure II.1.
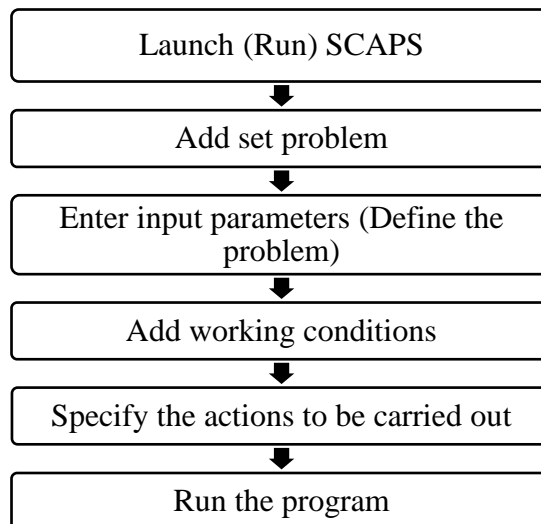
Figure II.1: SCAPS working procedure.

II.3. The beginning

First, to run the application, we double-click the file scaps3305.exe in the file manager (or any other SCAPS version). In the action panel, we click the icon **set problem**, and in the lower right of the panel that opens, we choose **load**. Select and open the file NUMOS CIGS baseline.def: that is the example problem file of the practicum session at the NUMOS workshop. This file is supposed to be in the folder /scaps/def, where /scaps/ stands for the directory where SCAPS is installed, and where the SCAPS .exe file resides. If necessary, browse to find this file. In case of adding a new cell, we click on the button **new**; add information about it, and save it by clicking the button **save**. We can also change all information about the cell later by clicking the **set problem** icon in the action panel.
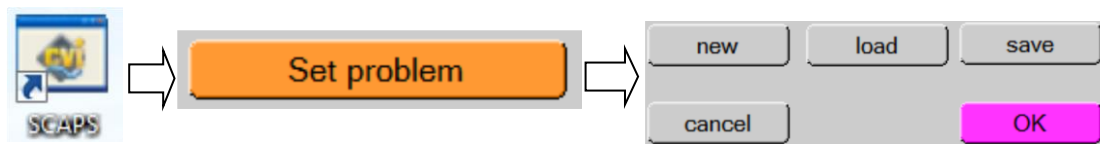
Figure II.2: Run and define the problem in SCAPS.

We specify information (parameters) about our work, or measurement that does not change during the simulation (remains constant when the simulation is performed) (see 3 in Figure II.3). Thus:

The temperature T: relevant for all measurements. Note that in SCAPS, only N_C (T), N_V (T), the thermal velocities, the thermal voltage kT, and all their derivatives are the only variables that have explicit temperature dependence. The corresponding materials parameters must be entered for each temperature.

The voltage V: is discarded in I-V and C-V simulation. It is the dc-bias voltage in C-f simulation and QE (λ) simulation. SCAPS always starts at 0 V and proceeds at the working point voltage in a number of steps that also should be specified.

The frequency f: is discarded in I-V, QE (λ), and C-f simulation. It is the frequency at which the C-V measurement is simulated.

The illumination: it is used for all measurements. For the QE (λ) measurement, it determines the bias light conditions. The basic settings are dark or light, choice of the illuminated side and choice of the spectrum. A one sun ($= 1000$ W/m^2) illumination with the (air mass 1.5, global) spectrum is the default, but it has a large choice of monochromatic light and spectra for specialized simulations. If there is a separate optical simulator, it can be loaded as a generation profile instead of using a spectrum.

II.4. Select the Measurement(s) to Simulate

In the action-part of the **Action Panel**, one or more of the following measurements to simulate: I-V, C-V, C-f, and QE (λ) can be selected. If necessary, the start and end values of the argument, and the number of steps can be adjudted. Initially, one simulation at a time is carried out. It should be noted that in a C-V simulation, the I-V curve is calculated as well; no need then to specify it separately (4 in
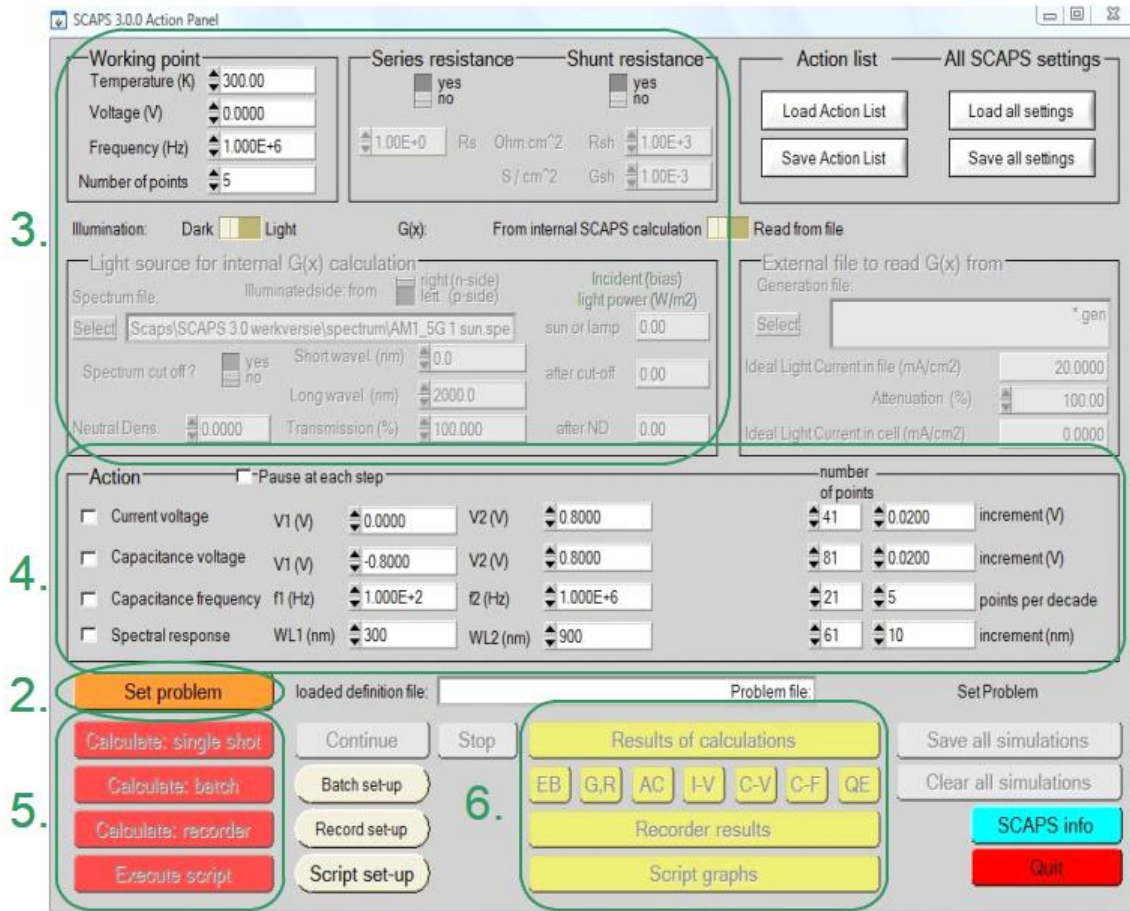
Figure II.**3**).

II.5. Shunt and series resistances

It is also possible to enter external values for parasitic resistances on the action panel (3   in
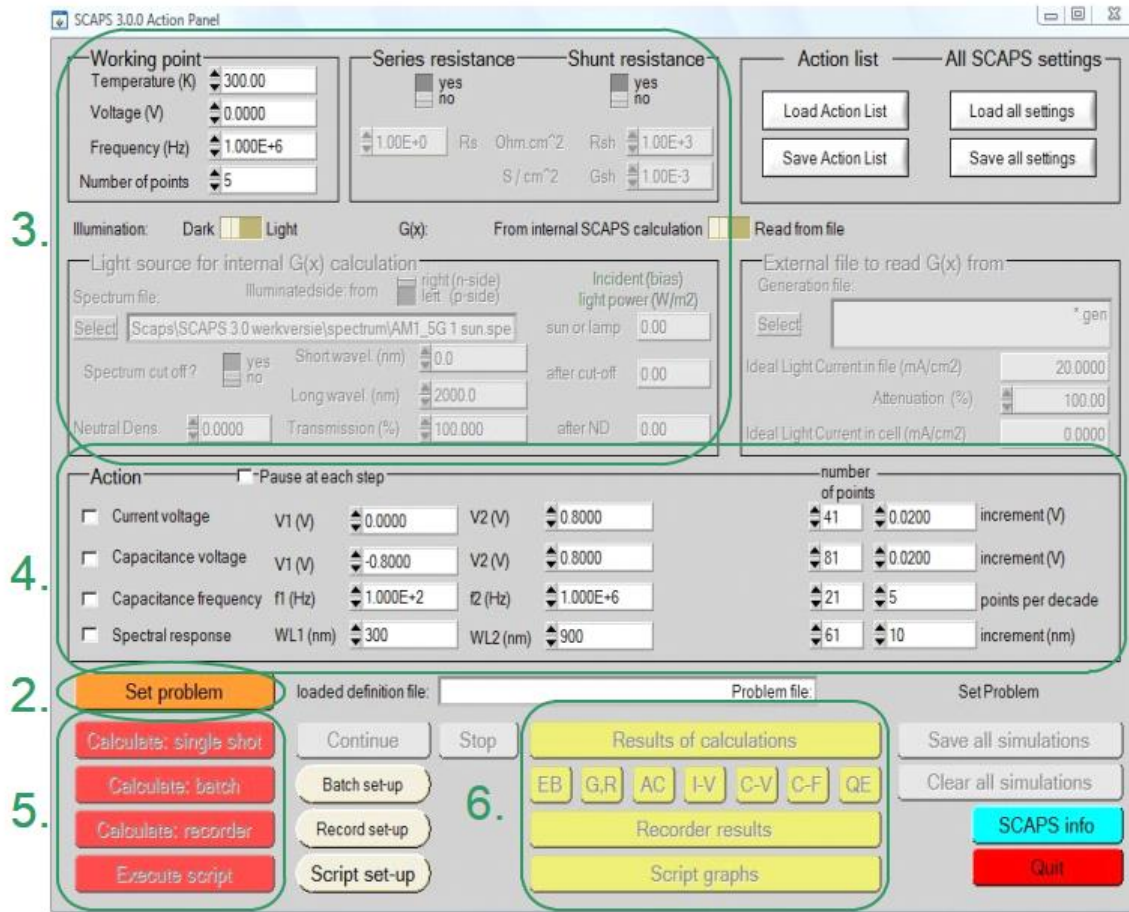
Figure II.**3**). To operate parasitic resistances the button **yes/no** is switched**.** Either resistance or conductance can be defined.

II.6. Start the calculation(s)

In the action panel, the icon **calculate: single shot** is clicked. The Energy Bands Panel opens, and the calculations start. At the bottom of the panel, a status line, iv from 0.000 to 0.800 Volt: V = 0.550 Volt can be seen, showing how the simulation proceeds. Meanwhile, SCAPS stands an animation how the conduction and valence bands, the Fermi levels and the whole caboodle are evolving (5 in Figure II.3). After that the results of the simulation are shown.
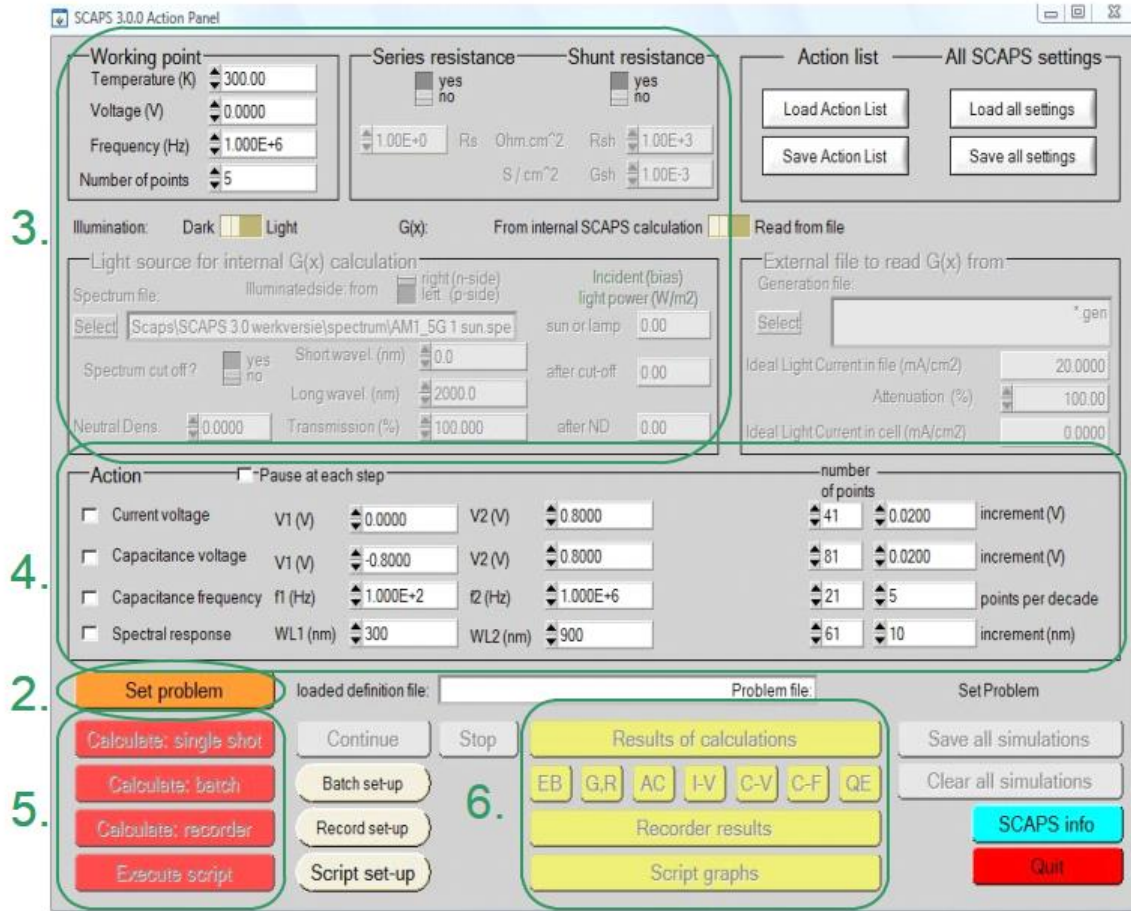
Figure II.3: The SCAPS start-up panel: the Action panel or main panel.

II.7. Solar Cell Definition

II.7.1. Editing a Solar Cell Structure

When clicking the 'Set Problem'-button on the action panel, the 'Solar cell definition'-panel is displayed. This panel allows create/edit solar cell structures and to save those to or load from definition files. These definition files are standard ASCII-files with extension '*.def', which can be read with notepad. Here, various properties about our cell located in it like band gap, electron affinity, thickness, defect, and others can be put. Layers, contact, and interface properties by clicking on the appropriate box as shown in Figure II.4 can also be added. Similarly, layers can be added by clicking 'add layer'. The user can input own reference conventions for the applied voltage V and the current density J in the external contacts.
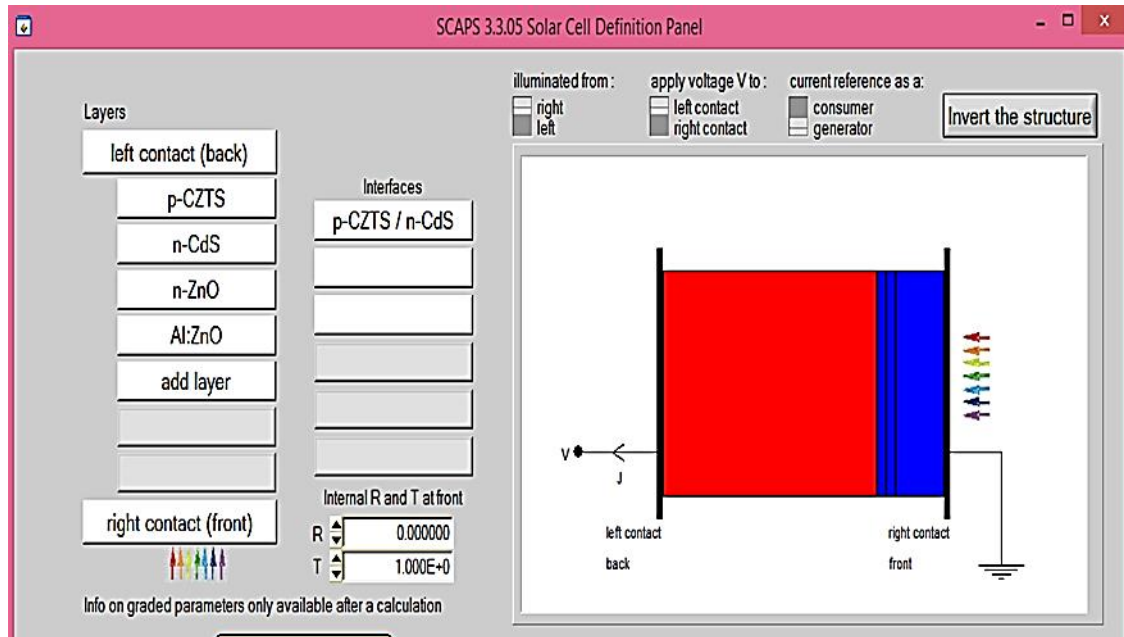
Figure II.4: Defining a solar cell structure.

In SCAPS 1D, there are many facilities such as:

'Apply voltage V to': when 'left' is set, then the right contact is the reference contact, and the voltage V is applied to the left contact; this is the default and the only possible option in SCAPS<4.0. When 'right' is set, the left contact is the reference contact, and the voltage V is applied to the right contact; in a JV curve, this corresponds to a reversal of voltage axis compared to the traditional JV curves in SCAPS (At the top of the Figure II.4).

'Current reference as a': when 'consumer' is set, then the current reference arrow is set such that P = J.V is the power consumed by the cell, and thus J.V is the power generated by the cell. When 'generator' is set, the current reference arrow is set such that P = J.V is the power generated by the cell, and thus J.V is the power consumed by the cell. The setting of the current reference arrow thus depends both on the selected voltage reference and on the consumer/generator selection (At the top of Figure II.4).

'Invert the structure': the solar cell structure is mirrored along the x-axis: the leftmost layer becomes the rightmost layer, and so on. This inversion of structure also swaps the interfaces, and all grading information in the layers and the defects. Clicking the inversion icon twice brings the original cell back. This inversion only concerns the structure: the

illumination side, the voltage and current reference settings all remain unchanged (At the top of Figure II.4).

Internally, in SCAPS only the default reference is used: voltage applied at the left contact and current reference arrow from left to right, resulting in a reference as a consumer. In all output (graphs, show/save tables), the result is shown consistent with the user's choice of reference. Note that the electric field in the SCAPS output is not subject to the user-set V and J references: it is always referred to the positive x-axis, thus from left to right.

II.7.2. Contact

The contact properties can be set by either clicking the front or back contact button on the cell definition panel, which opens the 'contact properties panel', see Figure II.5.

The metal work function Φ_m (for majority carriers) can be input by the user. However, the user can also choose the option "flat bands". In this case, SCAPS calculates for every temperature the metal work function Φ_m in such a way that flat band conditions prevail. We can edit value of 'thermionic emission/surface recombination velocity (cm/s)' for electrons and holes, also most of the cell electrical properties and optical properties can be added through this panel.

When the layer adjacent to the contact is n-type, Equation (II-6) is used. When it is p-type, Equation (II-7) is used. When it can be considered to be intrinsic, Equation (II-8) is used. As can be seen, only the shallow doping density is taken into account in order to calculate the flat band metal work function.

$$\Phi_m = \chi + k_B T \ln\left(\frac{N_c}{N_D - N_A}\right) \qquad\qquad \text{II-6}$$

$$\Phi_m = \chi + E_g - k_B T \ln\left(\frac{N_c}{N_A - N_D}\right) \qquad\qquad \text{II-7}$$

$$\Phi_m = \chi + k_B T \ln\left(\frac{N_c}{n_i}\right) \qquad\qquad \text{II-8}$$
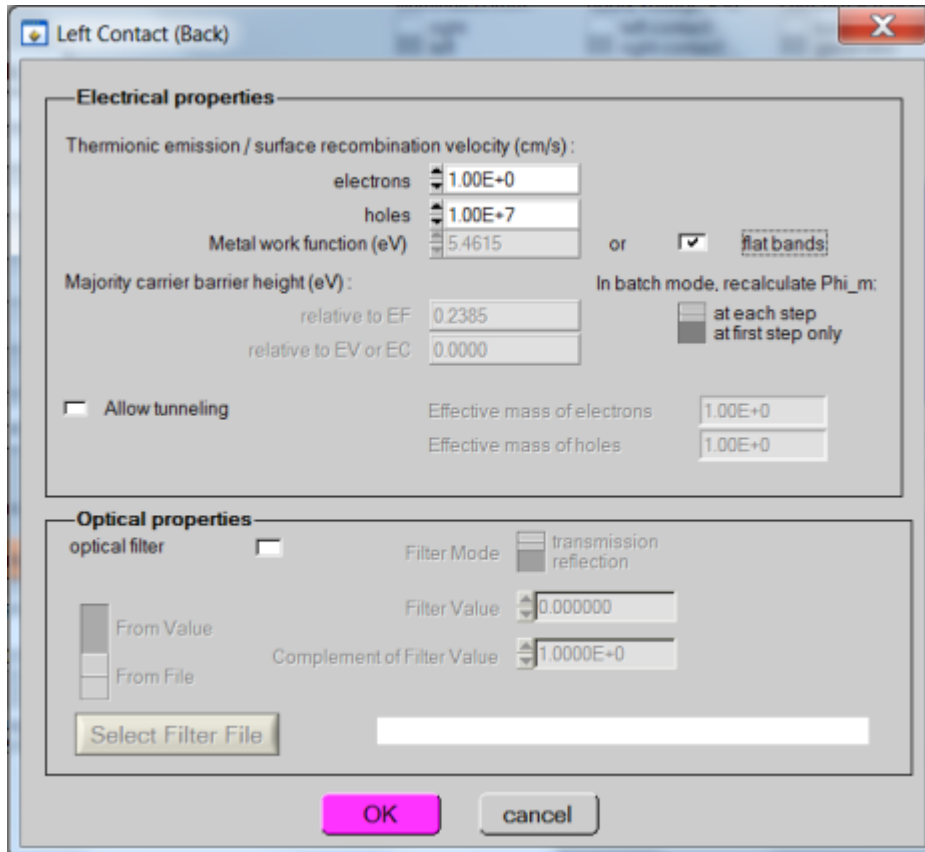
Figure II.5: Contact properties panel.

II.7.3. Defects and Recombination

In a diode, the current is converted from hole current at the p-contact to electron current at the n-contact. This means that somewhere in the diode recombination must take place, even in the most ideal device. So the user must specify recombination somewhere, at least at one place (in a layer, at contact, or an interface). If this is not done, a convergence failure will result in non-equilibrium conditions (non zero voltage, and/or illumination).

In the bulk of a semiconductor layer, three different kinds of recombination processes can be introduced: through defects, radiative, and Auger.

Figure II.6: Adding, editing, and removing defects.

Up to seven defects can be introduced in a semiconductor layer. The parameters governing each defect can be edited by clicking the appropriate Add/Edit-button, Figure II.6, which opens the 'defect properties panel'; this depends on the type of cell, the type of semiconductor, and the related defects (Figure II.7). And all that relates to the defects of one layer (Defect type, electron thermal capture cross section, hole thermal capture cross section, energetic distribution, and others).

Also, on one of the 'defect summary text boxes'; can be right-clicked where a panel then opens where a defect can be removed, duplicated or added, much the same as it was with removing, duplicating, and adding a layer.

Figure II.7: The defect properties panel.

II.7.4. Interfaces

Between any two semiconductor layers, an interface can be defined. The model which is implemented for interface transport in SCAPS is thermionic emission [17]. The thermal velocity of the interface transport equals the smallest thermal velocity of the two neighboring layers. The use of this model implies that there will always be a (small) step in the quasi-Fermi level energy values at an interface, even when there are no band offsets [8].

Just as in a bulk layer, recombination centers can be present at an interface. The definition of interface defects is very similar to bulk defects. However, there are only three possible defects, and there charge type cannot be multivalent. The interface defect can be edited by clicking for Checkbox of the interface. Then, defect parameters can be added.
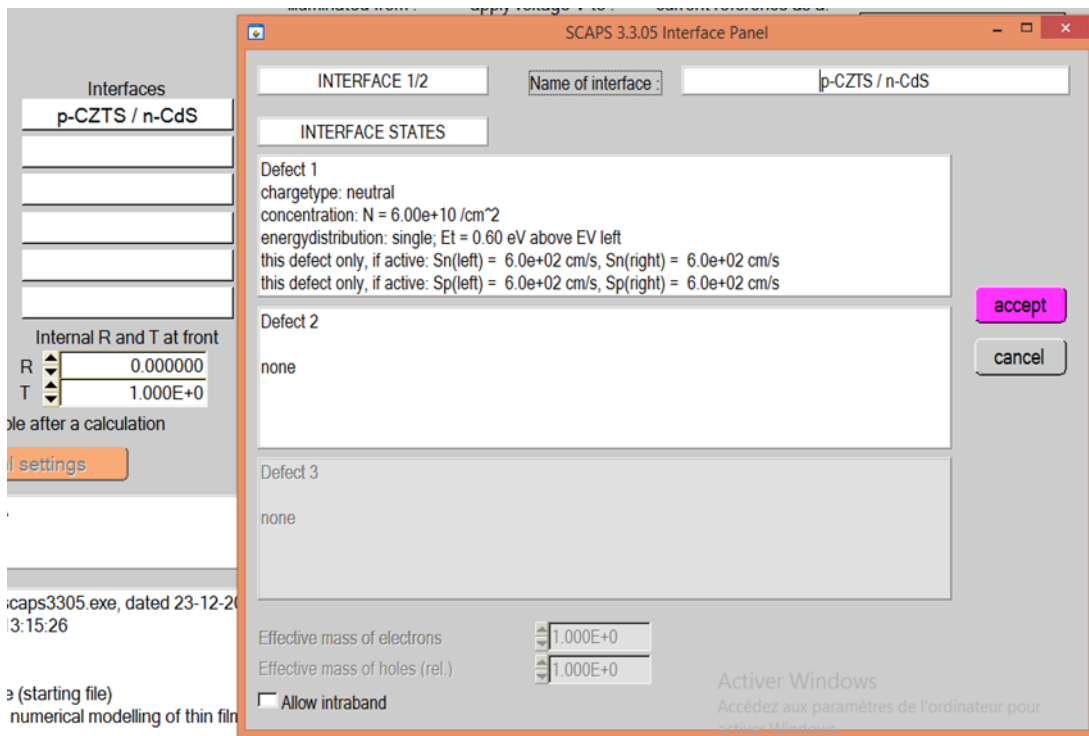
Figure II.8: Adding, editing, and removing interface defects.

II.8. Result Analysis

II.8.1. Navigation to the Analysis

SCAPS performs a lot of calculations any time the 'calculate'-button is clicked. We can analyze these results and provide a lot of help. Fortunately, there is a lot of help. The analysis-panels can easily be accessed from the action panel or any other analysis panel the analysis-panels can easily be accessed from the action panel or any other analysis panel, see Figure II.9.
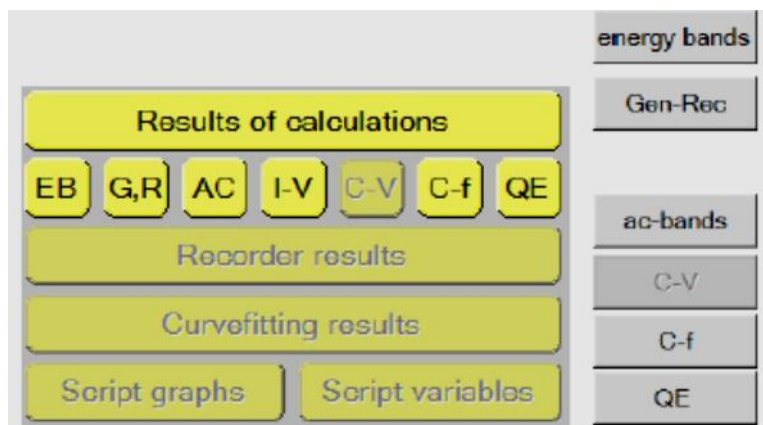
Figure II.9: Navigating to the results from the action panel (*left*) or any other panel (*right*).

Several options are available on every panel: saving data, showing data, saving graphs, and plotting the panel (sending to a printer). There are options available for scaling and zooming of graphs and to show more info about the plotted curves. Other options are panel specific.

At the bottom of every panel, there are two comment windows. The left window is auto generated and gives the definition file used with its last saving and when the simulation was performed. The right window can be used to write personal comments.

II.8.2. Zooming and Scaling

Most of the graphs are scalable. For most axes a logarithmic or linear scale can be chosen and/or the absolute value of the property can be plotted. The axis-range can be set by clicking a 'scale'-button, which opens the following pop-up menu.

- The scaling of both axes can be set automatically (default) or manually.
- A minimum/maximum value can be given.
- The settings on this panel can be saved/loaded (generating an ASCII-txt-file).

- Clicking the minimal positive button sets the y-axis scaling to manual and sets ymin to the smallest positive data point which needs to be plotted. This might be very useful when there are negative data points in a semilogarithmic diagram.
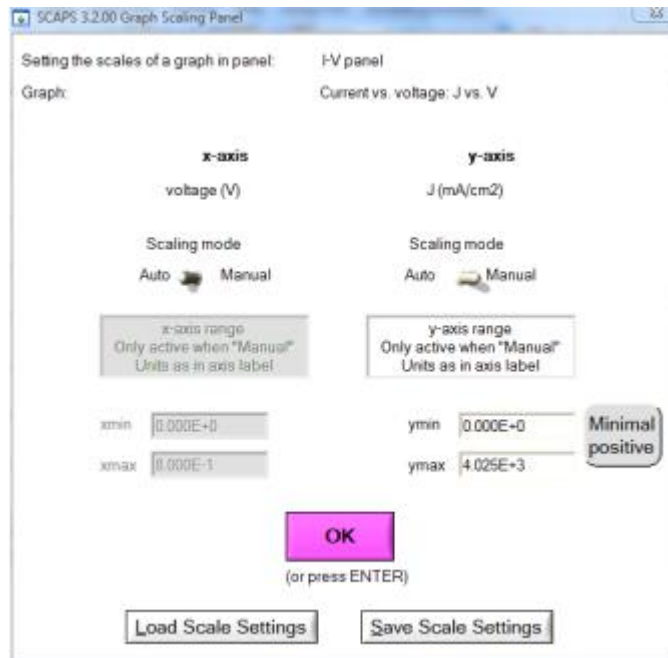
Figure II.10: The Scaling panel.

Almost all diagrams have zooming facilities. In order to zoom in, the CTRL-icon should be held pressed whilst drawing a rectangle with the mouse on a graph. For zooming out, the CTRL-icon should be held pressed whilst right-clicking with the mouse. Resetting the initial zooming can often be done as well by changing the log/lin property of the axes. This only works if the axes scaling is set to auto.

II.8.3. The IV-Panel

The results of the current-voltage simulations are shown on the IV-panel. The left graph displays all I-V simulations. The right graph gives detailed information about the recombination currents in the last simulation. This allows seeing the main recombination mechanism in the structure for varying voltages. If the simulation is performed under illumination, the solar cell parameters are calculated and shown under the graph I-V, see Figure II.11.
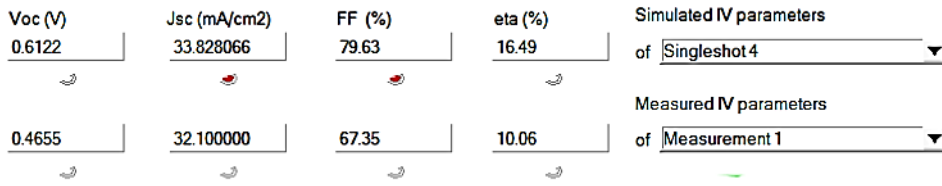
Figure II.11: Visualization of the solar cell parameters.

II.9. The batch set-up panel

The batch set-up panel allows to vary up to nine different parameters. An example of the batch set-up panel is shown in Figure II.12.
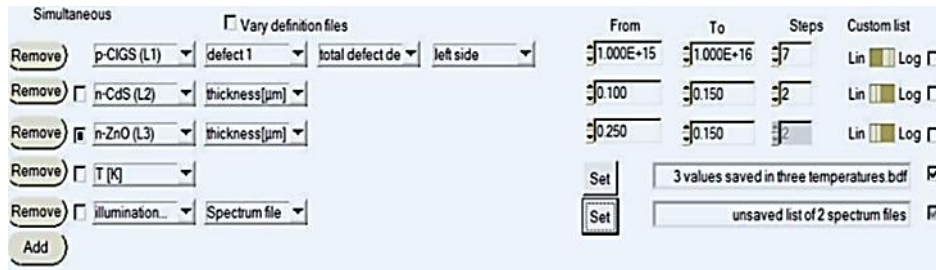
Figure II.12: The batch set-up panel, illustrating most of the options.

All (most of the) parameters present in the currently defined structure can be varied. Also, working point conditions can be varied.

When checking 'simultaneous', this parameter will be varied together with the parameter above (and thus in the same number of steps). If 'simultaneous' is not checked, the parameters are varied in a nested way.

Parameters can be varied in a linear, logarithmic, or a custom defined way.

Parameters that are filed can be varied by entering a list of file names: generation files, spectrum files, filter files, grading files, optical capture cross-section files and initial state work point files.

Some parameters can only take two values (on/off), e.g. illumination.

When changing any of the illumination parameters (ND filter, spectrum file…) as a batch parameter, the illumination is automatically switched on.

When changing one of the effective mass parameters, the accompanying tunneling mechanism is automatically switched on.

It is possible to save/load the parameters on the batch panel in a '*.sbf'-file which is a standard ASCII-file.

It is possible to print the batch panel in order to remember your settings.

II.9.1. Custom defined values

When checking the custom list option, a Set-icon appears which when clicking it opens a panel that allows to enter a list of parameter values.
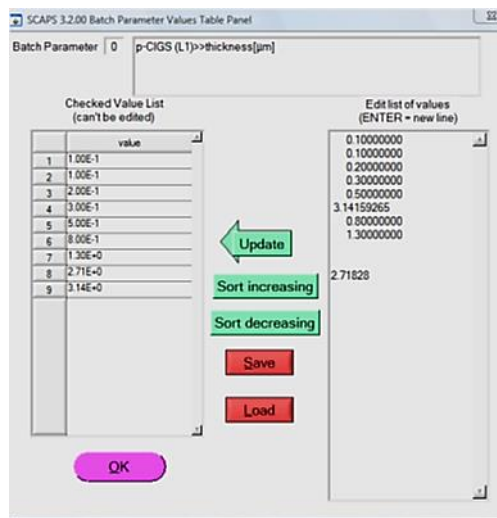
Figure II.13: Setting custom batch values.

• Parameters can be typed or copy/pasted in the right list interactively. Afterward 'Update' should be pressed to allow SCAPS to interpret the typing work. Data that cannot be interpreted as a number will be ignored.

• The values in the left list are the values SCAPS will use. These can be sorted.

• Parameter value lists can be saved and loaded. The resulting files are standard ASCII files with extension '*.bdf'. This allows to make custom lists with any other program (MS Excel, Origin, Matlab…) and load them in SCAPS. The layout of this file is rather tolerant. Just the parameter values can be added one below the other. All the lines which cannot be interpreted as only one number are ignored as being a comment. It is strongly recommend that the user add some comments to the file, so that what data are present in the file can be remembered, even after not using it for a while.

• Some parameters are files rather than numbers, e.g. a spectrum file. Then there is no choice but to vary the parameter in a custom way. Clicking the Set-icon will open a panel where a list of files can be set. Files can be added, removed or replaced. The order of the file-list can be changed. The list of files can be saved/loaded as well. This is again a standard ASCII file with the extension '*.bdf'. In the '*.bdf' file, the filenames of these files preceded by "file:" can be listed. All lines in the '*.bdf' which are not preceded by this will be treated as a comment. The listed files should be placed in the appropriate SCAPS folder: For example, the spectra and the generation files which are listed should be placed in the "spectrum" and "generation"-file of the working SCAPS-folder respectively.

II.10. Recorder Calculations

In a regular single shot or batch calculation, the detailed panels are only available for the last measurement point. To be able to see them as a function of the batch parameters you can launch a record calculation. You should first select the properties which you want to keep track of by clicking 'Record set-up'. By clicking 'calculate: recorder', a recorder calculation is launched. Cell parameters are varied according to the Batch set-up, and all simulations (and only those) are performed, which are needed to determine the asked properties. This means that the selected measurements on the action panel are ignored!
If this option is used with a little bit of imagination, you can devise all kinds of measurement simulations with SCAPS.

II.10.1.Setting a Recorder

With the Recorder facility, a batch calculation and register or record selected cell properties as a function of the batch parameter(s) can be done. For example, cell efficiency as a function of some doping density, $\eta \, (N_A)$, or whatever can be recorded. There are many possibilities.

The list of properties to be recorded is made in the Record Set-up. With the help of the five choice-menus (type-property-layer-defect-level), the user can choose a property and add it to the list on the left side of the panel using an Insert or Replace button. There are eight types of properties to be recorded: I-V characteristics, General properties, Cell definition, Interfaces, Energy band panel, Generation panel, Occupations, and AC panel.
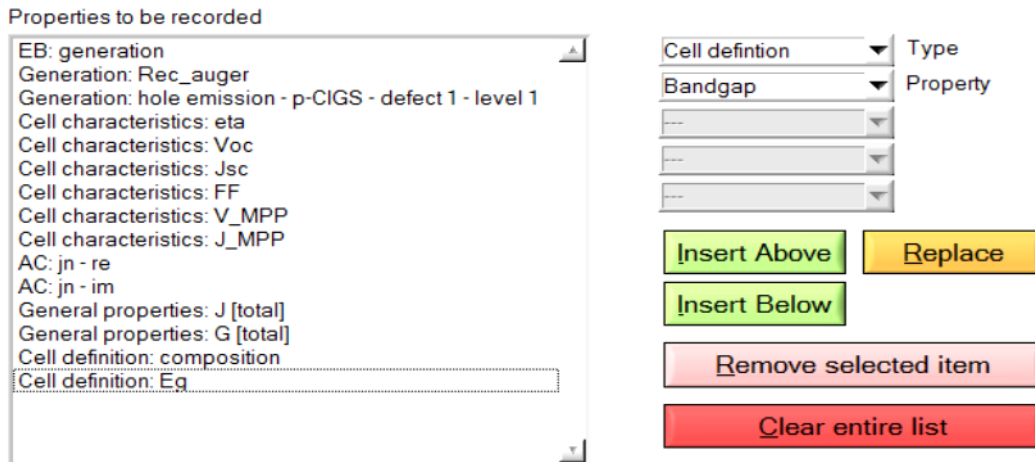
Figure II.14: Setting up a recorder.

II.10.2. Recorder Calculations

Clicking the 'Calculate: recorder'-button leads to a batch recording, which is only available when a batch is set. In this case, the action list, as it is set on the action panel, will be ignored. SCAPS will determine which calculations need to be done in order to record the asked properties. For example, when a property of the AC-panel is to be recorded SCAPS will perform a C-f simulation at the frequency determined by the working point. When a cell characteristic is to be recorded, an I-V simulation will be performed starting from 0 - V stopping at SCAPS does not a priori know the open-circuit voltage. Hence, it will perform an I-V simulation from 0 V up to a predefined maximum voltage with the 'stop at Voc' option on. This predefined maximum voltage can be set on the numerical panel and has a default value of 2.00V. the open-circuit voltage.

The accuracy of the determination of the cell characteristics is determined by the increment voltage used in the I-V simulation. SCAPS uses the value which is present on the

action panel unless it is larger than a predefined minimum value. This value can also be set on the numerical panel and has a default value of 0.05V.

| Maximum voltage for the recording of Solar cell characteristics (V) | 2.00 |
| Minimum voltage increment for the recording of Solar cell characteris | 0.05 |

Figure II.15: Recorder settings on the numerical panel.

II.10.3. Analyzing the Recorder Results

The results of a recording can be accessed through the 'Recorder Results' button on the action panel (or on the EB- or AC-panel). Recorded properties of the type IV characteristics, General properties, or Interfaces are immediately plotted as a function of one of the batch parameters. Record properties of the other types are plotted, as a function of the position in the cell (the mesh). The results can also be saved to a file, see Figure II.15. For each type of property type, a different file is saved. The user can choose which files are to be made using the checkboxes seen in Figure II.16. The show option has the same meaning as everywhere in SCAPS. But as not all property types can be showed in one window, only the last one (= the lowest checkbox checked on Figure II.16) will be shown.

☑ IV characteristics
☐ General properties
☑ Cell definition
☐ EB panel
☐ Interfaces
☑ Generation
☐ Occupations
☐ AC panel

save

show

Figure II.16: Saving and showing recorder results.

REFERENCES

[1]   P. A. Basore, "Numerical modeling of textured silicon solar cells using PC-1D," *IEEE Transactions on electron devices,* vol. 37, pp. 337-343, 1990.

[2]   J. G. Fossum, "Computer-aided numerical analysis of silicon solar cells," *Solid-State Electronics,* vol. 19, pp. 269-277, 1976.

[3]   R. Wei, "Modelling of perovskite solar cells," Queensland University of Technology, 2018.

[4]   J. Cai and L. Han, "Theoretical investigation on interfacial-potential-limited diffusion and recombination in dye-sensitized solar cells," *The Journal of Physical Chemistry C,* vol. 115, pp. 17154-17162, 2011.

[5]   J. Villanueva, J. A. Anta, E. Guillén, and G. Oskam, "Numerical simulation of the current−voltage curve in dye-sensitized solar cells," *The Journal of Physical Chemistry C,* vol. 113, pp. 19722-19731, 2009.

[6]   K. Ogiya, C. Lv, A. Suzuki, R. Sahnoun, M. Koyama, H. Tsuboi, N. Hatakeyama, A. Endou, H. Takaba, and M. Kubo, "Development of multiscale simulator for dye-sensitized TiO2 nanoporous electrode based on quantum chemical calculation," *Japanese Journal of Applied Physics,* vol. 47, p. 3010, 2008.

[7]   M. Burgelman, P. Nollet, and S. Degrave, "Modelling polycrystalline semiconductor solar cells," *Thin Solid Films,* vol. 361, pp. 527-532, 2000.

[8]   A. Niemegeers, S. Gillis, and M. Burgelman, "A user program for realistic simulation of polycrystalline heterojunction solar cells: SCAPS-1D," in *Proceedings of the 2nd World Conference on Photovoltaic Energy Conversion, JRC, European Commission, juli*, 1998, pp. 672-675.

[9]   M. Burgelman and J. Marlein, "Analysis of graded band gap solar cells with SCAPS," in *Proceedings of the 23rd European Photovoltaic Solar Energy Conference, Valencia*, 2008, pp. 2151-2155.

[10]   S. Utilisateur. (2019). *Simulation programme SCAPS-1D for thin film solar cells*. Available: https://photovoltaic-software.com/solar-tools/scientific-solar/simulation-programme-scaps-1d-for-thin-film-solar-cells

[11]   M. Mostefaoui, H. Mazari, S. Khelifi, A. Bouraiou, and R. Dabou, "Simulation of high efficiency CIGS solar cells with SCAPS-1D software," *Energy Procedia,* vol. 74, pp. 736-744, 2015.

[12]   R. E. Brandt, "Elucidating efficiency losses in cuprous oxide (Cu_2O) photovoltaics and identifying strategies for efficiency improvement," Massachusetts Institute of Technology, 2013.

[13]   D. Korfiatis, S. Potamianou, E. Tsagarakis, and K. T. Thoma, "Demixing profiles in oxides upon the application of an electrical field," *Solid state ionics,* vol. 136, pp. 1367-1371, 2000.

[14]   S. P. Gaur and D. H. Navon, "Two-dimensional carrier flow in a transistor structure under nonisothermal conditions," *IEEE Transactions on Electron Devices,* vol. 23, pp. 50-57, 1976.

[15]   H. Mathieu and H. Fanet, *Physique des semiconducteurs et des composants électriques: cours et exercices corrigés*: Dunod, 2009.

[16]   M. Burgelman, K. Decock, A. Niemegeers, J. Verschraegen, and S. Degrave, "SCAPS manual," ed: February, 2016.

[17]   H. Pauwels and G. Vanhoutte, "The influence of interface state and energy barriers on the efficiency of heterojunction solar cells," *Journal of Physics D: Applied Physics,* vol. 11, p. 649, 1978.

CHAPTER III

RESULTS AND

DISCUSSION

Chapter III.   Results and Discussion

III.1. Introduction

After making outs about solar cells, especially of the type of thin film based on P-CZTS, in this chapter we will tackle some of the parameters affecting these cells; where it contains two parts. In the first part, we dealt with comparing the results of our study edited cell to the experimental results *(Dhakal et al., Solar Energy, 100, 23-30,2014),* where we took some data, and introduced defects in the layer CZTS ,and the interface defect as well.

In the second, we studied the effect of some parameters on the performance of our cell, such as different buffer layers, affinity electronic, thickness, band gap energy, density carrier of absorber layer, defect on the absorber layer, and defect of the interface absorber/buffer. Because it is usually necessary to improve the parameters. Therefore, we study the impact of these parameters on performance in order to obtain maximum performance.

III.2. Ideal solar cell

In this study, the electrical characteristics (current voltage) were calculated using SCAPS simulator under AM1.5 illumination. The solar cell is based on p-type absorber CZTS layer together with the following material layers: TCO, ZnO and CdS buffer. The schematic structure of the cell is shown in Figure III.1.
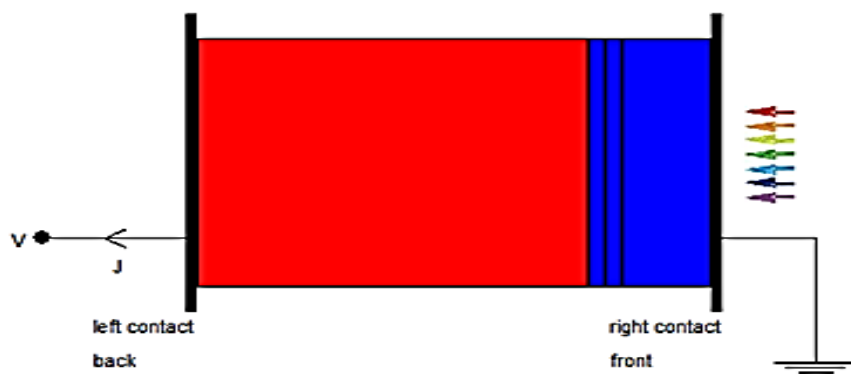
Figure III.1: A schematic representation of the CZTS solar cell

simulated in this work.

First of all, the solar cell is simulated considering ideal parameters for the absorber layer (CZTS) as well ZnO and CdS are simulated with their usual parameters used by SCAPS [1]. To be realistic, the effects of several types of defects were considered, this includes bulk deep acceptors and donors, as well as interface defects (CZTS/ CdS). A comparative study with experimental measurement[2] was carried out. The basic input parameters used in this simulation are shown in Table III-1 [2]. Additionally, the parasitic resistances reported by [2] were considered. The default illumination spectrum is set to the global AM 1.5. The front and rear contacts are modeled by a surface recombination rate of 10^7cm.s^{-1}. The CZTS absorption coefficient is 5 x 10^4 cm^{-1}; the series resistances and the shunt resistances are 5.61, 400 Ω.cm^2, respectively.

Table III-1: Parameters used in the simulation [2-5].

Parameters	Al:ZnO	n-ZnO	n-CdS	p-CZTS
Thickness (nm)	0.3	50	60	1300
Relative permittivity	9	9	9	10
Electron mobility μ_e (cm^2/Vs)	100	100	100	100
Hole mobility μ_h (cm^2/V s)	25	25	25	25
Acceptor concentration N_A(cm^{-3})	1×10^{17}	1×10^{17}	1×10^{17}	5.75×10^{16}
Donor concentration N_D (cm^{-3})	1×10^{17}	1×10^{18}	2×10^{17}	0
Band gap (eV)	3.3	3.3	2.4	1.53
Effective density of state N_C (cm^{-3})	2.2×10^{18}	2.2×10^{18}	2.2×10^{18}	2.2×10^{18}
Effective density of state N_V (cm^{-3})	1.8×10^{19}	1.8×10^{19}	2.4×10^{18}	1.8×10^{19}
Electron affinity (eV)	4.6	4.6	4.5	4.1
Optical Absorption constant (cm^{-1} eV$^{1/2}$)	5×10^4	scaps data	scaps data	scaps data

Table III-2: Device Parameters used in the Simulation [2, 5].

Cell properties	
Cell temperature	300 K
Back metal contact properties	
Electron work function of Mo	5 eV
Electron Surface recombination velocity (SRV)	10^5 cm/s
Holes SRV	10^7 cm/s
Front metal contact properties	
Electron work function	Flat band
Electron SRV	10^7 cm/s
Electron SRV	10^5 cm/s

Initially, we have considered an ideal structure without any defect and parasitic resistances Table 3.1; the obtained J-V characteristics are indicated in Figure III.2. The extracted figures of merit, in this case, are presented in Table III-3. It is obvious that the J-V characteristics and the extracted parameters are far away from measurements, except the short circuit current which is more or less comparable.
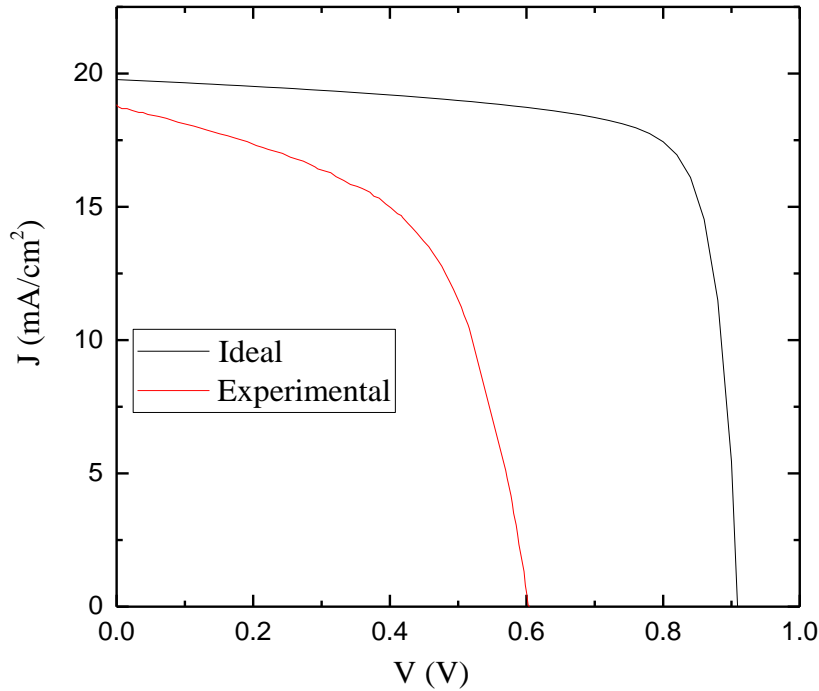
Figure III.2: The simulated J-V characteristics of an ideal solar cell compared with experimental solar cell [2].

Table III-3: The extracted output parameters from the J-V characteristics of the ideal solar cell compared to those evaluated from measurements [2].

	V_{OC} (mV)	J_{SC} (mA/cm^2)	FF (%)	η (%)
Simulation	910	20.21	81.02	14.92
Measurement	603	19.00	55.00	06.20

III.3. Effect of deep donor and a deep acceptor defect

III.3.1. Effect of deep donor and a deep acceptor defect without parasitic resistances

Next, the presence of a deep donor and a deep acceptor have been considered, separately. The parameters of such defects are demonstrated in Table III-4. The simulated J-V characteristics are presented in Figure III.3. It is also evident that the simulated results are not in good agreement with measurements.

Table III-4: The Parameters used for the bulk defects.

	p-CZTS		n-CdS	n-ZnO
Gaussian defect density, N_G (cm^{-3})	Acceptor 10^{15}	Donor 10^{15}	Neutral 10^{17}	Neutral 10^{17}
Capture cross section for electrons, σ_e (cm^2)	10^{-16}	10^{-14}	10^{-13}	10^{-12}
Capture cross section for holes, σ_h (cm^2)	10^{-14}	10^{-16}	10^{-13}	10^{-15}
$E_{A\,(D)}$ (eV)	0.6		1.2	1.65
$W_{A\,(D)}$ (eV)	0.1		0.1	0.1
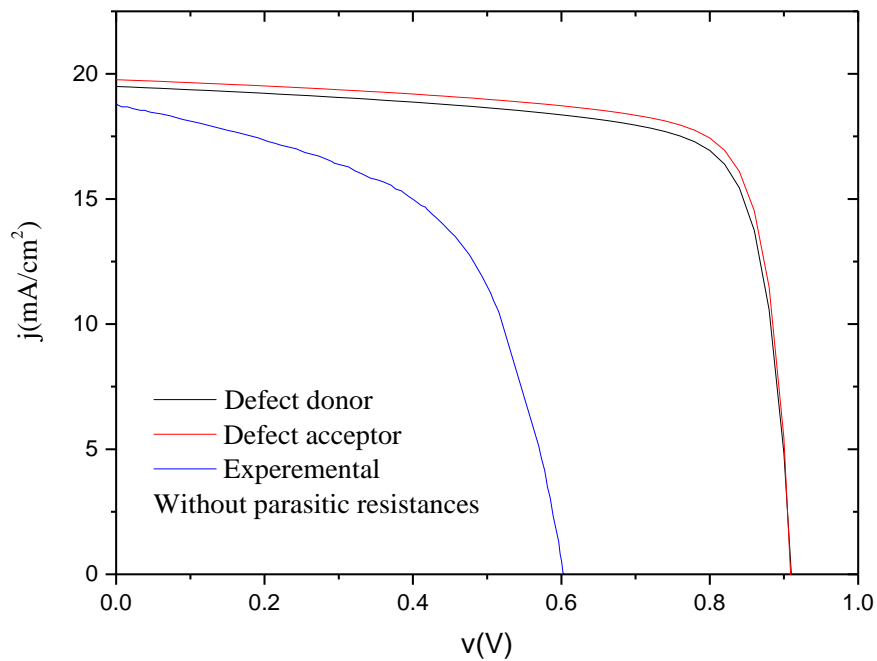
Figure III.3: The simulated J-V characteristics with deep defects [2].

It is worth to remember that the maximum theoretical efficiency for an ideal solar cell is of 14.92%. A slight decrease of the conversion efficiency has been observed in case of a donor or acceptor defect to 13.06% and 13.46% respectively. The loss in conversion

efficiency can be explained by the bulk defect density in the absorber layer which has a minimum density of around 10^{15} cm^{-3}, according to G. Hanna and co-workers [6, 7].

III.3.2. Effect of deep donor and a deep acceptor defect with parasitic resistances

The fill factor and J_{SC} follow the same trend as the conversion efficiency, although its variations do not exceed 5%. As expected, V_{OC} decreases slightly induced by interface recombination of photogenerated carriers [6, 8], and FF is affected by the presence of parasitic resistances[4]. These parasitic effects include the series (R_S) and shunt (R_{Sh}) resistances, which are not negligible in real cells. The resistance at the front and back electrodes and the interfacial resistances between different layers also contribute to the series resistance. The formation of sulphide (MoS$_2$ for Mo/CZTS) at absorber/back contact interface is also responsible for high series resistance of the CZTS based devices[9]. In Figure III.4,Table III.5), the efficiency of CZTS solar cell decrease from 13% to 10% (for donor defect and acceptor defect) in the presence of series resistance from 5.61 W cm^2. On the other hand, a finite shunt resistance leads to a leakage current in the device. In the actual CZTS thin film solar cells the shunt resistance is ~400 W cm^2 [2, 4].
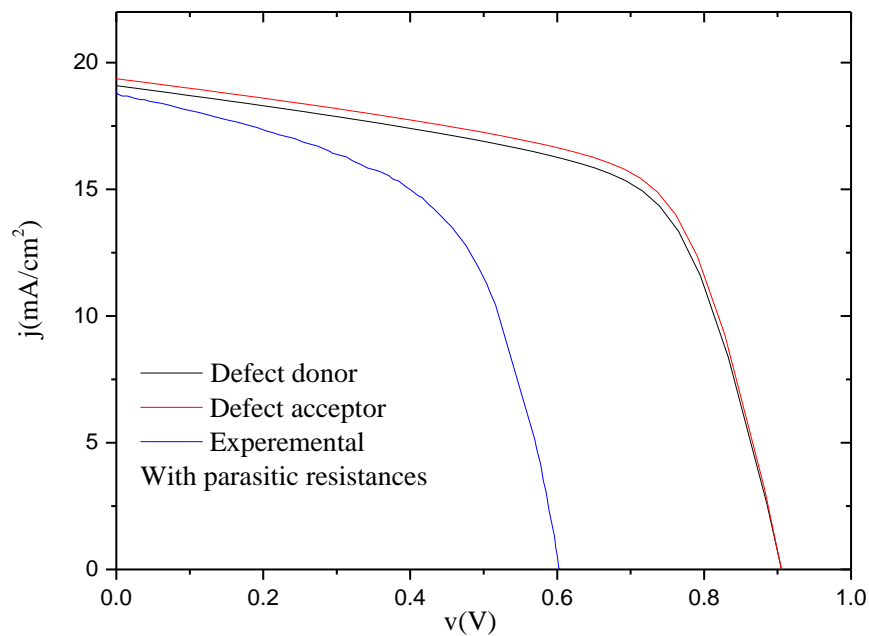
Figure III.4 : The simulated J-V characteristics in the presence of bulk defects with series resistance and shunt resistance [2].

Table III-5: The calculated output parameters compared to those evaluated from measurements [2].

	V_{oc} (mV)	J_{sc} (mA/cm²)	FF (%)	η (%)
Experimental data	603	19	55	6.2
Our results with donor defect	906	18.47	61.56	10.31
Our results with acceptor defect	906	18.75	62.48	10.62

III.4. Effect of interface state

Since neither donor nor acceptor bulk traps provide comparable simulation and measurement results, we have considered the existence of interface traps between the CZTS and CdS layers. Table III-6 presents the interface defect properties states parameters. The obtained J-V characteristics in this case are plotted in Figure III.5. It is evident that the simulated current versus voltage is very close to measurements [2].

Table III-6: The parameters used for the CZTS/CdS interface defect in the simulation.

CZTS/CdS interface defect properties	
N (cm^{-2})	N 6 X 10^{10}
σ_e (cm²)	10^{-15}
σ_h (cm²)	10^{-15}

Interface states existence can be explained by either the existence of a second phase which may be presented at the absorber/buffer layer interface, that boosts interface recombination [4]. It can also be due to the greater value of the defects density in the real samples. According to Table III.5, there is a good adjustable between the experimental data from the literature [2]and our model. Therefore, the set of parameters can be validated as a baseline for simulating the variation of absorber parameters influence on the solar cell performance [4]. This interface is also characterized by a high defect formation which may be due to the lattice, and thermal expansion mismatches as well. Furthermore, one of the most significant loss mechanisms in CZTS solar cells can be related to the trap-assisted tunneling through CZTS/CdS interface recombination [10, 11]. Moreover, the conduction band offset (CBO) between absorber and buffer materials have a large impact on device efficiency. Negative offset results in high recombination at the interface leading to low efficiency [10, 12].A cliff-like conduction band offset at the CZTS/CdS interface decreases

Voc by the trap state assisted recombination[8, 13]. However, since VBM (valence-band minimum) of CZTS is close to CBM of CdS, the recombination probability of majority carriers will be high, which will lead to reduced output voltage[14].
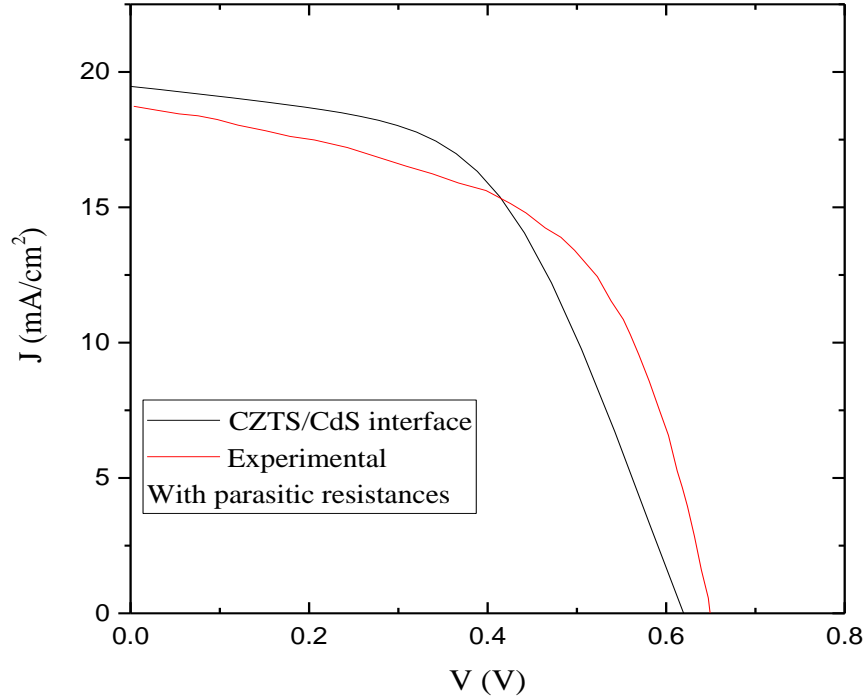
Figure III.5 : J–V graph of the CZTS solar cell experimental [2] and

simulation (CZTS/CdS defect).

III.5. Effect of buffer layer

In this part, we relied on the cell studied above with some modifications, and then we simulated the various parameters by SCAPS simulator under AM1.5 illumination, where electrical properties (voltage current) have been calculated. Used parameters summarized in the Table III-7.

Table III-7: parameters used in the simulation.

Parameters	Al:ZnO	n-ZnO	n- In_2S_3	ZnS	n-CdS	p-CZTS
Thickness (nm)	0.3	50	60	60	60	1300
Relative permittivity	9	9	13.5	9	9	10
Electron mobility μ_e (cm²/Vs)	100	100	400	100	100	100
Hole mobility μ_h (cm²/V s)	25	25	210	25	25	25
Acceptor concentration N_A(cm⁻³)	0	0	0	0	0	5.75×10^{16}
Donor concentration N_D (cm⁻³)	1×10^{17}	1×10^{18}	1×10^{17}	$1X10^{18}$	1×10^{17}	0
Band gap (ev)	3.3	3.3	2.5	3.1	2.4	1.52
Effective density of state Nc(cm⁻³)	2.2×10^{18}	2.2×10^{18}	1.8×10^{19}	$2.2X10^{18}$	2.2×10^{18}	2.2×10^{18}
Effective density of state Nv(cm⁻³)	1.8×10^{19}	1.8×10^{19}	4×10^{13}	$1.8X10^{19}$	2.4×10^{18}	1.8×10^{19}
Electron affinity (ev)	4.6	4.6	4.7	4.15	4.5	4.1
Coefficient d'absorption	scaps data	scaps data	scaps data [15, 16]	scaps data [6, 17, 18]	scaps data	$5X10^4$
Defect type	/	n	n	n	n	a/d/n
Defect distribution	/	Gaussian	Gaussian	Gaussian	Gaussian	Gaussian
Total Defect density (1/cm³)	/	$1x10^{17}$	$4.35x10^{16}$	$4.35x10^{16}$	$4.35x10^{16}$	$5x10^{15}$
σ_n (cm²)	/	10^{-12}	10^{-13}	10^{-13}	10^{-13}	10^{-16} /10^{-14} / 10^{-15}
σ_h(cm²)	/	10^{-15}	10^{-13}	10^{-13}	10^{-13}	10^{-14} /10^{-16} / 10^{-15}

CZTS/ZnS interface defect density: $6x10^{10}$ cm⁻² (single; neutral).

a :Acceptor, d: donor, n: neutral

In our simulation, we replace the buffer layer CdS with ZnS and In_2S_3. Consequently, we have noticed that using ZnS as a buffer layer provides a better efficiency 11.64% compared to CdS and In_2S_3, where the values are 6.33% and 3.16% respectively. In addition, the short circuit current density in the CZTS / ZnS solar cell is slightly larger than CZTS / CdS and CZTS / In_2S_3, as well as for FF and Voc a notable increase in CZTS / ZnS cases; this is due to band gap from ZnS (Eg = 3.1eV) [19-21], it is wider than CdS and In_2S_3 2.4eV and 2.5eV, respectively. The structural mismatches between In_2S_3 and other materials of the CZTS solar cell can lead to lower efficiency, as the affinity of In_2S_3 (4.7 eV) is greater than

CdS, ZnS 4.5 eV, and 4.15eV respectively. Also, the affinity of CZTS is 4.1eV, as well as making the band dfference of the conduction between the absorber / buffer layer (CBO or ΔE_c); or ΔE_c = -0.15 eV for the structure CZTS / ZnS, and 0.4 eV, 0.6 eV for CZTS / CdS and CZTS / In_2S_3 respectively.

Table III-8: The calculated output parameters.

	*V*oc (mV)	*J*sc (mA/cm²)	FF (%)	η (%)
SLG/Mo/CZTS/CdS/ZnO/Al:ZnO	0.604	19.00	55.15	6.33
SLG/Mo/CZTS/ZnS/ZnO/Al:ZnO	0.905	19.59	65.66	11.64
SLG/Mo/CZTS/In₂S₃/ZnO/Al:ZnO	0.387	19.04	42.84	3.16
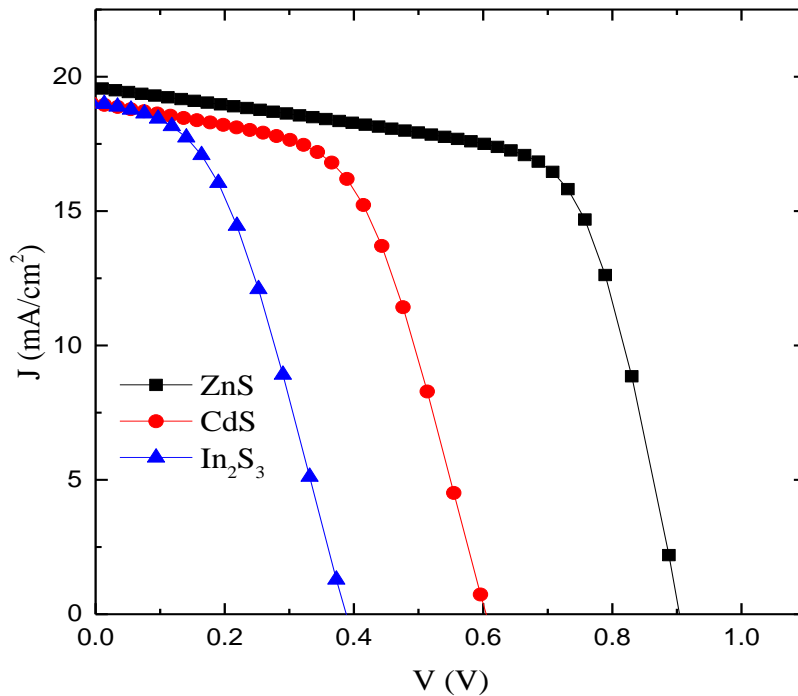
Figure III.6: J–V graph of the CZTS solar cell with ZnS, CdS, and In_2S_3 buffer layer.
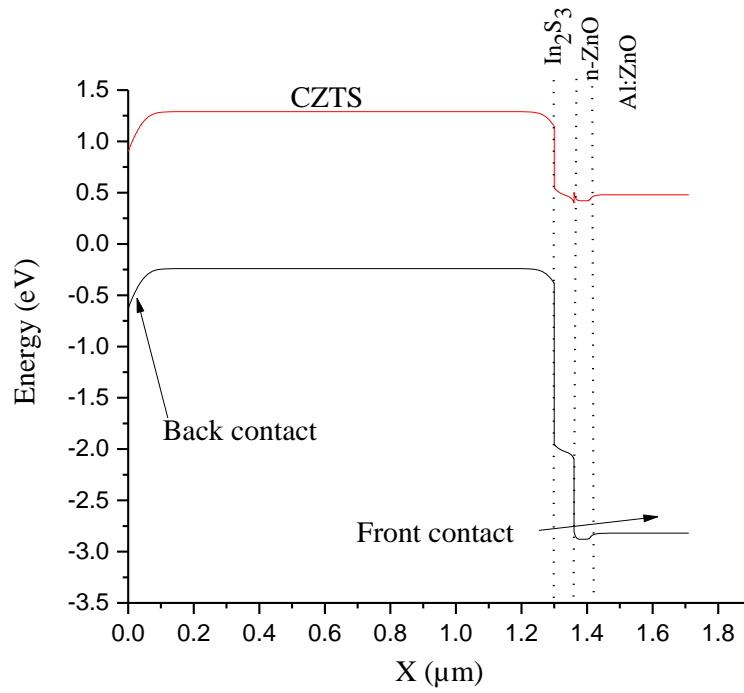
Figure III.7: Graphical representation of the band alignments within CZTS/In$_2$S$_3$ solar cell.
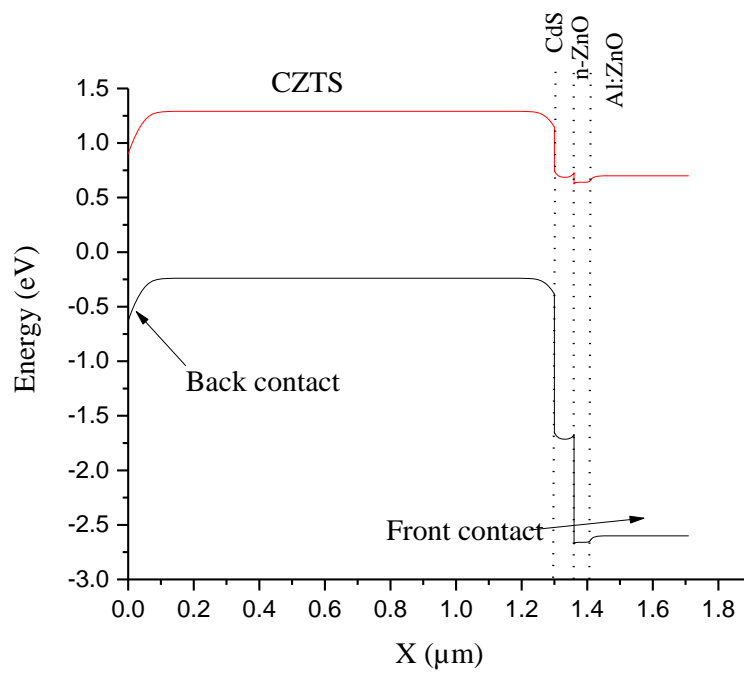
Figure III.8: Graphical representation of the band alignments within CZTS/CdS solar cell.
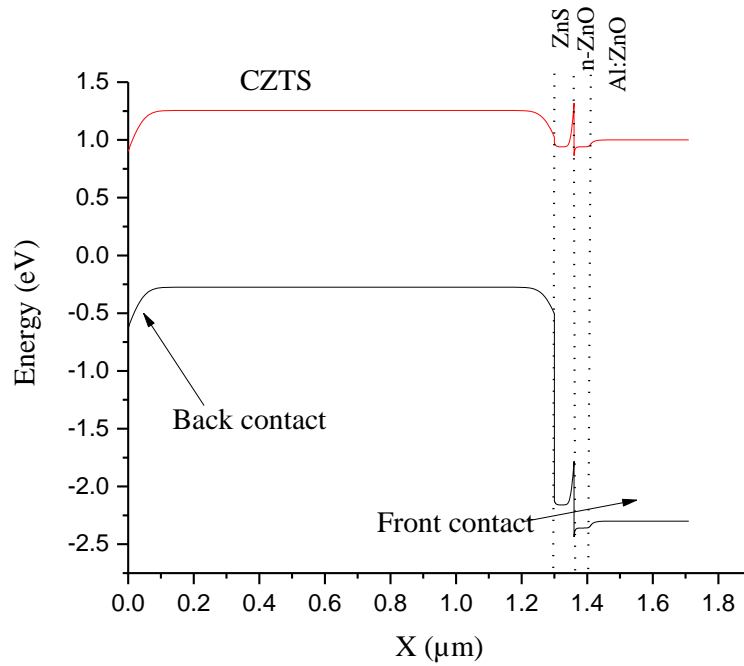
Figure III.9: Graphical representation of the band alignments within CZTS/ZnS solar cell.

III.6. Effect of CZTS absorber layer

III.6.1. Effect of CZTS layer affinity

Figure III.11 represent, respectively, the J-V characteristic of our photovoltaic cell with various electronic affinity of the CZTS absorber layer and the variation of solar cell performance parameters for a thickness 1300 nm of CZTS.

We observe that the I-V characteristic curves have two different zones:

- 0-0.1V: I-V curves are apparently identical (look the same), the augment in electron affinity does not have a significant influence on the characteristic of I-V up to a voltage of 0.8V.
- 0.1-0.9V: The curves are subject to change.
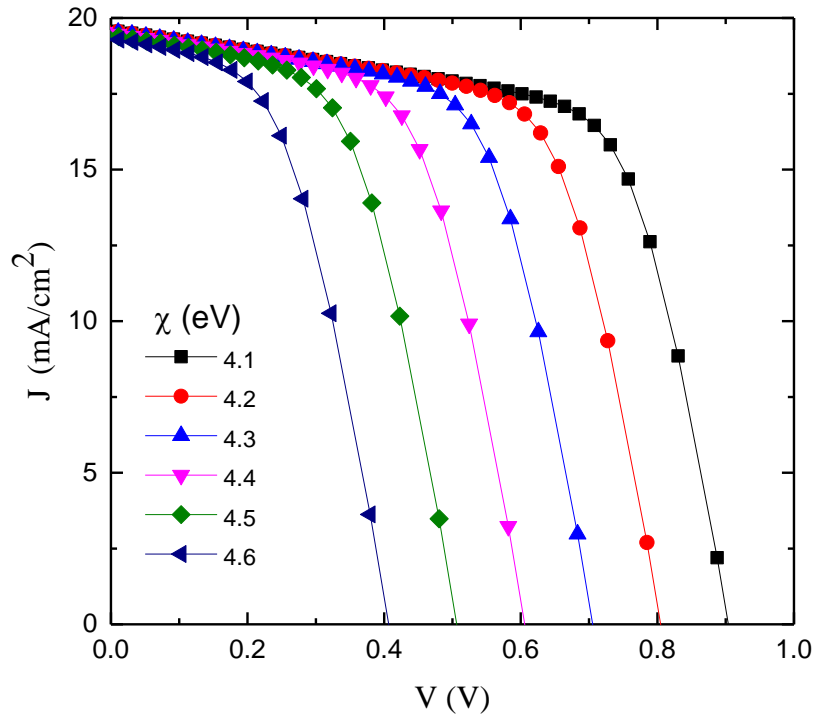
Figure III.10: The simulated J-V characteristics for variable electron affinity of CZTS.
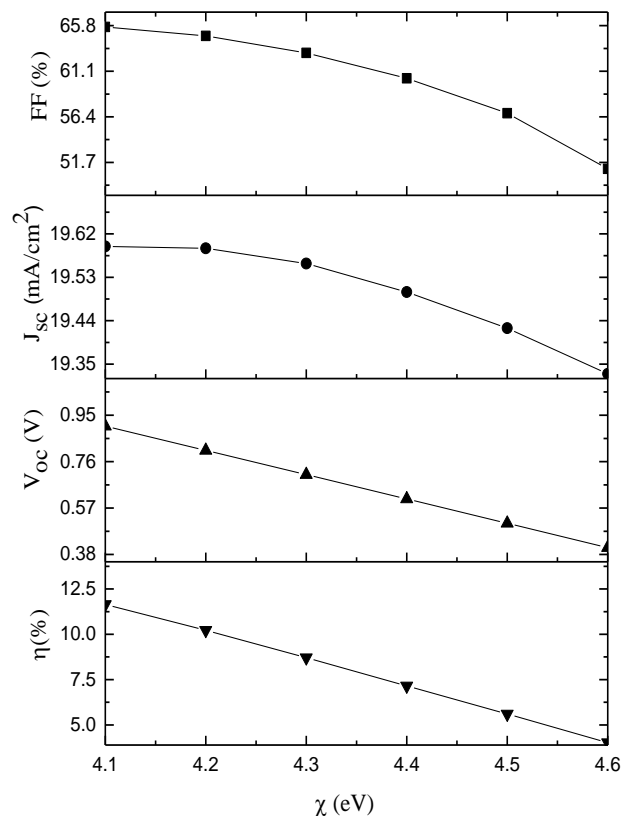
Figure III.11: The effect of CZTS electron affinity on the solar cell performance

parameters.

We notice on Figure III.10 and Figure III.11, that the more you increase the electron affinity of CZTS absorber layer, different parameters and characteristics are decreasing (a remarkable decrease in electrical efficiency, fill factor , open circuit voltage, and slight decrease for short-circuit current density). For an electron affinity $\chi = 4.6$eV, an efficiency of 4.02%, fill factor of 51.02% are obtained .

The interface strongly depends on the respective electron affinities (χ), which can be varied by modifying the deposit conditions. Deposition methods and post-deposition conditions can have a significant impact on the nature of CZTS / CdS heterojunctions and therefore band alignment [4, 22]. The heterojunction interface can give rise to type I (CBO) (spike type, the positive) or type II (cliff type,the negative) depending on the difference in electronic affinity of the absorber and the buffer layer. The large spike CBO at the buffer/absorber interface also decreases the solar cell's performance as it severely decreases the photocurrent. This positive offset band constitutes a large potential barrier between the minimum CB in the absorber layer and the maximum CB in the buffer layer that impedes the photogenerated electrons [23]. In the present simulation, the electron affinity of CZTS, which is dependent on its growth conditions, varied from 4.1 to 4.6 eV, and its effect on the J-V characteristics of the PV cell was issued. We can observe with an increase in χ. The efficiency is the highest ($\sim 11.64\%$) for $\chi = 4.1\ eV$.

III.6.2. Effect of CZTS band gap energy Eg

Figure III.12 and Figure III.13 represent respectively the J-V characteristic of our photovoltaic cell as function of bandgap energy Eg of the CZTS absorber layer, and the variation of solar cell performance parameters when the values of 1300 nm of CZTS.

We have also evaluated, in this study, the impact of different gap energies of the CZTS absorber layer on the performance of the cell; layer P is the absorber layer or so-called active layer or base. The gap energy has been varied from 1.4 eV to 1.63 eV, these values are found within the typical range of literature modeling CZTS solar cells [5, 10, 24-29]. The optical band-gap (*E*g) was affected by varying Zn, Sn and S precursor concentrations[30].
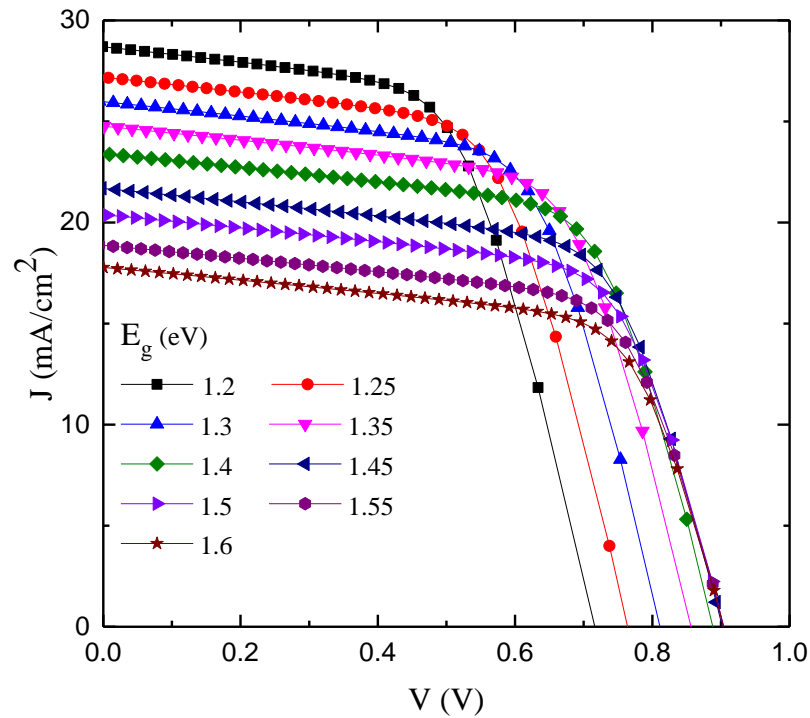
Figure III.12: The simulated J-V characteristics for variable band gap energy of CZTS.

We can notice the changes in the values of Jsc, Voc, FF and the efficiency .The figure shows that when the band gap is equal to 1.6 eV, Voc is 0.904 V and FF reached the value of 65.6. From the figure, it appears that rising Eg from 1.2 to 1.6 eV caused a decrease to value 10.56 % in efficiency and decrease in current density of short circuits to value of 17.77mA/cm^2. The explanation for this is that rising Eg leads to reducing the absorption, leading to a decrease in Jsc and efficiency. Additionally, Voc is increasing because of its direct proportionality to Eg. It shows that Voc and FF grow significantly to 1.35 eV, and remain almost unchanged after this value while Jsc is decreasing linearly. This decrease can be explained by the fact that the wide gap absorbers do not absorb photons wavelengths. As a result, a small amount of electron-hole pairs can be observed and a small amount of free carriers collected; which could reduce the value of Jsc. Decreasing efficiency after 1.35 eV is due to the reduce of Jsc as Voc and FF remain almost constant after this value [31].
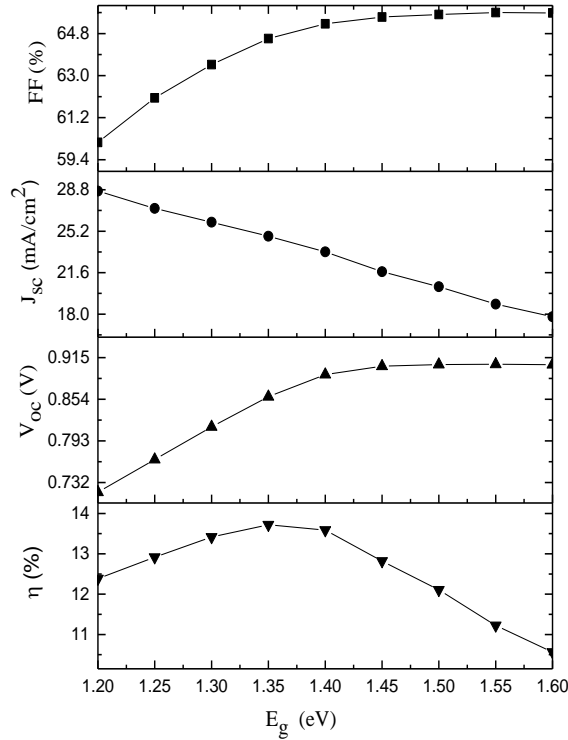
Figure III.13: The effect of CZTS bandgap energy on the solar cell performance parameters.

III.6.3. Effect of CZTS thickness

The effect of the thickness of the CZTS absorber layer on the performance of the cell has been studied by varying it from 1 to 3.5 microns meter. The Figure III.14 and Figure III.15 show the different effects of this variation on the cell performance parameters such as short-circuit current density (Jsc), open circuit voltage (Voc), fill factor (FF), and efficiency. Note in the Figure that Jsc, Voc, and η increase consistently with the boost in the absorber layer thickness. This could be due to the fact that more photons with long wavelengths are absorbed by the absorber when it is wider and, therefore, an increased number of electron-hole pairs is remarked. This will therefore produce enhancements in the values of Jsc, Voc, and therefore efficiency. Note that FF decreases with boosting thickness from the value 2 µm. Wider thicknesses introduce resistive components which can affect the fill factor [5].

However, the growth of thicker absorber layers is not profitable. In addition to this, for thicker CZTS films the secondary phases (ZnS, Cu_2S and Cu_2SnS_3, for example) should be more numerous and tough to detect experimentally [4].
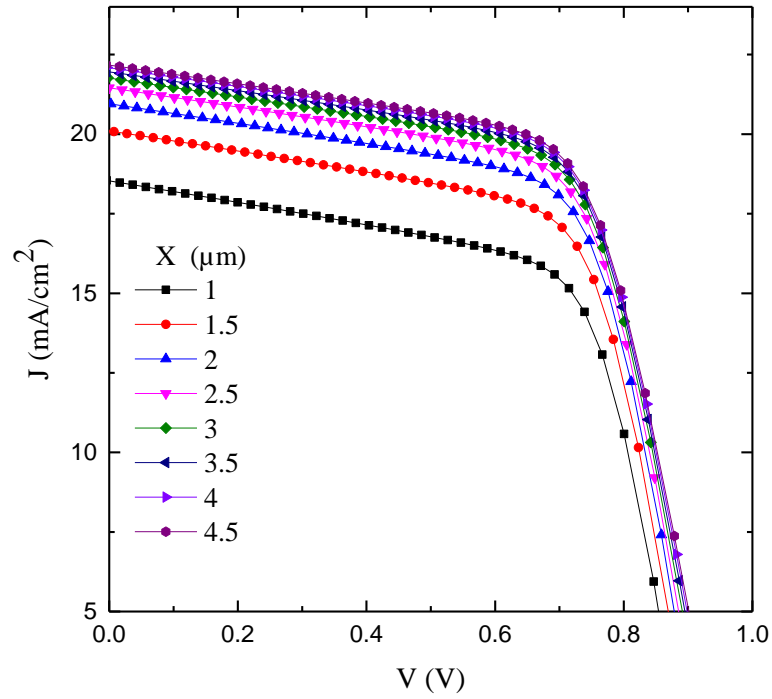
Figure III.14: The simulated J-V characteristics for variable thickness of CZTS.
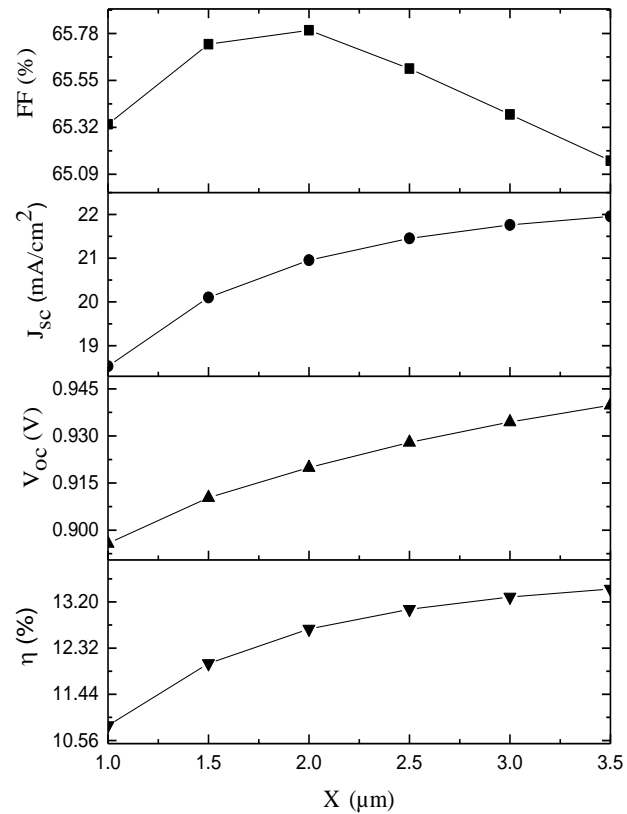
Figure III.15: The effect of CZTS thickness on the solar cell performance parameters.

III.6.4. Effect of the concentration of the Na absorber layer of CZTS

The Figure III.16 and Figure III.17 illustrate the J-V characteristics of cells with various carrier densities (N_A) in the CZTS absorber. Our model of solar cell has been simulated for the values of N_A in the margin 10^{13}-10^{17}, since the experimental results have shown that the minimum and maximum values of N_A are about 1.2×10^{15} cm^{-3}[5, 32] and 3.1×10^{20} cm^{-3} [32, 33] respectively . This indicates that the Voc, FF, and η increase with the concentration of carriers and the Jsc decreases with it. As the absorber carrier densities N_A increase, the saturation current I_0 decreases and then the V_{oc} increases.

However, with rising carrier densities, the short-circuit current will decrease. This is mainly because the higher carrier densities increase the recombination process and the probability of formation of photon-generated electron. At a hole concentration amount 10^{17} / cm^{-3} the efficiency as well as FF are found to be maximum.With increased carrier density, the difference in quasi-Fermi levels corresponding to minority carriers on both sides of the junction becomes wide. This leads to an increase in V_{OC} up to a certain critical concentration after that the semiconductor makes degeneration. In degenerate situation, the length of the carrier diffusion is very small,this results in a drastic reduction of the open-circuit voltage and hence in efficiency. It is also observed that the quantum efficiency is reduced for higher densities of the acceptors due to increased recombination process [4, 34].

Where the efficiency is enhanced to a value of 11.82% for its density 10^{17}cm^{-3}. When the concentration of carriers increases in the absorber layer, the semiconductor becomes degenerate and this is a valid reason for limiting the large values of N_A.
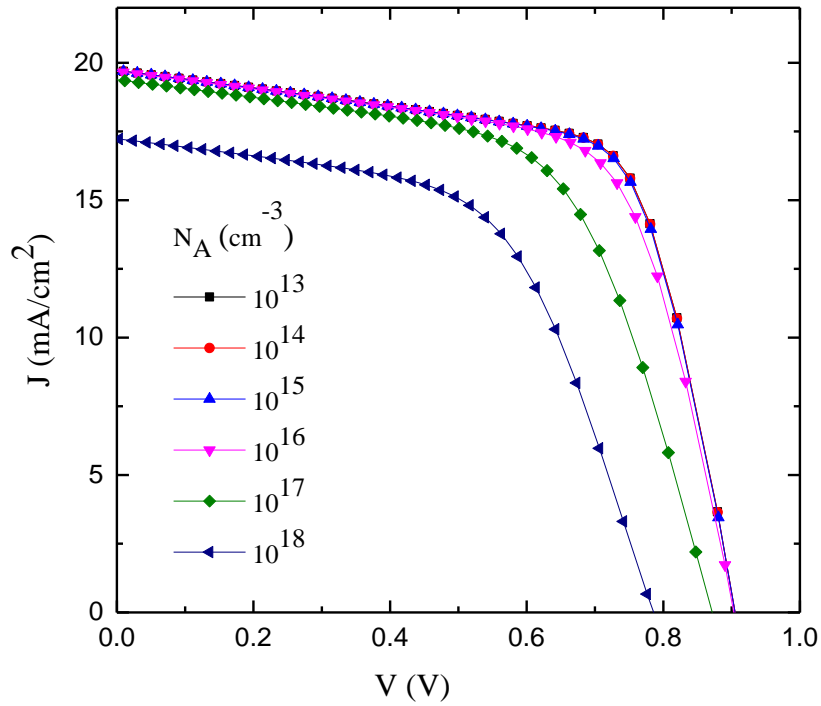
Figure III.16: The simulated J-V characteristics for variable doping density of
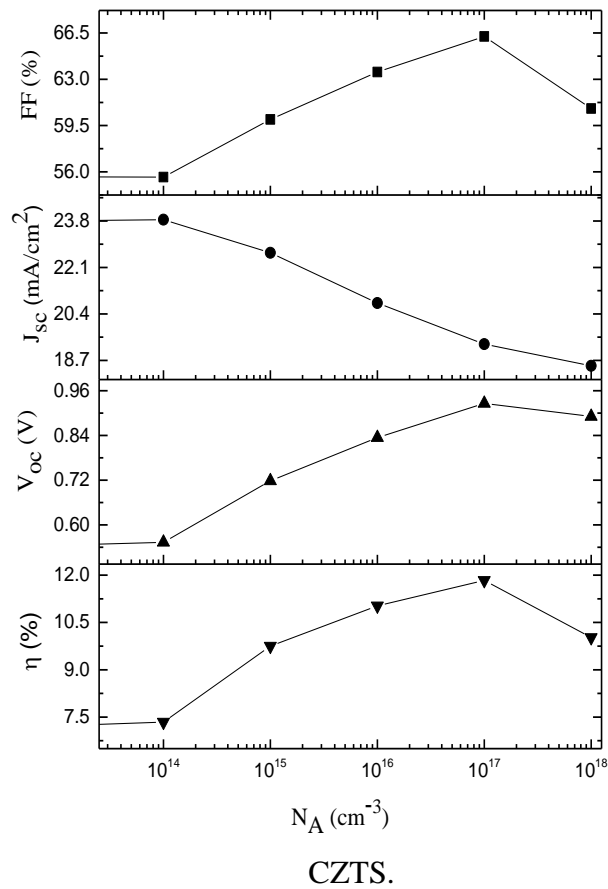
CZTS.

Figure III.17: The effect of CZTS doping density on the solar cell performance

parameters.

III.6.5. Effect of defect in CZTS

CZTS has a wide variety of points that include: The point defects of the acceptor in CZTS which are vacant: V_{Cu}, V_{Zn}, V_{Sn}, and the antisites: Cu_{Zn}, Cu_{Sn}, Zn_{Sn} , whereas the donor as defects consist of vacancy: V_S, interstitials: Cu_i, Zn_i, and antisites: Zn_{Cu}, Sn_{Cu}, Sn_{Zn}. deep acceptor levels of Cu_{Sn} and Cu_{Zn} are considered to be one of the most active SRH recombination centers for CZTS-based devices [4, 32, 35-38]. Deep donor defects such as defects (V_S and Sn_{Zn}) also contribute significantly to the recombination of SRH [37, 39]. On the other hand, the self-compensating neutral defect of complexes like $[Cu_{Zn}^- + Zn_{Cu}^+]$ et $[V_{Cu}^- + Zn_{Cu}^+]$ act as passivation centers for these types of deep level faults [4, 32, 35-38, 40], where the concentration of defects is as mentioned in some studies is ~ (10^{18}cm^{-3} -10^{21}cm^{-3}) [32, 37, 41].

The defect states can introduce additional carrier recombination centers in CZTS solar cells, especially SRH recombination. Enhance the recombination process of photogenerated carriers, leading to increased reverse saturation current density, reduced short-circuit current, cell efficiency, and open-circuit voltage [4, 34, 42].

a. Influence of neutral defect

The Figure III.18 and Figure III.19 demonstrate the current-voltage characteristics of solar cells as function defects densities of the neutral type with a variable concentration from 10^{13}cm^{-3} to 10^{17}cm^{-3}.
$Nt < 10^{16}$cm^{-3}: the Jsc, FF, Voc, and η decreases slowly. $Nt > 10^{16}$cm^{-3}: enough marked decrease in Jcc, FF, and η ; As for the voltage decreases to the value of 0.861V at 10^{17}cm^{-3}.

In the CZTS layer, we introduce Gaussian defect states with energy 0.6 EV which was selected above CZTS valence band edge.
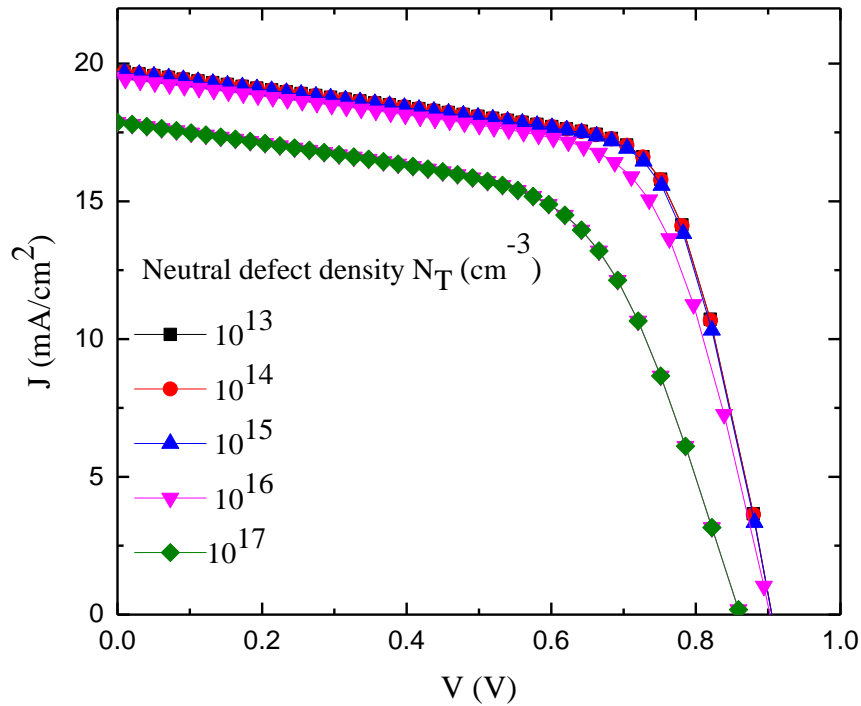
Figure III.18: The simulated J-V characteristics for variable of neutral defect density of CZTS.
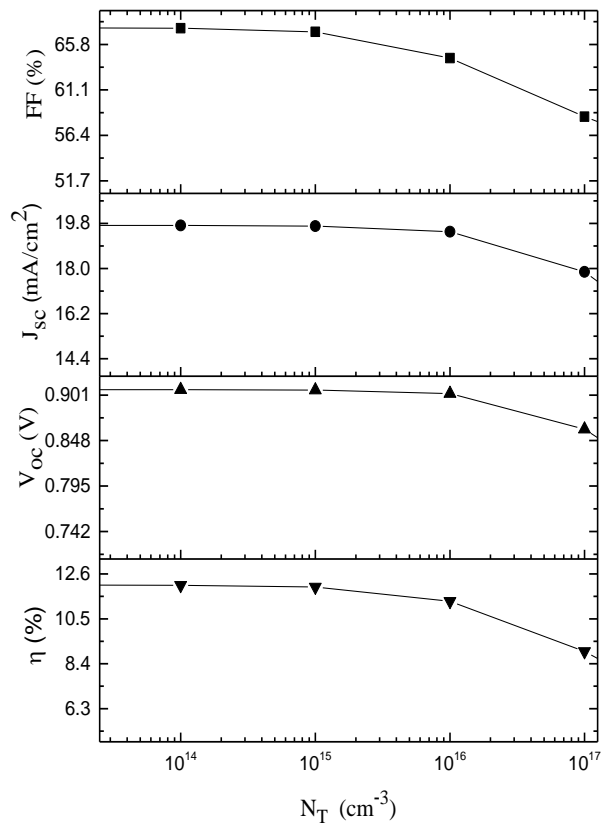
Figure III.19: The effect of CZTS neutral defect density on the solar cell performance

parameters.

b. Influence of acceptor defect

The Figure III.20 and Figure III.21 demonstrate the current-voltage characteristics of solar cells as function defects densities of the acceptor type with a variable concentration from 10^{13} cm^{-3} to 10^{18} cm^{-3}.

Almost the same as in the case of neutral defect where we notice that there is a slight decrease in Jsc, FF, η, and Voc.
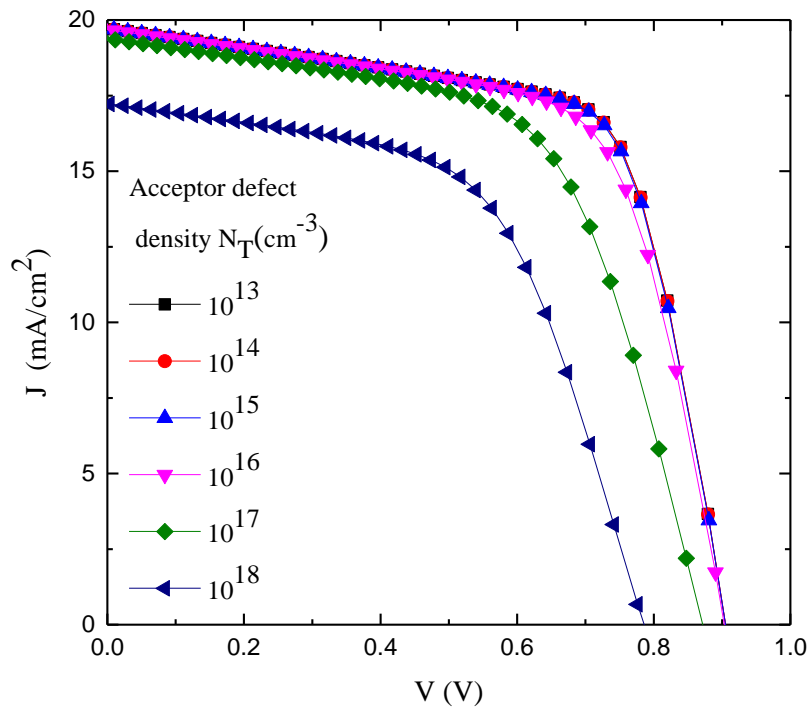
Figure III.20: The simulated J-V characteristics for variation of acceptor defect density of CZTS.
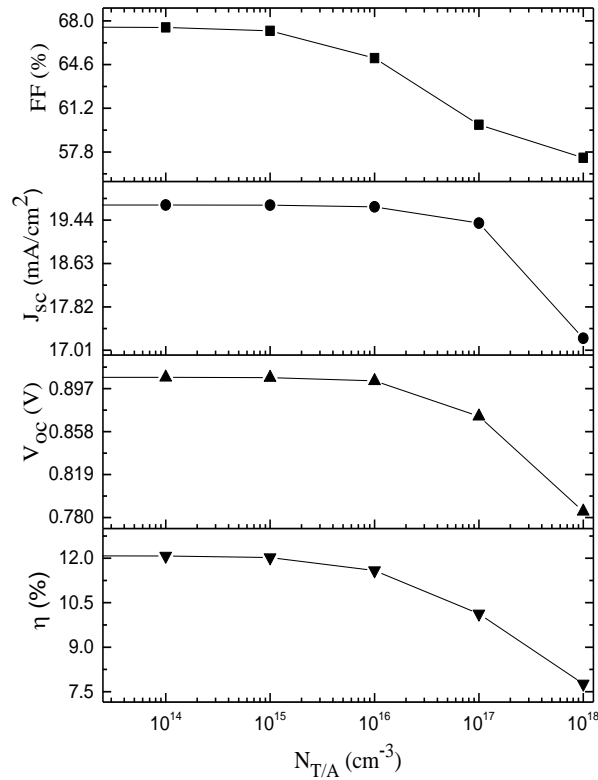
Figure III.21: The effect of CZTS acceptor defect density on the solar cell performance parameters.

c. Influence of donor defects

The figure represents the current-voltage characteristics in diodes with donor type defect of variable density from 10^{13}cm^{-3} to 10^{17}cm^{-3}. It can be seen that the current decreases when the concentration of defects in the active layer increases. Nevertheless, this influence is slight for density less than 10^{16}cm^{-3}. The same for FF, η, and Voc. Then, we notice a significant decrease when the density is greater than 10^{16}cm^{-3}.
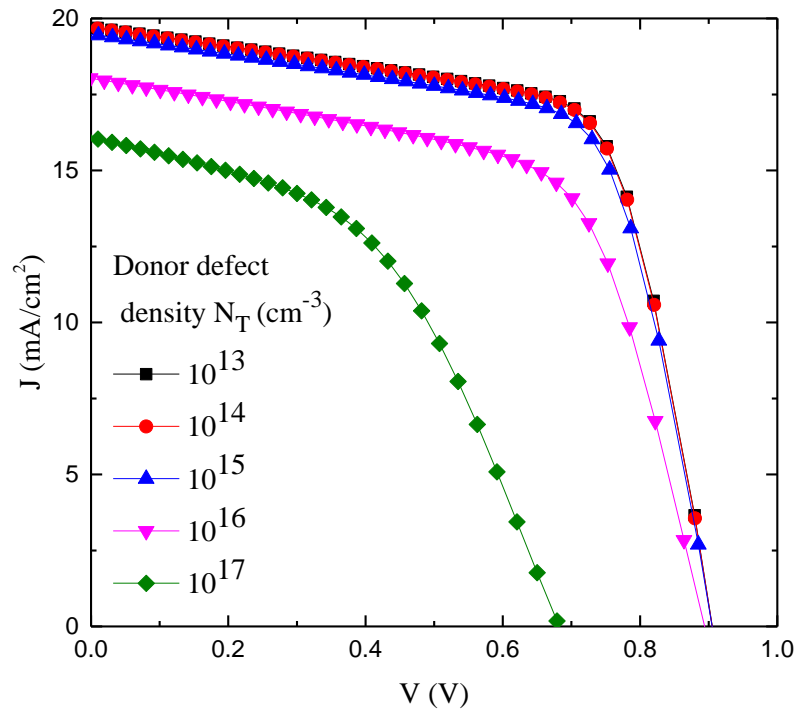
Figure III.22: The simulated J-V characteristics for variation of donor defect density of CZTS.
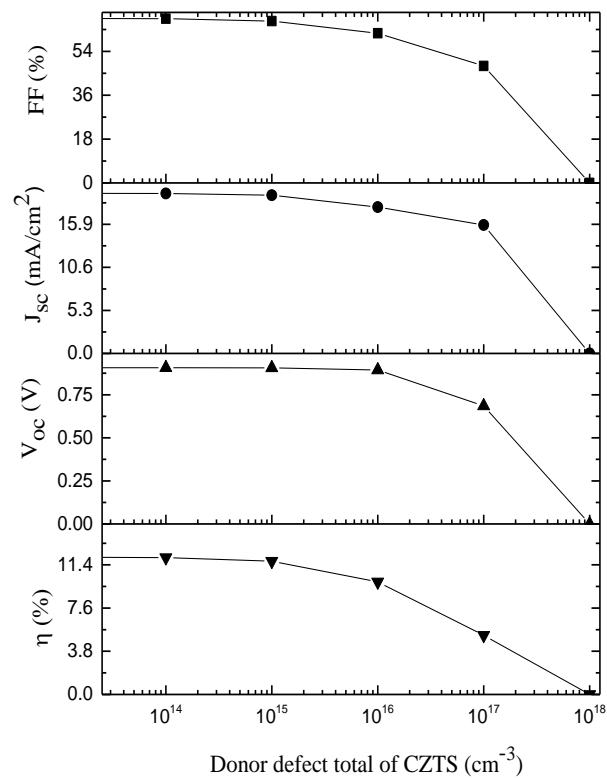
Figure III.23: The effect of CZTS donor defect density on the solar cell performance parameters.

III.7. Influence of CZTS / ZnS interface defect

The Figure III.24 and Figure III.25 represent, respectively, the J-V characteristic of our photovoltaic cell as function of total defect of interface CZTS/ZnS, and the variation of solar cell performance parameters.
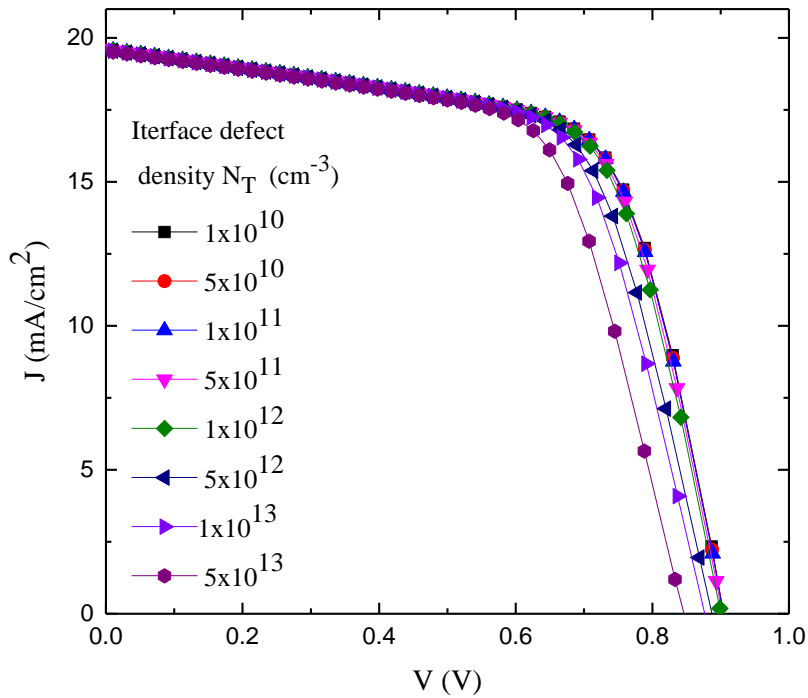
Figure III.24: The simulated J-V characteristics for variation of interface defect density of CZTS.
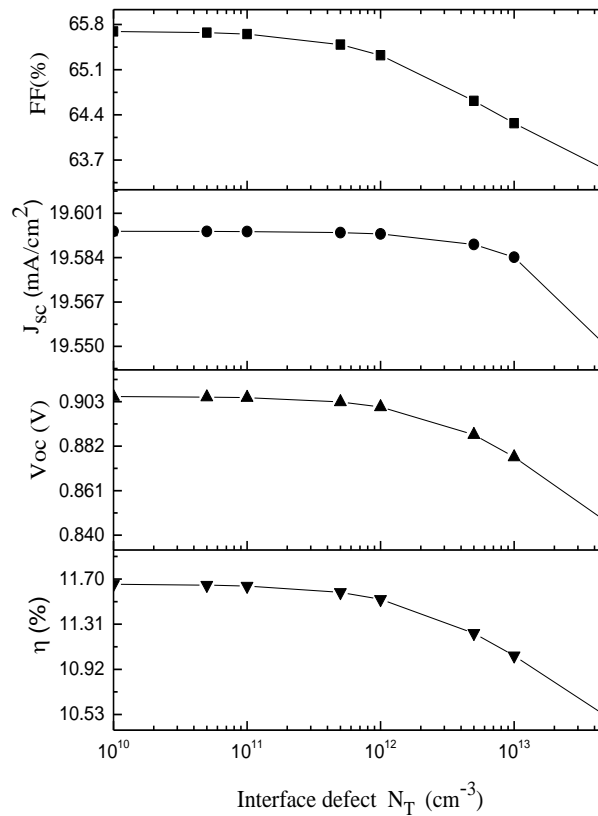
Figure III.25: The effect of CZTS/ZnS interface defect density on the solar cell performance parameters.

CZTS / ZnS interface defect is varied between the values 10^{10}-10^{13} cm^{-3} [43-45], the Influence of CZTS / ZnS interface defect this causes the J-V characteristics of the solar cell to decrease. Moreover, the neutral defects in the CZTS / ZnS interface are also principal centers for recombining carriers. They are formed mainly due to the difference between the two layers and are a major source of SRH recombination in thin film PV cells [4, 34, 42].

Table III-9 : The Optimal parameters

Band gap	Electron affinity	Thickness	Acceptor density	the neutral defect concentration	CZTS / ZnS interface defect
1.35eV	4.1eV	2μm	1x 10^{17} cm^{-3}	5x 10^{15} cm^{-3}	6x 10^{10} cm^{-3}
Ƞ=15.21%		FF=65.19%		J_{SC}=26.43mA/cm^2	V_{oc}=0.882V

REFERENCES

[1]   M. Burgelman, P. Nollet, and S. Degrave, "Modelling polycrystalline semiconductor solar cells," *Thin Solid Films,* vol. 361, pp. 527-532, 2000.

[2]   T. P. Dhakal, C. Y. Peng, R. R. Tobias, R. Dasharathy, and C. R. Westgate, "Characterization of a CZTS thin film solar cell grown by sputtering method," *Solar Energy,* vol. 100, pp. 23-30, 2014.

[3]   C. Mebarkia, D. Dib, H. Zerfaoui, and R. Belghit, "Energy efficiency of a photovoltaic cell based thin films CZTS by SCAPS," *Journal of Fundamental and Applied Sciences,* vol. 8, pp. 363-371, 2016.

[4]   S. Meher, L. Balakrishnan, and Z. Alex, "Analysis of Cu 2 ZnSnS 4/CdS based photovoltaic cell: a numerical simulation approach," *Superlattices and Microstructures,* vol. 100, pp. 703-722, 2016.

[5]   M. Patel and A. Ray, "Enhancement of output performance of Cu2ZnSnS4 thin film solar cells—A numerical simulation approach and comparison to experiments," *Physica B: Condensed Matter,* vol. 407, pp. 4391-4397, 2012.

[6]   A. Sylla, S. Touré, and J.-P. Vilcot, "Numerical modeling and simulation of CIGS-based solar cells with ZnS buffer layer," *Open Journal of Modelling and Simulation,* vol. 5, p. 218, 2017.

[7]   G. Hanna, A. Jasenek, U. Rau, and H. Schock, "Influence of the Ga-content on the bulk defect densities of Cu (In, Ga) Se2," *Thin Solid Films,* vol. 387, pp. 71-73, 2001.

[8]   H. Sun, K. Sun, J. Huang, C. Yan, F. Liu, J. Park, A. Pu, J. A. Stride, M. A. Green, and X. Hao, "Efficiency Enhancement of Kesterite Cu2ZnSnS4 Solar Cells via Solution-Processed Ultrathin Tin Oxide Intermediate Layer at Absorber/Buffer Interface," *ACS Applied Energy Materials,* vol. 1, pp. 154-160, 2017.

[9]   A. D. Adewoyin, M. A. Olopade, and M. Chendo, "Enhancement of the conversion efficiency of Cu2ZnSnS4 thin film solar cell through the optimization of some device parameters," *Optik-International Journal for Light and Electron Optics,* vol. 133, pp. 122-131, 2017.

[10]   M. Courel, J. Andrade-Arvizu, and O. Vigil-Galán, "Loss mechanisms influence on Cu2ZnSnS4/CdS-based thin film solar cell performance," *Solid-State Electronics,* vol. 111, pp. 243-250, 2015.

[11]   M. Courel, J. A. Andrade-Arvizu, and O. Vigil-Galán, "Towards a CdS/Cu2ZnSnS4 solar cell efficiency improvement: A theoretical approach," *Applied Physics Letters,* vol. 105, p. 233501, 2014.

[12]   I. ETCMOS Services, *ETCMOS 2017 Vol. 2: Circuits and Systems Track: Presentation Slides*, 2017.

[13]   T. Minemoto, T. Matsui, H. Takakura, Y. Hamakawa, T. Negami, Y. Hashimoto, T. Uenoyama, and M. Kitagawa, "Theoretical analysis of the effect of conduction band offset of window/CIS layers on performance of CIS solar cells using device simulation," *Solar Energy Materials and Solar Cells,* vol. 67, pp. 83-88, 2001.

[14]   W. Bao and M. Ichimura, "First-Principles Study on Influences of Crystal Structure and Orientation on Band Offsets at the CdS/Cu2ZnSnS4Interface," *International Journal of Photoenergy,* vol. 2012, pp. 1-5, 2012.

[15]   C. Mebarkia, D. Dib, H. Zerfaoui, and R. Belghit, "Energy efficiency of a photovoltaic cell based thin films CZTS by SCAPS," *Journal of Fundamental and Applied Sciences,* vol. 8, p. 363, 2016.

[16]   P. McElhany and J. Arch, "Numerical Simulation of Cu2ZnSnS4 Based Solar Cells with In2S3 Buffer Layers by SCAPS-1D," *Appl. Phys,* vol. 64, p. 1254, 1988.

[17]   M. B. Hosen, A. N. Bahar, M. K. Ali, and M. Asaduzzaman, "Modeling and performance analysis dataset of a CIGS solar cell with ZnS buffer layer," *Data Brief,* vol. 14, pp. 246-250, Oct 2017.

[18]   N. M. Saeed, "Structural and Optical Properties of ZnS Thin Films Prepared by SprayPyrolysis Technique," *Journal of Al-Nahrain University-Science,* vol. 14, pp. 86-92, 2011.

[19]   J. Huso, L. Bergman, and M. D. McCluskey, "Bandgap of cubic ZnS1-xOx from optical transmission spectroscopy," *Journal of Applied Physics,* vol. 125, p. 075704, 2019.

[20]   J. Shenoy, J. N. Hart, R. Grau-Crespo, N. L. Allan, and C. Cazorla, "Mixing thermodynamics and photocatalytic properties of GaP–ZnS solid solutions," *Advanced Theory and Simulations,* vol. 2, p. 1800146, 2019.

[21]   O. Toma, L. Ion, S. Iftimie, V. Antohe, A. Radu, A. Raduta, D. Manica, and S. Antohe, "Physical properties of rf-sputtered ZnS and ZnSe thin films used for double-heterojunction ZnS/ZnSe/CdTe photovoltaic structures," *Applied Surface Science,* 2019.

[22]   A. T. Ngoupo, S. Ouédraogo, and J. Ndjaka, "Numerical analysis of interface properties effects in CdTe/CdS: O thin film solar cell by SCAPS-1D," *Indian Journal of Physics,* pp. 1-13, 2019.

[23]   M. D. Wanda, S. Ouédraogo, and J. Ndjaka, "Theoretical analysis of minority carrier lifetime and Cd-free buffer layers on the CZTS based solar cell performances," *Optik,* vol. 183, pp. 284-293, 2019.

[24]   S. Vallisree, R. Thangavel, and T. Lenka, "Theoretical investigations on enhancement of photovoltaic efficiency of nanostructured CZTS/ZnS/ZnO based solar cell device," *Journal of Materials Science: Materials in Electronics,* vol. 29, pp. 7262-7272, 2018.

[25]   J. Li, M. Wei, Q. Du, W. Liu, G. Jiang, and C. Zhu, "The band alignment at CdS/Cu2ZnSnSe4heterojunction interface," *Surface and Interface Analysis,* vol. 45, pp. 682-684, 2013.

[26]   J. Paier, R. Asahi, A. Nagoya, and G. Kresse, "Cu2ZnSnS4as a potential photovoltaic material: A hybrid Hartree-Fock density functional theory study," *Physical Review B,* vol. 79, 2009.

[27]   W. Li, J. Chen, C. Yan, and X. Hao, "The effect of ZnS segregation on Zn-rich CZTS thin film solar cells," *Journal of Alloys and Compounds,* vol. 632, pp. 178-184, 2015.

[28]   D. Nam, S. Cho, J.-H. Sim, K.-J. Yang, D.-H. Son, D.-H. Kim, J.-K. Kang, M.-S. Kwon, C.-W. Jeon, and H. Cheong, "Solar conversion efficiency and distribution of ZnS secondary phase in Cu2ZnSnS4 solar cells," *Solar Energy Materials and Solar Cells,* vol. 149, pp. 226-231, 2016.

[29]   A. Nagoya, R. Asahi, and G. Kresse, "First-principles study of Cu2ZnSnS4 and the related band offsets for photovoltaic applications," *Journal of Physics: Condensed Matter,* vol. 23, p. 404203, 2011.

[30]   M. Patel, I. Mukhopadhyay, and A. Ray, "Structural, optical and electrical properties of spray-deposited CZTS thin films under a non-equilibrium growth condition," *Journal of Physics D: Applied Physics,* vol. 45, p. 445103, 2012.

[31]   H. Arbouz, A. Aissat, and J. Vilcot, "Simulation and optimization of CdS-n/Cu2ZnSnS4 structure for solar cell applications," *International Journal of Hydrogen Energy,* vol. 42, pp. 8827-8832, 2017.

[32]   S. Chen, A. Walsh, X. G. Gong, and S. H. Wei, "Classification of lattice defects in the kesterite Cu2ZnSnS4 and Cu2ZnSnSe4 earth-abundant solar cell absorbers," *Advanced Materials,* vol. 25, pp. 1522-1539, 2013.

[33]   C. Chan, H. Lam, and C. Surya, "Preparation of Cu2ZnSnS4 films by electrodeposition using ionic liquids," *Solar Energy Materials and Solar Cells,* vol. 94, pp. 207-211, 2010.

[34]   P. Lin, L. Lin, J. Yu, S. Cheng, P. Lu, and Q. Zheng, "Numerical simulation of Cu2ZnSnS4 based solar cells with In2S3 buffer layers by SCAPS-1D," *Journal of Applied Science and Engineering,* vol. 17, pp. 383-390, 2014.

[35]   W. Xiao, J. Wang, X. Zhao, J. Wang, G. Huang, L. Cheng, L. Jiang, and L. Wang, "Intrinsic defects and Na doping in Cu2ZnSnS4: A density-functional theory study," *Solar Energy,* vol. 116, pp. 125-132, 2015.

[36]   T. Gershon, T. Gokmen, O. Gunawan, R. Haight, S. Guha, and B. Shin, "Understanding the relationship between Cu 2 ZnSn (S, Se) 4 material properties and device performance," *Mrs Communications,* vol. 4, pp. 159-170, 2014.

[37]   M. Kumar, A. Dubey, N. Adhikari, S. Venkatesan, and Q. Qiao, "Strategic review of secondary phases, defects and defect-complexes in kesterite CZTS–Se solar cells," *Energy & Environmental Science,* vol. 8, pp. 3134-3159, 2015.

[38]   S. Chen, J.-H. Yang, X.-G. Gong, A. Walsh, and S.-H. Wei, "Intrinsic point defects and complexes in the quaternary kesterite semiconductor Cu 2 ZnSnS 4," *Physical Review B,* vol. 81, p. 245204, 2010.

[39]   V. Kosyak, N. Mortazavi Amiri, A. Postnikov, and M. A. Scarpulla, "Model of native point defect equilibrium in Cu2ZnSnS4 and application to one-zone annealing," *Journal of Applied Physics,* vol. 114, p. 124501, 2013.

[40]   S. K. Wallace, D. B. Mitzi, and A. Walsh, "The steady rise of kesterite solar cells," *ACS Energy Letters,* vol. 2, pp. 776-779, 2017.

[41]   D. Huang and C. Persson, "Band gap change induced by defect complexes in Cu2ZnSnS4," *Thin Solid Films,* vol. 535, pp. 265-269, 2013.

[42]   S. Çetinkaya, "Study of electrical effect of transition-metal dichalcogenide-MoS2 layer on the performance characteristic of Cu2ZnSnS4 based solar cells using wxAMPS," *Optik,* vol. 181, pp. 627-638, 2019.

[43]   S. Guitouni and N. Attaf, "Elaboration et étude de structures à base de couches minces de ZnO et de chalcogénures (CIS, CZTS) pour des applications photovoltaïques," 2016, جامعة الإخوة منتوري قسنطينة.

[44]   F. Z. Boutebakh and N. Attaf, "Realization and electrical characterization of thin film heterojunction for photovoltaic application," جامعة الإخوة منتوري قسنطينة.

[45]   F. Boutebakh, M. L. Zeggar, N. Attaf, and M. Aida, "Electrical properties and back contact study of CZTS/ZnS heterojunction," *Optik,* vol. 144, pp. 180-190, 2017.

GENERAL

CONCLUSION

GENERAL CONCLUSION

Throughout this research, we have studied solar cells of the kind thin films based on CZTS. We used a numerical simulation program SCAPS to determine the best parameters for each solar cell based on CZTS, in order to improve the performance of the cell.

The first phase of the work was devoted to the study of the cell CZTS/ CdS/ ZnO/ Al:ZnO where we studied the effect of defects of the donor type and acceptor (Gaussian) in addition to the shun resistance and serie resistance. As we noted the effect of the defects of the interface CZTS/CdS in the performance of this cell, and that is from showing the curves of current density voltage (J-V).

In the second phase, we showed the change in the current density voltage (J-V). First, we indicated the effect of buffer layers as CdS, ZnS, and In_2S_3 on cell performance. Then, we represented the effect of electronic affinity, concentration, band-gap energy, thickness, the presence of deep defect (donor or acceptor) of the CZTS layer, and defect of interface CZTS/ZnS on the short circuit current, the open circuit voltage, the fill factor, and efficiency of CZTS/ ZnS/ ZnO/ Al:ZnO.

The results of the simulation demonstrated that:

- For the CZTS/ CdS/ ZnO/ Al:ZnO cell, we found that we can compare simulation values with experimental values when adding defects of interface the values are converging.
- Of the three layers, CdS, In_2S_3, and ZnS, we find that the latter provides a better performance to the cell.
- For the CZTS/ ZnS/ ZnO/ Al:ZnO cell, efficiency, J_{sc}, V_{oc} and FF are decreasing for increase the electronic affinity of CZTS.
- FF and V_{oc} are increasing to boost the band-gap energy of CZTS, while the J_{sc} is decreasing, the efficiency is increasing even the $E_g = 1.35eV$, then it is reduce.
- Efficiency, J_{sc} and V_{oc} are increasing by augment the thickness of CZTS, while the FF is increasing even value 2µm, and then it is reducing.
- When N_A increases, J_{sc} is reduce; while the efficiency, V_{oc}, and FF are increasing to value 10^{17} cm^{-3}, then it decreases.

- The effect of defects leads to deteriorate of cell performance, especially the donor defects whose effect is clear.